

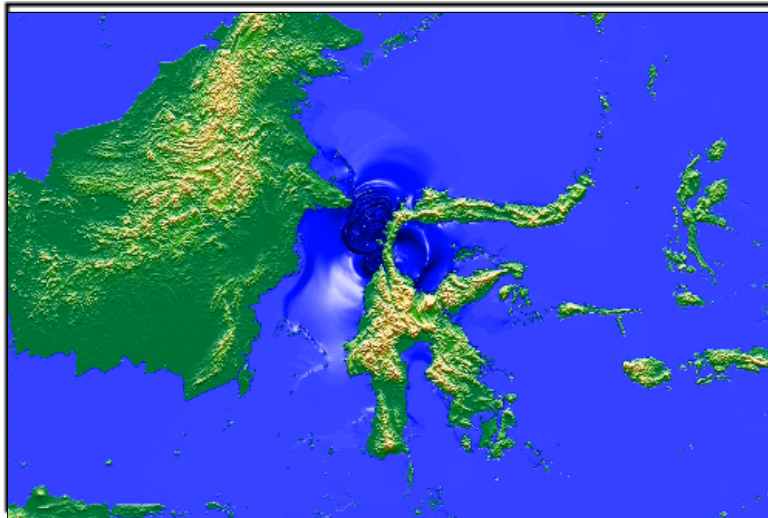
## Master of Science in Environmental Science

### Tsunami simulation and sensitivity analysis using MIRONE (Case study: Tsunami Palu 2018)

---

Katrin Serafina

Sous la direction du Prof. Grégoire Mariéthoz  
Codirection du Dr. Joaquim Luis



June – 2022

**Information importante:** Le texte de ce travail n'a pas été rédigé en vue d'une publication ou dans l'optique d'une édition ou diffusion ; son format et tout ou partie de son contenu répondent donc à cet état de fait. Les contenus n'engagent pas l'Université de Lausanne.

Ce texte n'en est pas moins soumis aux règles et droits usuels sur les droits d'auteur. A ce titre, les citations tirées du présent mémoire ne sont autorisées que dans la mesure où la source et le nom de l'auteur.e sont clairement cités. La loi fédérale sur le droit d'auteur et les droits voisins (LDA) est en outre applicable.

### **Convention de transmission des travaux de master en Sciences de l'Environnement déposés dans les archives de la Bibliothèque des Sciences de la Terre**

Les travaux de masters en Sciences de l'Environnement sont juridiquement considérés comme des copies d'examen et sont, à ce titre, confidentiels.

Cependant, la confidentialité peut être exceptionnellement levée avec l'accord de l'auteur du travail de master et du directeur du travail de master pour des **motifs de recherche scientifique, sans but commercial**.

- Par sa signature, l'auteur du travail de master en autorise la transmission sous format papier et électronique pour des motifs de recherche scientifique, par la bibliothèque des Sciences de la Terre.
- Le directeur du travail doit indiquer si le travail contient des données juridiquement confidentielles (par ex. des données de compagnies pétrolières ou minières) ne pouvant pas être diffusées.
- Le directeur du travail peut en outre décider d'une période d'embargo durant laquelle le travail ne sera pas transmis, même pour des motifs de recherche scientifique. La période d'embargo s'éteint automatiquement au plus tard à la retraite du directeur du travail ou lorsque le directeur quitte l'université de Lausanne.

Titre du travail :

Auteur :

Directeur :

---

J'autorise la transmission de mon travail de master pour des motifs de recherche scientifique sans but commercial.

Lausanne, le....., signature de l'étudiant

---

Le travail contient des données confidentielles et ne peut pas être transmis      oui / non

Le travail est soumis à un embargo jusqu'au ..... (date)

L'embargo peut être levé avant la date indiquée moyennant mon accord      oui / non



Lausanne, le ....., signature du directeur

*Unil*

## Contents

1. Introduction	8
1.1 Background	8
1.2 Research aims and hypotheses	10
2. Case Study: Tsunami Palu 2018	11
2.1. Tsunami	11
2.1.1. Description and causes	11
2.1.2. Characteristics and Damages	11
2.1.3. Generation Mechanism	14
2.1.4. Tsunamis in Indonesia	15
2.1.5. Indonesian Tsunami Early Warning System (Ina-TEWS)	17
2.2. Event of Interest: Tsunami Palu 2018	18
2.2.1. Recorded Data	20
2.2.2. Survey Data	21
2.2.3. Initial conclusion	22
3. Methodology	23
3.1. Workflow	23
3.2. Model Selection	24
3.2. Selected Model: MIRONE	28
4. Initial Model	31
4.1. Process	31
4.1.1. Bathymetry Map	31
4.1.2. Seismic Elastic Deformation	34
4.1.3 Tsunami Palu 2018 Initial model	36
4.2. Result	48
4.2.1. Recorded Data	49

4.2.2. Survey Data	50
5. Sensitivity analysis	53
5.1. Process	53
5.1.1. Bathymetry Map	54
5.1.2. Seismic Elastic Deformation	55
5.2. Result	59
5.2.1. Bathymetry Map	59
5.2.2. Seismic Elastic Deformation	60
6. Discussion	70
6.1. Initial model	70
6.1.1. Computational limitations	70
6.1.2. Landslide induced tsunami	71
6.2. Sensitivity analysis	73
6.2.1. Bathymetry Map	73
6.2.2. Seismic Elastic Deformation	75
7. Conclusion	81
References	84
Appendix A: Finite-Source Rupture Model from USGS	89

## List of Figure

Figure 1 Various tsunami wave heights	11
Figure 2 Topographic and tectonic map of the Indonesian archipelago and surrounding region	15
Figure 3 Tectonic setting of the 2018 Mw 7.5 Palu earthquake	18
Figure 4 Tide Gauge Mamuju Result	20
Figure 5 Workflow	22
Figure 6 Moving boundary example	24
Figure 7 Flowchart of numerical modeling procedure	29
Figure 8 Obtaining GEBCO Bathymetry	31
Figure 9 Loaded GEBCO Bathymetry in MIRONE	31
Figure 10 Obtaining National Bathymetry (BATNAS)	32
Figure 12 Loaded National Bathymetry in MIRONE	33
Figure 13 Loaded Finite Source Rupture Model in MIRONE	35
Figure 14 Coastal Area in Google Earth	36
Figure 15 GEBCO Coastal Area in MIRONE	37
Figure 16 BATNAS Coastal Area in MIRONE	38
Figure 17 Loaded Finite Source Rupture Model and Bathymetry in MIRONE	39
Figure 18 Characteristics of the Fault in MIRONE	41
Figure 19 Masinha Fault Computation	42
Figure 20 TINTOL Environment	43
Figure 21 Load *.nc file	44
Figure 22 Creating the movie	45
Figure 23 Simulation from 00:00 every 5 seconds until 01:00	46
Figure 24 Maximum Wave Height Initial Model	47
Figure 25 BMKG Model Result	48
Figure 26 Mamuju Tide Gauge Wave Height	49
Figure 27 National Bathymetry (Batimetri Nasional – BATNAS) in MIRONE	53
Figure 28 GEBCO Combined with National bathymetry (Batimetri Nasional – BATNAS) in MIRONE	54
Figure 28 Definition sketch of fault plane dimension and geometry	56
Figure 30 New Fault by MIRONE	58
Figure 31 Maximum Wave Height (New Fault)	58

Figure 32 Maximum Wave Height (BATNAS)	59
Figure 33 Maximum Wave Height (GEBCO Combined with BATNAS)	60
Figure 34 Maximum Wave Height with Depth Variation	61
Figure 35 Maximum Wave Height VS Depth to Top	62
Figure 36 Maximum Wave Height with Slip Variation	63
Figure 37 Maximum Wave Height VS Depth to Top	63
Figure 38 Maximum Wave Height with Width Variation	64
Figure 39 Maximum Wave Height VS Width	65
Figure 40 Maximum Wave Height with Rake Angle Variation	66
Figure 41 Maximum Wave Height VS Rake Angle	67
Figure 42 Maximum Wave Height with Dip Angle Variation	67
Figure 43 Maximum Wave Height VS Dip Angle	68
Figure 43 Bathymetric data processing flow chart (modified from Hsiao et al., (2016))	73

## List of Table

Table 1 Causes of tsunamis in the Pacific Ocean Region (2000 years period)	11
Table 2 Damage caused by tsunamis	13
Table 3 Characteristics of the current tsunami numerical models	28
Table 4 Differences between Okada Deformation Model and Real Tsunami	41
Table 5 Characteristics of USGS Fault	42
Table 6 Surveyed Data from Meteorology, Climatology, and Geophysical Agency	50
Table 7 Wave Height Comparison from Simulation Data and Surveyed Data	51
Table 8 Characteristic of New Fault by MIRONE	57
Table 9 Maximum Wave Heights from Different Bathymetries	61
Table 10 Maximum Wave Height with Depth Variation	62
Table 11 Maximum Wave Height with Slip Variation	64
Table 12 Maximum Wave Height with Width Variation	65
Table 13 Maximum Wave Height with Rake Angle Variation	67
Table 14 Maximum Wave Height with Dip Angle Variation	69

subduction

## 1. Introduction

### 1.1 Background

Tsunami is a disaster with a relatively low frequency of occurrence, causes extensive damage and loss of life, and results in large financial, social and environmental impacts that last for years. A tsunami is generated from a series of long waves caused by the displacement of a large volume of water and occurs rapidly. Tsunami waves are very different from waves generated by the wind. While winds produce waves that only move near sea level water and have small wavelengths measured in meters, in contrast, tsunamis include the seabed water's movement which can produce 100 kilometers or more wavelengths. This event is mostly triggered by underwater earthquakes, but can also be caused by volcanic eruptions, landslides, or by meteor impact (Nahak et al., 2017).

Being a country which is located in the area of three active tectonic plates makes Indonesia very prone to tsunamis. The Indo - Australian plate moves north - northeast at a speed of 7 cm/year, the Eurasian plate moves relative to the Southeast at a speed of 0.4 cm/year and the Pacific with 2 plates namely, the Philippine Micro plate which moves relative to the west - northwest at a rate of 10.2 cm/year (Simandjuntak & Barber, 1996). As a result, subduction zones were formed. This leads to frequent earthquakes, tsunamis or volcanic eruptions in Indonesia, including the recent tsunami that happened in Palu, 2018 (Bock, 2003).

On September 28, 2018, a 7.5 magnitude earthquake in Palu, Indonesia triggered several disasters, landslides, liquefaction and tsunamis which resulted in various damages, economic losses and loss of lives (Goda et al., 2019). Preliminary analysis shows shallow left-lateral, strike-slip faulting mechanism along the Palu-Koro Fault which trends generally north-south from the subduction zone of North Sulawesi in the Sulawesi Sea to the Makassar Strait in the west of Sulawesi and to Palu Bay (Paulik et al., 2019).

This particular tsunami has caused a total economic loss of 1.1 billion U.S. dollars (Goda et al., 2019), which leads to some questions regarding the reliability of tsunami early warning system in Indonesia. Even though after the Indian Ocean tsunami that hit Indonesia in 2004, a tsunami early warning system (Indonesian Tsunami Early Warning

of plate convergence / Formating

The frequency is a consequence. Not of high speeds.

Doesn't make much sense (the sentence)

System - Ina-TEWS) was built under the coordination of the Ministry of Research and Technology, and is operated by the Meteorology, Climatology and Geophysics Agency (BMKG) (Kurniasih et al., 2020), unfortunately, Ina-TEWS failed to detect the tsunami in 2018 in Palu, according to both media coverage and official statements from BMKG.

Built on this incident, it is relatively safe to say that Ina-TEWS is still not able to meet the desired expectations in minimizing the occurrence of casualties and losses due to the tsunami. Therefore, improvements are well-needed to prevent similar fatalities, especially regarding the available tsunami early warning system in Indonesia.

This thesis focuses on the numerical modeling of tsunami waves. It is essential to have an improved model of tsunamis which concentrates more towards the tsunami generation mechanisms. Consequently, authors propose a framework to the phenomenon of the tsunami wave and will highly be influenced by the tsunami in Palu 2018. There are many available data records and information from various sources which allow simulation with numerical modeling. Then, the result of this simulation will be ~~calibrated~~ by comparing it with the collected data from the true event.

MIRONE is the main software for this research which uses TINTOL (NSWING) code to perform numerical tsunami models that results in tsunami modeling of propagation and inundation (Luis, 2007). This wonderful software by Dr. Joaquim Luis is an open source code written in MATLABs 6.5 and its main purpose is to visualize and operate Generic Mapping Tools (GMT) Network Common Data Form (netCDF) grids. The Generic Mapping Tools (GMT) can be utilized for multiple purposes, such as geophysics, geodynamics, geodesy, oceanography, and so on (Wessel et al., 2019).

To realize that, this model uses the bathymetry grid taken from Badan Informasi Geospasial (Geospatial Information Agency) and the initial deformation from United States Geological Survey (USGS) will be identified by the Okada (1985) model. The calculation and simulation of the tsunami wave will produce important data such as wave height and travel time. These data are extremely useful in tsunami hazard evaluation and could definitely improve the available tsunami early warning system.



6 cm?  
That can never  
cause massive  
destruction

## 1.2 Research aims and hypotheses

The core aim for this study was to analyze the wave propagation of the Palu 2018 tsunami due to the interesting recorded wave height of 6 cm which then unfortunately caused a massive destruction with a wave height up to 11 m. Therefore, this would provide significant data for the government and scientific community which can improve tsunami early warning system and reduce future losses due to similar events. This can be elaborated into several methodological steps:

- a) Identify and understand the data needed to make a tsunami wave propagation simulation using NSWING code in MIRONE
- b) Identify and analyze the sensitivity of wave propagation simulation in Palu 2018
- c) Identify and analyze the gap of data received from another organization and the real event

Therefore, the project is focused on one main hypothesis:

- H1: Are earthquake properties (bathymetry, fault) sufficient to explain the recorded data and surveyed data of tsunami Palu 2018?

A favorable tsunami generation model can provide appropriate initial conditions for the following propagation model and the inundation model.

The preparation of the research requires direct and specific data and literature. The project uses both field data collection and computational modeling. The main data will be taken from Badan Informasi Geospasial (Geospatial Information Agency), United States Geological Survey (USGS), Badan Meteorologi, Klimatologi, dan Geofisika (Meteorology, Climatology, and Geophysics Agency) of Indonesia. Other than that, additional data might be able to be obtained from other literature. To process the data, MIRONE, open source software, will be further assessed to check the compatibility.

The result of the numerical computation is the tsunami travel times to many locations around the impacted area and the estimated maximum amplitude of the tsunami. In short, a proper tsunami generation model is able to deliver suitable initial conditions for the following propagation model and the inundation model. In result of the improvement on the accuracy of the initial condition, the tsunami early warning systems can be improved.

## 2. Case Study: Tsunami Palu 2018

### 2.1. Tsunami

#### 2.1.1. Description and causes

Tsunami comes from a Japanese word which consists of 2 kanji words which are, “Tsu” which means port and “Nami” which means wave. Therefore, it can be derived as big or high waves that hit the harbor/beach (Bryant, 2008; Roy, 2014). Tsunamis occur due to a sudden change or displacement of water masses triggered by changes in the vertical surface of the earth, tectonic earthquakes that have large strengths, landslides, seabed volcanic eruptions, and the result of falling meteors in the sea (Parker, 2010). The distribution of the cause of tsunamis in the Pacific Ocean region can be seen in Table 1 below.

**Table 1 Causes of tsunamis in the Pacific Ocean Region (2000 years period)**

Cause	Number of events	Percentage of events	Number of deaths	Percentage of deaths
Earthquakes	1,172	82.4%	620,796	89.7%
Unknown	121	8.5%	5,364	0.8%
Volcanic	65	4.6%	51,643	7.5%
Landslides	65	4.6%	14,661	2.1%
Total	1,423	100%	692,464	100%

Source: Intergovernmental Oceanographic Commission (1999), United Nations (2006), National Geophysical Data Center and World Data Center A for Solid Earth Geophysics (2007) in Bryant, 2008

*The data cannot add more complexity.*

In addition to that, the data from The National Geophysical Data Center website add more complexity to the cause of tsunami because these processes can work in combination with each other which further enhance the scales of the tsunamis, for example submarine landslides are often accompanied by large earthquakes as well as collapses of volcanic cones (Jinsong Xie, 2007).

2.1.2. Characteristics and Damages

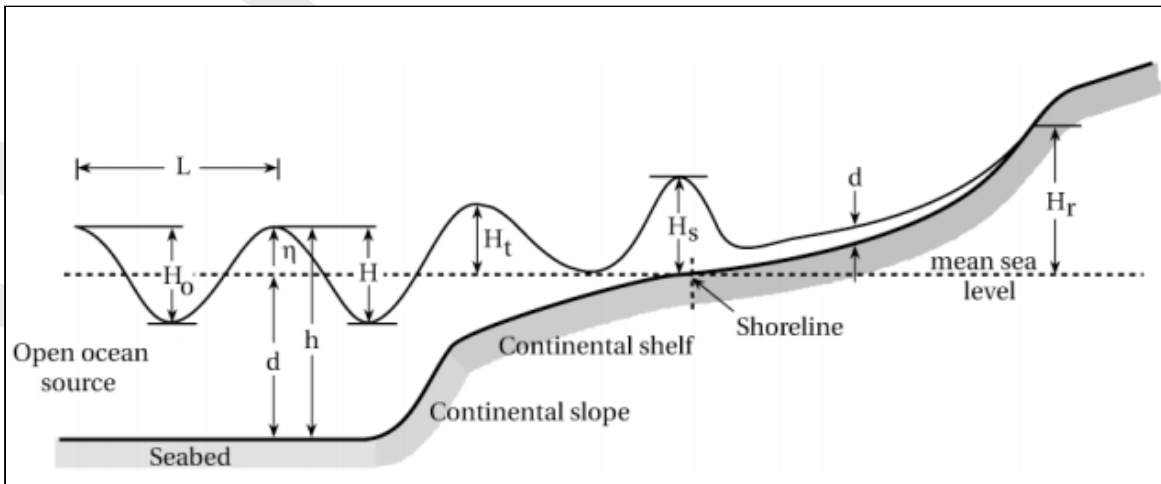
Tsunamis have specific characteristics that differentiate them from other waves (Jinsong Xie, 2007):

- Enormous energy
- Rapid propagation
- Mobile great trans-oceanic distances with little energy loss.

*this comes from where?*

*What tsunami?*  
Based on North East Atlantic and Mediterranean Tsunami Warning System (NEAMTWS), this local tsunami could reach a distance of  $< 400$  km. In addition, tsunamis of this type are generated by local earthquakes (or underwater landslides) which have an impact on a very limited area. However, this type of tsunami can still cause damage. In contrast, a distant (or transoceanic/basin) tsunami can reach the coast several hours after the trigger occurred at a very remote location. Tsunamis that occur throughout the ocean can impact the entire ocean and are caused by large earthquakes and reach distances  $> 400$  km. The tsunami in Aceh was a distant tsunami in the Indian Ocean and caused damage not only to Indonesia but also to Thailand, Malaysia, Sri Lanka, India and the coasts of East Africa.

*again*



Source: Bryant, 2008

Figure 1 Various tsunami wave heights

Each tsunami case has various and different wave characteristics but in most cases, tsunami has a period over four to six hours starting from initial wave. Each tsunami window

*4-6 hours? No. ~ 20 min.*

has different wave velocity based on the depth, as seen in Figure 1, which are (Bryant, 2008):

1.  $H_o$  (deepest part of ocean) = 600 – 900 km/h
2.  $H_t$  (continental shelf) = 100 – 300 km/h
3.  $H_s$  (shore) = around 36 km/h

Based on those characteristics, the wavelength of a tsunami is between 10 km and 500 km.

must be.

To be considered as a hazardous or significant tsunami, the amplitude of the wave when it reached the target is at least 0.5 m (Papadopoulos et al., 2014). Coastal features, namely reefs, bays, entrances to rivers, undersea features and the slope of the beach help modify the tsunami shape and energy which therefore can determine the size and impact of tsunami waves. Moreover, the shape of the earthquake's fault plays a big role when the earthquake is close to the epicenter. Different types of tsunamis can be distinguished according to their energy and distance before they reach the coast, which will be linked to their damaging effects as well. The wave-front of tsunami becomes rapid and bigger as it reaches the coast; can even reach a height of 20 meters or more. Some hydrodynamic features can increase and/or prolong the tsunami wave height with the right circumstances. The energy of an incident tsunami can be redistributed in time and space with the characteristics which differ from the original (incident) wave.

Typically, tsunami waves continue to move inland until the energy is finally degenerate through bottom friction, influence of obstacles, and/or increasing slope of the land (Xie, 2007). When the tsunami reaches land, it remains to push itself onward causing severe damage to anything in its path. The height of the generated wave itself is enough to destroy objects in its path, even enormous objects such as ships. Those objects could be carried inland and even for some cases, the harbors can be wiped out, meaning that tsunamis have abundant potential that would first erode the coastal vegetation and then crush homes and other coastal structures. These would add debris to the tsunami waves and act as the added cause of death and damage. The damage caused by previous tsunami events can be seen in Table 2.

The shape? What do you mean?

Not correct

No need to exaggerate.

Then, its wavy nature pull it back

It moves inland during 1/2 period.

Table 2 Damage caused by tsunamis

Tsunami event	Location	Method	Frame	Number of building
Multiple events	Various (Matsutomi and Harada, 2010)	Field survey	Wood, concrete block, RC	-
Indian Ocean tsunami, 2004	Southern Thailand (Suppari, et. al., 2011) Banda Aceh, Indonesia (Valencia, et. al., 2011) Sri Lanka (Murao and Nakazato, 2010)	Field survey  Field survey and satellite imagery Field survey	Wood RC with brick wall Wood RC with brick wall  Non solid Solid	20 120  161 from fielded survey and 2576 from satellite imagery 1202 333
Java tsunami, 2006	South Java, Indonesia (Reese, et. al., 2007)	Field survey	Wood/bamboo, brick (traditional/ with RC column), RC with brick wall	-
South Pacific tsunami, 2009	American Samoa and Samoa (Reese, et. al., 2011)	Field survey	Wood Masonry RC	24 135 16
East Japan tsunami, 2011	Miyagi Prefecture, Japan (Suppari, et. al., 2012c)	Field survey	Wood	150

Source: Suppasri et al., 2013

### 2.1.3. Generation Mechanism

In general most tsunamis will undergo these stages (André & Conde, 2012; Chenan et al., 2010):

#### 1. Generation

The first stage happened in the seabed, where it is deformed and caused the water to be vertically displaced. This is why earthquake tsunamis are the most destructive compared to volcanic ones. In this stage, period of a tsunami can range from 5

Now is 2h.

When is this number coming from?

minutes to 2 hours and the wavelength can be as high as 500 km and tsunamis will always behave as shallow water waves due to the ratio between the wavelength and the depth of the ocean is over 20, which follows the shallow-water equations.

The velocity of a shallow-water wave:

$$v = \sqrt{g \cdot h} \text{ (Eq. 1)}$$

g: gravity (9.8 m/s<sup>2</sup>)

h: depth of the water column

As mentioned in the previous part, in deep sea tsunami will propagate at high speed, for example in the Pacific Ocean, where the average depth is approximately 4000 m, the velocity of a tsunami in this water mass could reach 200 m/s.

km/h to be consistent

## 2. Split

Once the wave is generated, the wave will split into two directions, one leads to open sea and another one leads to the coastal area. The tsunami wave's speed depends on its water depth; therefore the open sea (distant) tsunami is faster than the coastal tsunami.

## 3. Amplification

For coastal tsunami (local tsunami) the speed decreases fast due to the decrease in depth, and this leads to a significant increase in wave height. This consequence is also known as **shoaling**. The small wave height (which is around 0.3 m in the deep sea) could be intensified to several meters. This can be seen in the equation where the wave energy density  $E$ , the amplitude  $A$ , and the wavelength  $\lambda$

$$E \propto A^2 \lambda \propto A^2 v \propto A^2 \sqrt{g h} \text{ (Eq. 2)}$$

if  $A$  and  $E$  remain constant,

$$A \propto \frac{1}{\sqrt{h}} \text{ (Eq. 3)}$$

Need to format better the equations

From the equation, it can be calculated that a 1 m high wave at 1000 m depth could reach 5.62 m at 1 m depth.

## 4. Run-up (could also be drawback)

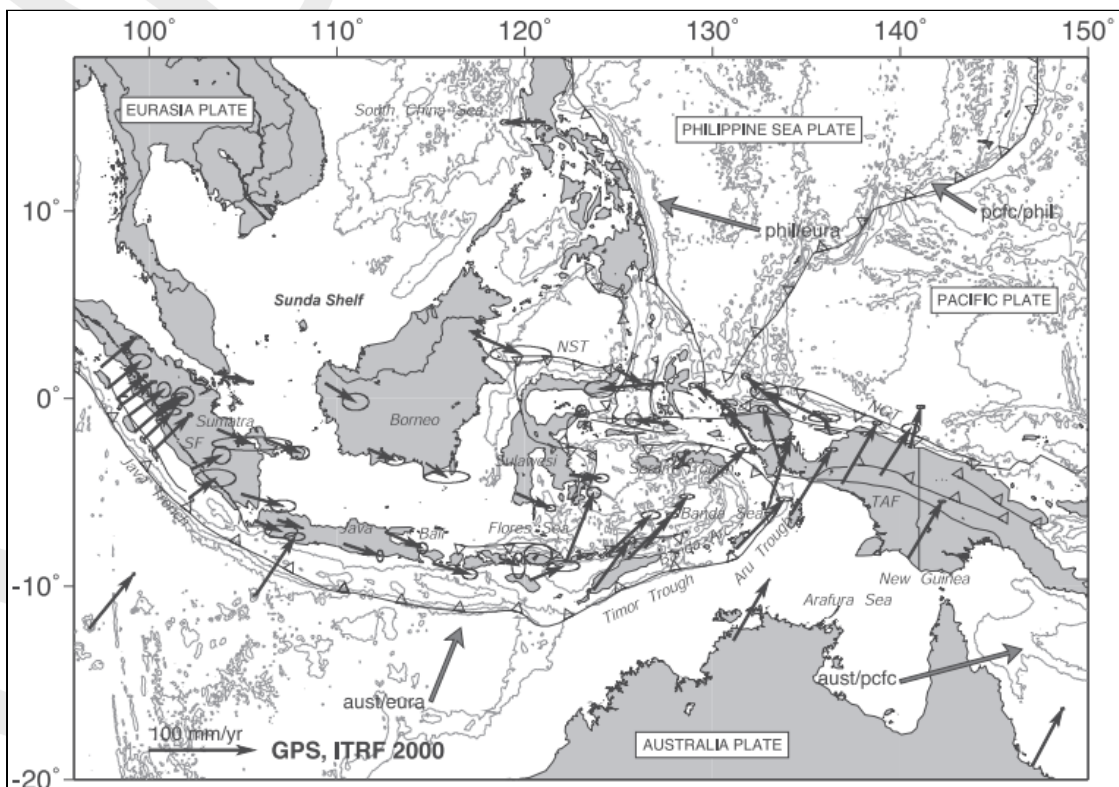
This stage represents the wave that approached the coastal area and is higher than average wave height. Either run-up or drawback could happen depend on where the first part tsunami reaches. If the tsunami wave reaches the trough first, then, the drawback would happen instead of run-up. It also happen when the coast is on the side of the tectonic plate below is below the other adjacent plate.

rephrase

rewrite

#### 2.1.4. Tsunamis in Indonesia

Indonesia is a country traversed by three active tectonic plates in the world, namely the Eurasian plate, the Australian plate and the Pacific plate as seen in Figure 2. This location therefore makes Indonesia one of the countries with the highest number of volcano eruptions and earthquakes. Around 25% of the volcanoes are located in the Sunda Banda arc and there are at least 9 volcano induced tsunamis in Indonesia. In addition to that, Indonesia has many active faults which are located near the subduction zone or seismic zone. The subduction zone can be referred as a prone to earthquakes area (Bock, 2003).



Source: Bock, 2003

**Figure 2 Topographic and tectonic map of the Indonesian archipelago and surrounding region**

This condition often leads to geological disasters that can trigger tsunami generation. National Board for Disaster Management (BNPB) recorded about 3810 geological disasters over the period of 10 years (2005-2015) (Kurniasih et al., 2020). These disasters include earthquakes, tsunamis, volcanic eruptions, and landslides and represents



Earthquakes with magnitude  $\geq 5$ , do not produce tsunamis. Page 18

approximately 22% of the total natural disasters. There are around 460 earthquakes every year with the magnitude of  $\geq 4.0$  which could trigger tsunami (HAMZAH et al., 2000). There are 246 tsunamis recorded in Indonesia, with 10 tsunami events that caused casualties of more than 100 people. Dominating with 90%, the trigger of tsunamis in Indonesia is by earthquakes, followed by around 9% by volcanoes and lastly 1% by landslide (Triyono et al., 2018). Although based on the number of occurrences, geological disasters are not as common compared to other natural disasters, however, based on the resulting impacts, geological disasters would cause more significant impacts (Amri et al., 2016 in Kurniasih et al., 2020).

Due to tsunami, the average number of economic loss is approximately 71 trillion rupiah and the average number of threatened people is approximately 4 million (Amri et al., 2016 in Kurniasih et al., 2020). Since the number of population in Indonesia keeps increasing, it is quite certain that the number of people who are in danger of the tsunami will also increase. The data shows the high number of casualties in the earthquake and tsunami that occurred in the waters of the Sunda Strait and Sulawesi in 2018.

### 2.1.5. Indonesian Tsunami Early Warning System (Ina-TEWS)

One of the biggest tsunami that occurred in Indonesia is the Indian Ocean tsunami 2004. After the Indian Ocean tsunami, Indonesia has built a tsunami early warning system (Indonesian Tsunami Early Warning System - Ina-TEWS) under the Ministry of Research and Technology, and is operated by the Meteorology, Climatology and Geophysics Agency (BMKG). Ina-TEWS is then being evaluated by the joint rapid assessment team on the famous tsunami and several other later tsunamis, one of them is Aceh tsunami which happened on 11 April 2012. According to the team, the devices such as sirens didn't work properly even though the warning has been issued by the BMKG. Therefore, the sirens had to be manually activated 10 minutes after the warning; but some of them even couldn't be activated. Evaluation of the system shows that the tsunami buoy in Aceh waters is completely damaged so that it cannot detect sea level differences (Kurniasih et al., 2020).

The tide gauge instrument was delayed by approximately 15 minutes. Although in the end the earthquake only triggered a small tsunami and it didn't cause casualties, the results of the evaluation show that the early warning system has not been running well (Joint Rapid

what does this mean?



Assessment Team, 2012 in Kurniasih et al., 2020). Based on media coverage and BMKG statements, the tsunami early warning system failed to detect the tsunami in 2018 in Palu causing many casualties. In addition, verification of the incident in Palu could not be carried out because there was no working telephone line in Palu shortly after the earthquake.

Seeing these incidents, Ina-TEWS is considered unable to meet the desired expectations in minimizing the incidence of casualties and losses due to the tsunami.

## 2.2. Event of Interest: Tsunami Palu 2018

The 2018 Sulawesi tsunami was simply the most shocking tsunami since the 2004 Indian Ocean tsunami. A shocking Mw 7.5 Sulawesi earthquake occurred in Palu, Indonesia on Friday, 28 September 2018 at 18:02:44 local time (GMT + 8). The epicenter was detected at  $-0.22^{\circ}$  S and  $119.85^{\circ}$  E at a depth of 10 and 27 km northeast of Donggala City (BMKG, 2018 in Widiyanto et al., 2019). The earthquake was followed by a series of tsunami waves. The biggest impact of the tsunami hit Palu City and Donggala Regency. Furthermore, low-amplitude tsunami waves were also identified in Mamuju, a city overlooking the Makassar Strait and outside Palu Bay. The tsunami hit the coast, houses, various objects and washed out the coastal area of Palu Bay, Central Sulawesi Province (Widiyanto et al., 2019a).

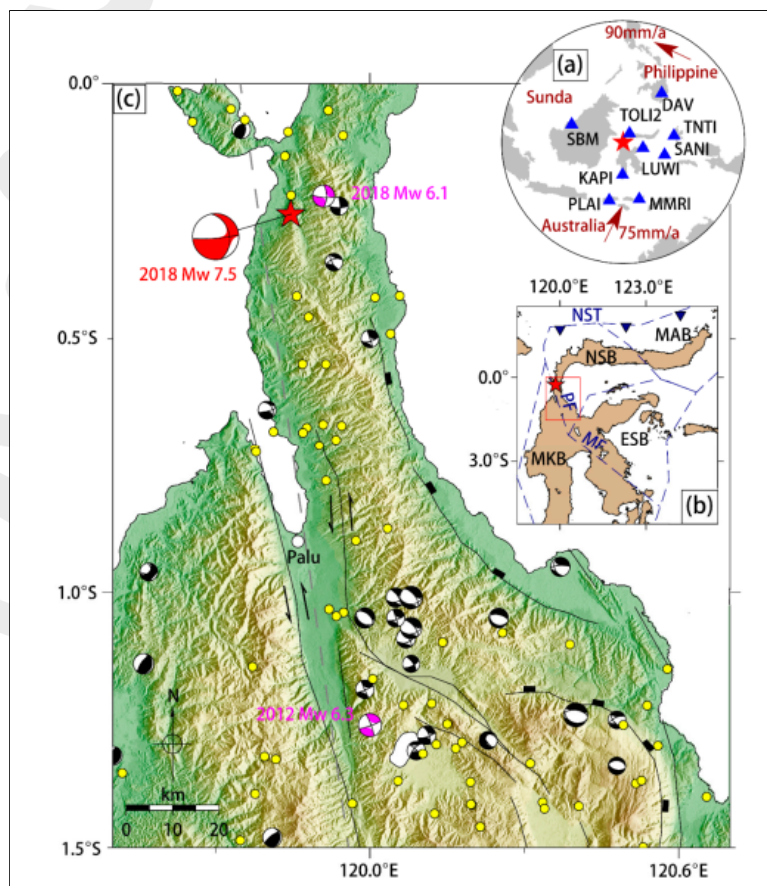
The earthquake was a supershear strike-slip earthquake with a rupture velocity of 4.1 km/s which was situated in Palu-Koro strikeslip fault, which has been determined by several sources: CPPT (Centre Polynésien de Prévention des Tsunamis, the French Polynesia Tsunami Warning Center), USGS (US Geological Survey), GFZ (GeoForschungsZentrum, German Research Centre for Geosciences), IPGP (Institut de Physique du Globe de Paris, Institute of Earth Physics of Paris), gCMT (the global Centroid Moment Tensor catalog) (Fang et al., 2018). In addition, the hypocenter depths were shallow, approximately at 10-22 km (Sotiris Valkaniotis et al., 2018). As seen in Figure 3, Palu-Koro strike-slip fault goes offshore over the Palu Bay to the north part of Sulawesi, linked with the North Sulawesi trench and extends to the south direction with the Matano fault in the southeast. Even though the zone is seismically active, the seismic level of Palu-Koro fault is relatively low, which has a recurrence interval of around 700 years for Mw ~7-8

Was it? And the Japan 2011

Fig. 3  
reference

But with a recurrence of ~700 years it cannot be that high!

earthquakes (Bellier et al., 2001). Due to its active structures, Palu–Koro fault potentially gives a great seismic hazard in the Sulawesi region (Bao et al., 2019), which therefore, a strong earthquake is expected on this fault. At the location of the earthquake, the Sunda plate moves south with respect to Molucca Sea plate at a velocity of about 30-40 mm/year (Sotiris Valkaniotis et al., 2018). Although before the large earthquake, there was a series of small-to-moderate sized earthquakes over the hours. The USGS identified four other earthquakes which have a magnitude of  $M=4.9$  and larger around the epicentral area. It began with an  $M=6.1$  earthquake three hours earlier at the south of the main  $M=7.5$  earthquake. There was also an aftershock sequence in the first five days following this earthquake which is a total of 40 events with magnitudes of  $M=4.4$  and larger. The largest aftershock in this time-frame was  $M=5.8$ , about 12 minutes after the  $M=7.5$  earthquake (Sotiris Valkaniotis et al., 2018).



Source: Fang et al. (2018)

Figure 3 Tectonic setting of the 2018 Mw 7.5 Palu earthquake

Legend:

(a) Dark red arrows: the convergent rates between the Philippine Sea, Australian, and Sunda plates.

Red star: the epicenter of the 2018 Palu earthquake.

Blue triangles: the broadband regional stations used in this study.

(b) Microblock model of Sulawesi with the block boundaries depicted by dark blue dashed lines (modified from Wang et al. [4]). Red rectangle outlines the bounds of the panel (c). PF, Palu–Koro fault; MF, Matano fault; NST, North Sulawesi trench; NSB, North Sulawesi block; MAB, Manado block; ESB, East Sulawesi block; MKB, Makassar block.

(c) Close-up of the epicenter region. The white circle shows the location of the city of Palu. The focal mechanism plotted in red represents the 2018 Mw 7.5 Palu earthquake. The magenta ones denote the 2018 Mw 6.1 foreshock and the 2012 Mw 6.3 earthquake. The black ones denote the  $M_w \geq 5.5$  historical earthquakes. The yellow dots are the aftershocks within nearly four months following the 2018 Palu earthquake. All the focal mechanisms are from the global centroid moment tensor (gCMT) solution. The gray dashed line depicts the fault trace used in the joint inversion. Black lines denote the regional fault traces, with the fault mechanism shown as well.

Where?

The timeline for the event of September 28, 2018 is retrieved from the information published in the official website of BMKG and also from UNESCO/IOC (2019):

- 07.00 UTC: First earthquake (fore shock) occurred ( $M=6.1$ )
- 10.02 UTC: First strong earthquake (main shock) occurred ( $M=7.5$ )
- 10.06 UTC: First tsunami wave during the first earthquake
- 10.07 UTC: BMKG issued a potential tsunami statement. BMKG has activated tsunami early warning with 'ALERT' status (high potential tsunami 0.5 - 3 meters) on the western Donggala coast, and 'WASPADA' status (tsunami potential height of less than 0.5 meters) on northern Donggala coast, northern Mamuju and West Palu City.
- 10.10 UTC: Second tsunami wave
- 10.27 UTC: 6 cm change in sea level rise recorded at tide gauge in Mamuju
- 10.36 UTC: Based on the observation of the 6 cm height change from the updated data and due to earthquake source mechanism with strike type was assumed wouldn't cause tsunami, the Tsunami Early Warning (Peringatan Dini Tsunami - PDT) was ended.

07:00?

Where!

Map?

Therefore in total, the warning only lasted for half an hour and it didn't even reach the residents.

**2.2.1. Recorded Data**

The main recorded data during this event is the tide gauge data. A tide gauge is used to continuously measure the sea level change in respect to a vertical datum by recording the water height (Khare et al., 2019). There are two tide gauge stations that could be used as a reference: Mamuju and Pantoloan tide gauges. Unfortunately, at that time the is the only source of data came from Mamuju tide gauge because the Pantoloan tide gauge was inactive based on the press release from the Meteorology, Climatology, and Geophysical

phrase.

The press release inactivated it?

Agency of Indonesia (BMKG) No: UM.505/9/D3/IX/2018 and statement from BMKG in Kompas, Tuesday, 02 Oct 2018, p.2.

Mamuju tide gauge is located at Mamuju City, West Sulawesi. To be more exact, the coordinate for this tide gauge is Lat/Lon: -2.666982 / 118.893349. For the tsunami event, the tide gauge recorded that the tsunami wave arrived ~~after~~ 18 min after the earthquake. Makassar Strait, which connects the earthquake epicenter with Mamuju City, has a ~~moderate~~ depth of approximately 2000 m. Therefore, a tsunami traveling with an estimated speed of 250 km/h requires at least 1 h to travel the length of Makassar Strait at a speed of 250 km/h. Together, these facts indicate the tsunami that generated the signal at Mamuju tide station was not due to the aforementioned strike-slip earthquake but had a source close to the Mamuju tidal station inside Palu bay.

Then, the results of the tide gauge observations in Mamuju was also observed, it was visible that there was a change in sea level rise as high as 6 cm at 17:27 WIB (See Figure 4).

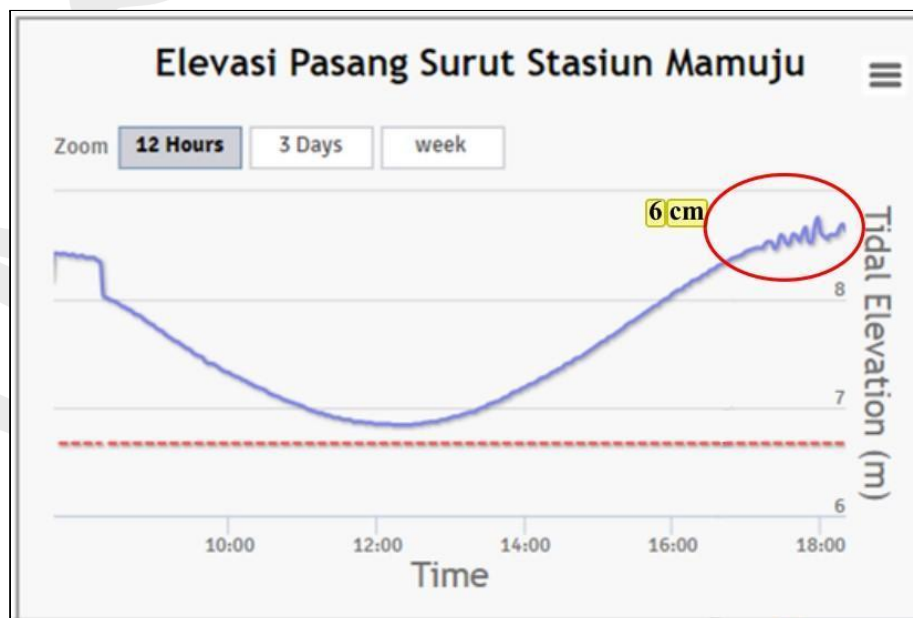


Figure 4 Tide Gauge Mamuju Result

Based on the earthquake source mechanism which is strike slip and the results of observations of tsunami wave heights in Mamuju tide gauge, also noticing that the

estimated time of tsunami arrival has passed, the Tsunami Early Warning (PDT) is ended at 17.36.12 WIB (UNDRR and UNESCO/IOC, 2019).

### 2.2.2. Survey Data

The result of immediate field surveys of the impacted areas after the earthquake discovered that the local tsunami reached 10 m wave height above sea level around Palu Bay (Muhari et al. 2018 in Widiyanto et al., 2019). After that, the Meteorology, Climatology, and Geophysical Agency (Indonesian: Badan Meteorologi, Klimatologi, dan Geofisika, abbreviated BMKG) released a survey report which stated that the maximum wave height was 11.3 m (Pribadi et al., 2018). The main impacted area of the September 2018 tsunami is Palu Bay on Sulawesi Island, and Central Sulawesi Province. Although the epicenter was at the further border of Palu Bay, interestingly, the most severe damage happened in Palu City. This area is located about 70 km from the epicenter which is at the end of the bay. This city is the capital of Central Sulawesi Province, has a population of around 380 000 people. Additionally, the disaster area also included Donggala Regency, and Sigi District. Although Sigi Regency did not suffer loss from the tsunami, but large-scale liquefaction led to a significant number of deaths and disappearances in this area. As of February 2019, the number of deaths/missing and injured exceeded 4,340 and 4,438, respectively. The number of buildings damaged is greater than 68,451, and the total economic loss of the event was estimated at 1.1 billion U.S. dollars (PuSGen, 2018).

TTT of hour of TTT  
It wasn't > 1 hour of TTT  
at 250 km/hr?

### 2.2.3. Initial conclusion

This particular event surprised the society, especially the scientific community. This type of fault commonly does not cause significant deformation that could trigger a huge tsunami because the plates move horizontally. This caused two different opinions, on one hand Ulrich (2019) considers that a cause related to earthquake displacements is probable and that land sliding maybe not the main source of the tsunami. On the other hand, Takagi et al. (2019) concludes that landslides produced the tsunami.

Due to that peculiarity, it is quite understandable to see the response of the Meteorology, Climatology, and Geophysical Agency of Indonesia. During the event, immediately after the initial earthquake (at 18:02 local time) the BMKG issued a tsunami warning showing possible wave heights of 0.5 to 3 m for coastal areas, including Sulawesi Island (the warning was subsequently lifted at 18:39 local time). However, a newspaper article

(Suroyo and Ungku, 2018 in Harnantyarı et al., 2019) reported that no one received any warnings nor heard sirens during the disaster, although, the possibility that the power transmission lines were damaged due to the earthquake could be considered. Then, the tsunamis reached coastal areas within several minutes after the earthquake (Takagi et al., 2019).



### 3. Methodology

This chapter will first describe the workflow of this research. There are several steps that need to be carried out due to a realization that the model has to achieve the best fitting result compared to the recorded data and the real event data. In addition, this chapter will also elaborate how the model was selected.

#### 3.1. Workflow

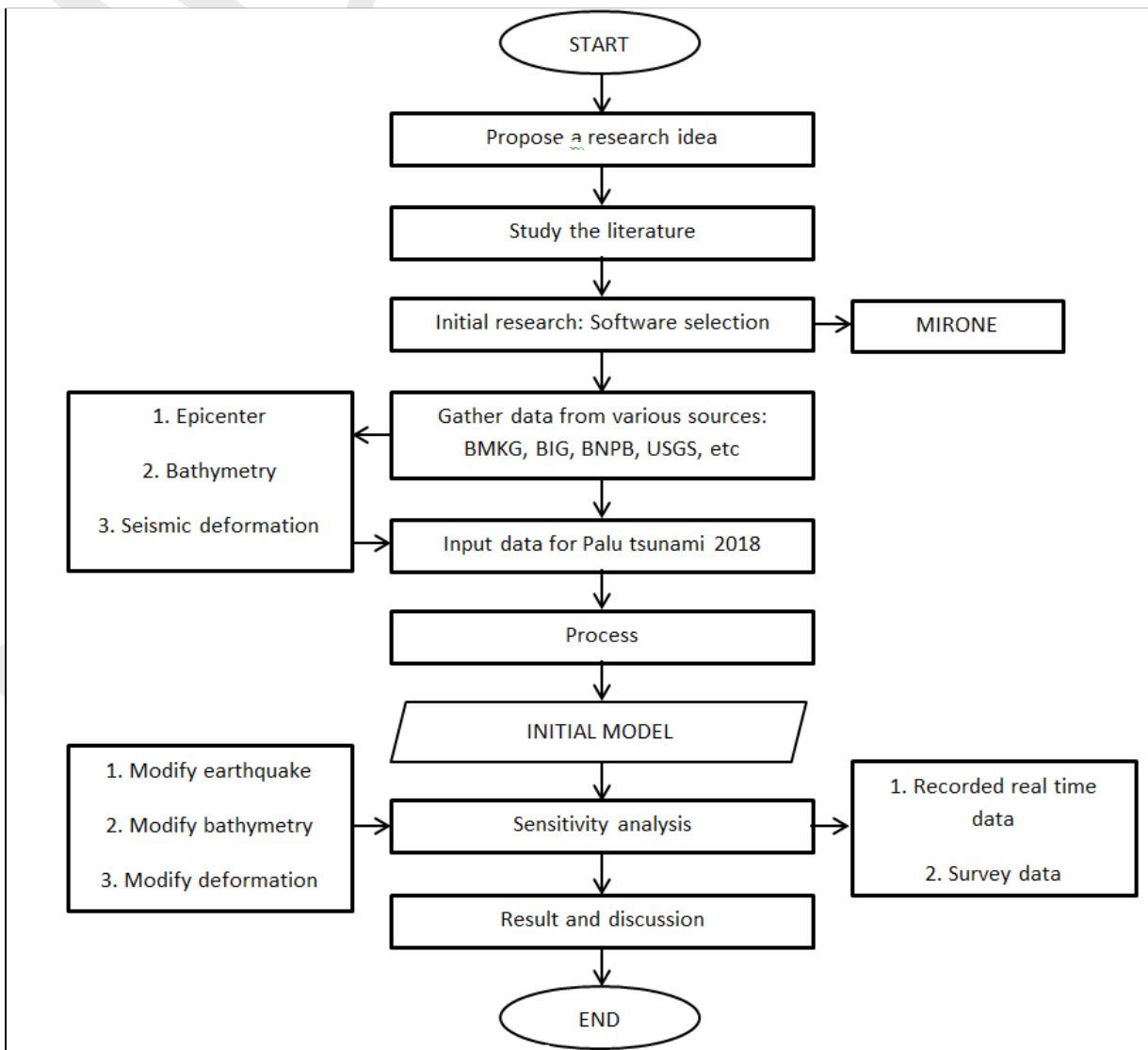


Figure 5 Workflow



### 3.2. Model Selection

There are numerous ways to derive shallow water equations, assuming that the flow is vertically hydrostatic (vertical acceleration of water particles is insignificant). Maximum tsunami height, commonly several hours after the first arrival, can result from reflection at a coast or resonance within a bay, based on bathymetry and local coastal shape.

To make sure that the results bear a resemblance to the real situation, there are several safety measures as shown below are used for the shallow water models (Jinsong Xie, 2007):

1. The wave length for propagation has to be 40 times longer than the depth of deep ocean. *The  $\lambda$  is the earthquake that determines*
2. The period for propagation can't be too short. It has to be longer than 15 minutes.
3. The slope for flooding has to be bigger than 2%. *???*
4. The period for flooding can't be too short. It has to be longer than 10 minutes
5. The wave source must have a length that is 10 times its depth.
6. The period for run-up can't be too short. It has to be longer than 15 minutes.

*→ Sorry, nothing of this makes really sense.*

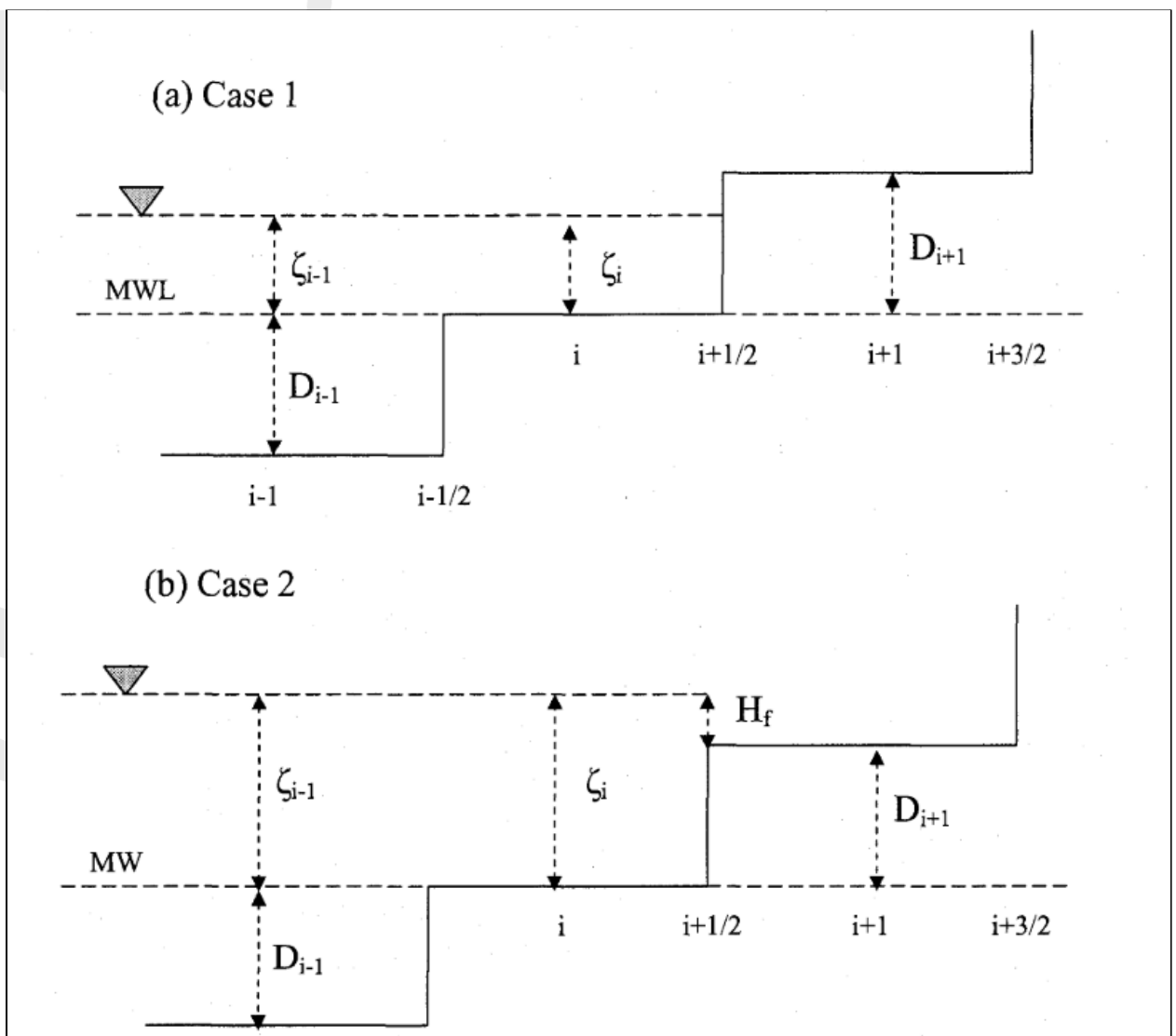
For tsunami modeling, the mathematical problems are caused by the various spatial scales of flows. On one hand, for the deep ocean, tsunami wavelengths are frequently around several hundred kilometers, which would require a large computational domain. On the other hand, in the near shore region, tsunami energy is compressed and focused by bathymetry that could be unpredictable that would require smaller grid spacing that is orders of magnitude. Due to this problem, mathematical model have to be able to model global propagation as well as local inundation simultaneously. Based on the above analysis, and considering the planetary ocean bathymetry and topography as an example, at least five aspects must be taken into account (Jinsong Xie, 2007):

#### 1. Boundary conditions

Suitable boundary conditions have to be identified in order to obtain solutions of the wave propagation over a fixed domain. The horizontal velocity normal to the wall is always zero for a vertical wall that is faultlessly reflective. However for the near shore areas, the boundaries consist of dry and wet points. The dry points represent the coastal area, where the normal velocity is set to zero. Then, due to run-up or run-down, the new wet and dry points is possibly created even with the large space step. Therefore, a mathematical system for both wetting and drying need to be available. The main parameter to see the



presence of wet or dry points is the total depth expressed with  $d = \text{ocean depth } (D) + \text{sea level } (\zeta) - \text{bottom displacement } (\eta)$  (Flather et al. and Heaps et al. (1975); Imamura et al. (1996) in Jinsong Xie (2007)). The wet and dry points are found by setting the average undisturbed ocean depth as positive values (wet points) and elevations as the negative values (dry points). Therefore to simplify, the dry point would equal to total depth of 0 ( $D + \zeta = 0$ ). With the intention of diminishing the reflective wave in coastal areas, the vertical movable boundary should be set.



Source: Jinsong Xie (2007)

**Figure 6 Moving boundary example**

Moving boundary can be explained by Figure 6. As seen in both cases, the recorded grid points are:  $i-1$ ,  $i-1/2$ ,  $i$ ,  $i+1/2$ ,  $i+1$  and lastly  $i+3/2$ . Total depths ( $h$ ) are recorded at  $i-1$ ,  $i$  and

$i+1$ , meanwhile the flux are recorded at  $i-1/2$ ,  $i+1/2$ , and  $i+3/2$ . In Case 1, the  $i$  cell is wet since the depth is negative and the fluxes at  $i+1/2$  are 0. Then, if the same cell ( $i$ ) is examined in Case 2, it is clear that the depth in  $i$  cell is positive, therefore the fluxes at  $i+1/2$  can't be 0. This means that the shoreline is somewhere between  $i$  and  $i+1/2$ .

In order to create a quick computing process, the areas that characterize permanent dry (such as land) are excluded from the computation by fixing a limit for the depth. Furthermore, the connected bottom friction becomes very large when  $H$  is very small, so a lower value of the water depth is applied in order to avoid problems. The estimated difference is fixed for the continuity equation. This fixed value would later be applied for the total depth values that are available on every side of a computational grid. When the total depth for all sides on a grid cell is observed to be negative or zero, then the grid cell is considered as dry cell.

In addition, there is a problem that could occur since the typical tsunami modeling code carries out a linear extrapolation for a continuous boundary. The conditions for continuous boundary are built on the conservation of mass, where there is an equal value for the input and output of the boundary. Therefore, this code could be executed when the wave arrives simultaneously, but unfortunately if the wave that arrives is curved, a false wave could be created, that is known as reflective wave. MIRONE software could minimize this problem by using cosine curve. Once it's used on arrays, the water depth would be reduced and it would greatly affect the wave speed, since the speed is formulated by  $\sqrt{gh}$ . In result, the wave would have a very slow speed. Based on this fact, MIRONE builds an imaginary border where depth progressively decreased to zero. Ideally, if this is applied, the wave never reaches the border and therefore is not reflected. So far, boundary conditions have been successfully constructed in numerical models.

These are code details that may or may not be connect (don't remember)

Where is this coming from?

You are describing sponge borders.

2. Cyclic boundary condition  
Cyclic boundary condition for E-W velocity as well as for the sea level on the meridian is needed for the computational domain because the globe is spheroid and it's cut lengthwise the meridian longitude.

The latitude/longitude boundaries of custom grid in degrees and minutes (precision is to the nearest minute) must be chosen. In addition, there are several conditions that must be

???

NSWING does not do that (no need)

taken into account. These conditions require a strong understanding of both geography, which focused on topography and bathymetry:

- The value of grid: between  $0^\circ$  and  $180^\circ$ .
- The value of latitudes: from  $90^\circ$  North to  $90^\circ$  South.
- The value of longitude values: from  $180^\circ$  west to  $180^\circ$  east.
- If the grid is spanned the entire globe longitudinally (for the case of the ETOP02 Global Topography), the condition is a bound of  $180^\circ$ W to  $180^\circ$ E, or from  $0^\circ$ E to  $0^\circ$ E.

There is Antarctica at S-pole

Modeling can be done in cartesian coordinates as well!

### 3. Bottom friction and Coriolis force

Theoretically, the effect of both bottom friction and Coriolis force are examined by all numerical codes. However, the calculation domain is small in reality. Therefore, since the Coriolis force is considered as a secondary effect on tsunami waves, it is most likely to be ignored. But Kowalik et al. (2005) did a research on the 2004 Indian Ocean tsunami and included the Coriolis force to simulate the tsunami. The results showed that the Coriolis force has an important effect on the tsunami wave.

### 4. Model schemes

Model schemes are based on 3 discretization elements that have some advantages and disadvantages:

- Finite difference: finite difference algorithms are widely used in contemporary tsunami numerical models with upwind and downwind schemes; finite differences are the simplest to work with.
- Finite volume: finite volume offers the best stability and efficiency.
- Finite element algorithms: these models offer the best geometric flexibility.

What is efficiency?

### 5. Nested-grid schemes

There are some numerical difficulties related to simultaneously modeling global propagation and local inundation due to diverse flow regimes. Globe scale tsunami waves move throughout the entire area, which need various levels of modifications at different times and locations. Nested-grid schemes (adaptive mesh refinement) would give a possibility for a coarse grid to cover parts with no significant waves available on the domain. Higher level of modification is also possible with nested-grid schemes by the

Global?

They are not faster.

— ?

you read this in  
moving? Geoclaw?

application of an algorithm that could adjust the appearance of set moving sub-grids at any time. This would users to track waves' motion in deep ocean.

rewrite

The capabilities of various tsunami models are listed in Table 3. A good representation of accurate bathymetry must be spherical coordinate system to accurately project 3-D globe to 2-D map. If the plane coordinate system is used, the projection could be misrepresented.

This is wrong. Not all tsunamis are ocean wide. AMIGA to Australian code uses only UTM or Mercator grids.

Table 3 Characteristics of the current tsunami numerical models

Model Factor	LGW	COMCOT	SWAN	MIRONE	ZUNI	MOST	TSUN2	UAF
Generation	Y	Y	Y	Y	Y	Y	Y	Y
Propagation	Y	Y	Y	Y	Y	Y	Y	Y
Inundation	Y	Y	Y	Y	Y	Y	Y	Y
Wave theory	Airy	Airy	Airy	Airy	Stokes	Airy	Airy	Airy
Nonlinear	Linear	Linear	Non-linear	Nonlinear	Nonlinear	Nonlinear	Linear	Linear
Finite Difference	Y	Y	Y	Y	Y	Y	Y	Y
Coordinate System	Plane	Plane	Spherical	Spherical	Plane	Spherical	Spherical	Spherical
Coriolis	N	N	Y	Y	N	Y	Y	Y
Friction	Y	Y	Y	Y	N	Y	Y	Y
Surface Stress	N	N	N	N	N	N	N	N
Boundary Condition	bad	good	bad	bad	bad	better	good	better
Nested Grid	N	Y	Y	Y	Y	Y	Y	Y
Dispersion	N	N	N	N	Y	Y	Y	Y

\*'Y' = used; 'N' = not used, 'better' = perform better compared with all other models

Source: (Jinsong Xie, 2007)

### 3.3. Selected Model: MIRONE

The MIRONE software will be used to simulate tsunami propagation in this research. MIRONE is a MATLAB-based framework tool that could be accessed with Windows and it is a set of unified numerical codes intended for simulating tsunami generation, propagation and subsequent run-up onto the shoreline. It allows the display and manipulation of a huge number of grids format by its interface with GDAL library. Furthermore, the equations were expressed in spherical polar coordinates which are great for the purpose of simulating the tsunami generation and propagation. The main purpose of that is to create a graphical

and Cartesian.

and cartesian.

Bad?? NSWING  
VMS name BC  
as COMCOT.

interface that would be easy to use. However, it also suffers from important limitations, such as speed and memory consumption (Luis, 2007).

what? It has many drawbacks but not there.

MIRONE software embedded numerical code NSWING which stands for Non-linear Shallow Water Model with Nested Grids to model the tsunami (Miranda et al., 2015) which is highly motivated by Liu et al., 1998 (Miranda et al., 2015). NSWING works with a system of nested grids which can solve shallow water equations for both linear and nonlinear expressions. For the nonlinear expressions, it utilizes an upwind scheme and for the linear expressions, it utilizes an advanced leapfrog numerical scheme. In addition, NSWING employs a radiating boundary condition which is based on "wet" and "dry" cells, and allows NSWING to track shoreline movement during inundation. This further allows wave motion to move from one area to another with minimal reflections (Wronna, 2015). In addition, the deformation in this model is rendered by Okada, 1985 theory in the seabed (Luis, 2007).

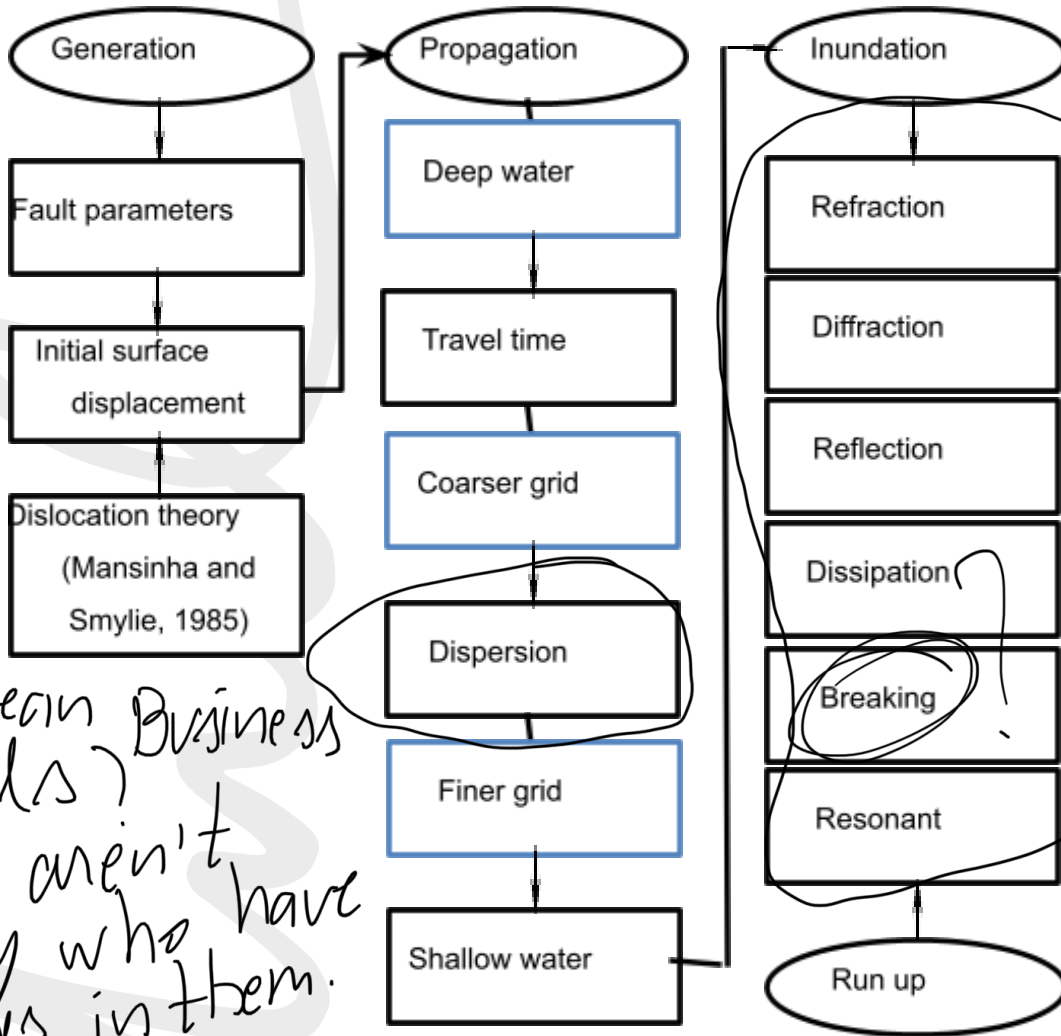
MIRONE implement the TSUNAMI N2 in order to model shoaling, flooding and coastal amplification of the tsunami waves. While NSWING and TSUNAMI N2 are two completely separate models, both can simulate tsunami generation, propagation and inundation. These two models are combined with their own role. NSWING is for the propagation model and TSUNAMI N2 is for the inundation model (Jinsong Xie, 2007).

Lastly, the steps for this project can be seen below. The steps are encouraged by a research done by Jinsong Xie (2007):

1. Obtain the fault parameters and the bathymetry
2. Use the MIRONE software, obtain the initial surface displacement
3. Obtain the initial tsunami simulation
4. Do sensitivity analysis with multiple parameters.
5. Compare the results from the calibrated MIRONE models with observations to see whether the model truly represent the event.

I have told since the beginning that we do NOT calibrate the models.

This is FALSE. TSUNAMI N2 was a older code that was abandoned NSWING does NOT use TSUNAMI N2 anywhere. Where did you see this?



Why is this in a workflow? Users do not control this.

You mean Business models? There aren't many who have Business in them.  
Source: Jinsong Xie (2007)

Figure 7 Flowchart of numerical modeling procedure

## 4. Initial Model

In this chapter, I will discuss the initial model of tsunami Palu 2018. The initial model serves a purpose to see the range of the tsunami wave using the available data that will be explained below.

### 4.1. Process

The process of creating initial model involves several data and steps. The data needed are: bathymetry map and seismic elastic deformation. Then, this data will be processed by the selected software, MIRONÉ.

The generation of tsunami because of an earthquake, the commonly applied theory is the dislocation theory developed by Mansinha and Smylie in 1971.

#### 4.1.1. Bathymetry Map

The bathymetry data that will be used in this initial model is the data in Sulawesi, Java, and some part of Borneo Island. The reason why a wide area is used in this model is to see how far the tsunami wave will initially grow. There are two bathymetry data that are taken as consideration for the initial model. Both are open source from different sources with different resolution which has their own pros and cons. The two data used are: GEBCO 2020 grid and National bathymetry (Batimetri Nasional – BATNAS).

##### 1. GEBCO 2020 grid

The GEBCO 2020 Grid provided by the General Bathymetric Chart of the Oceans (GEBCO) and it is labeled as the latest global bathymetric product. This bathymetry data can be accessed openly and is available at <https://download.gebco.net/>. It has a total of 3,732,480,000 data points, divided in 43200 rows x 86400 columns. The resolution delivered by GEBCO\_2020 is 15 arc-second (GEBCO Bathymetric Compilation Group 2020, 2020).

As seen from Figure 8, the GEBCO 2020 bathymetry data can be obtained by selecting an area in the map. Therefore, in order to know the initial impact of the initial tsunami model, there are several tiles that need to be obtained. I decided to focus on the whole Sulawesi and Java islands including islands around them, and parts of Kalimantan and Papua.

grid

expand?

This is not the resolution (with is much worse)  
It is the grid step. grid step and resolution are two different things.



Once all the GEBCO 2020 bathymetry data for the desired area was selected, the data is later downloaded as \*.tiff and file \*.grd and it can be loaded in MIRONE. (Figure 9).

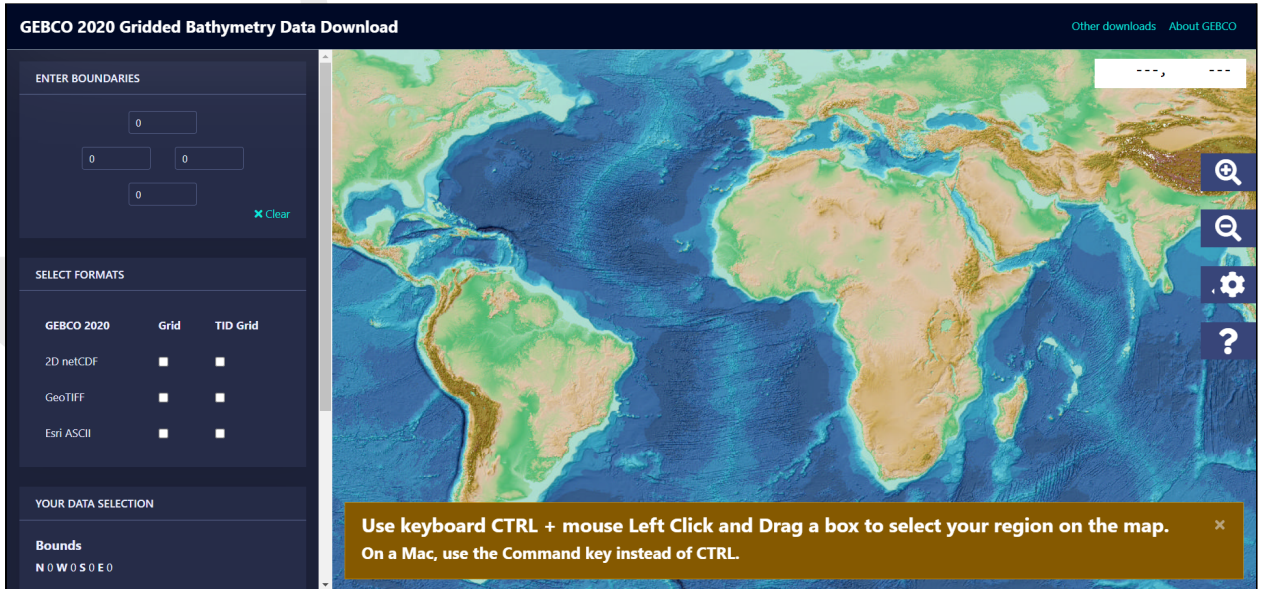


Figure 8 Obtaining GEBCO Bathymetry



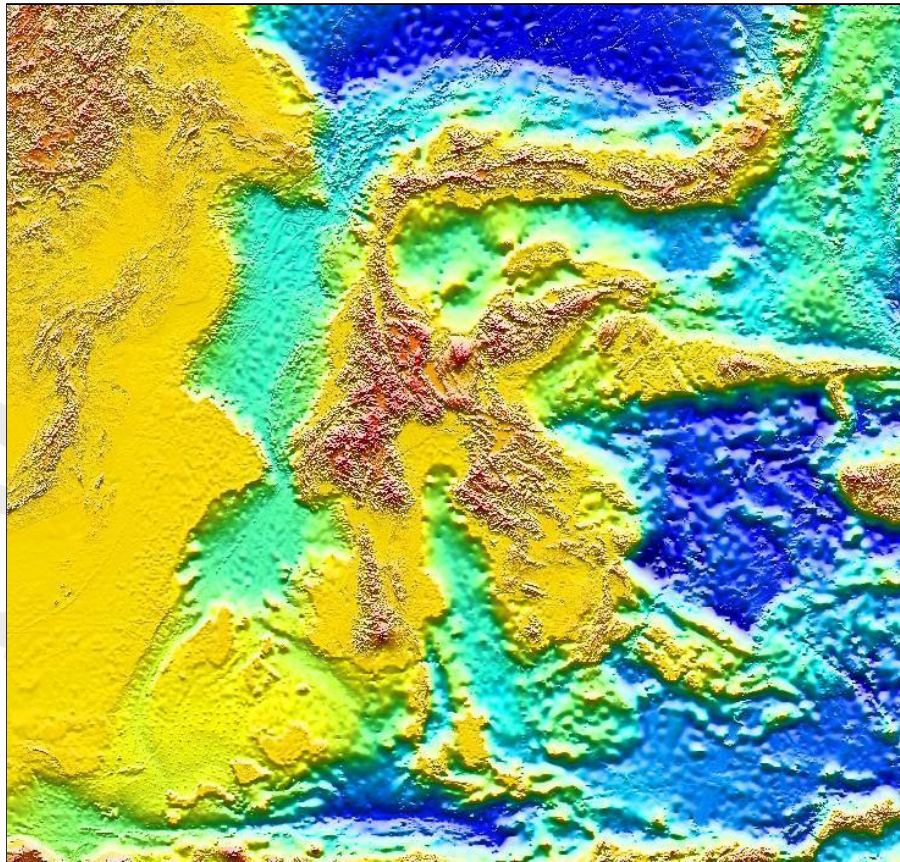
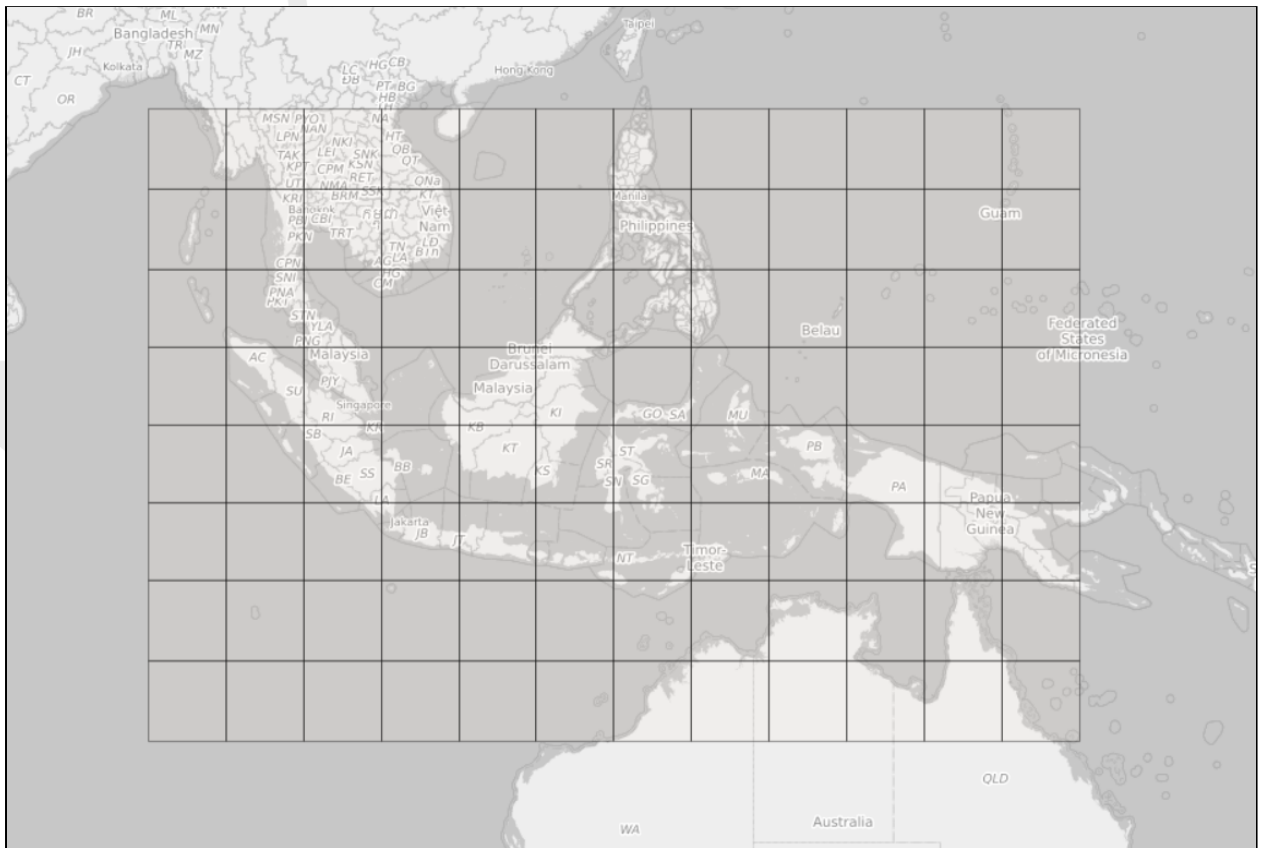


Figure 9 Loaded GEBCO Bathymetry in MIRONE

## 2. National bathymetry (Batimetri Nasional – BATNAS)

Geospatial Information Agency (Indonesian: Badan Informasi Geospasial, abbreviation: BIG) and can be accessed openly. To access the data, user has to create an account in <http://tides.big.go.id/DEMNAS/login.php>. Then, a wide range of Indonesian bathymetry data can be obtained directly which is easily accessible, as seen in Figure 10.

→ All figures MUST have coordinates, and color scale.



**Figure 10 Obtaining National Bathymetry (BATNAS)**

Source: <http://tides.big.go.id/BATNAS/>

National bathymetry (Batimetri Nasional – BATNAS) data is created from the results of inversion of gravity anomaly data from altimetry data processing by adding sounding data carried out by multiple institutions, such as Geospatial Information Agency (BIG), National Geophysical Data Center (NGDC), The Agency for the Assessment and Application of Technology (BPPT), Indonesian Institute of Sciences (LIPI), and others with single or multibeam surveys. The spatial resolution of the national bathymetry data is 6arc-second using the MSL datum.

National bathymetry with a resolution of 30 s and has a scope of area from 90 to 150 East Longitude and from 20 South latitude to 20 North latitude.

As seen from Figure 9, the national bathymetry data can be obtained in in small tiles. Therefore, in order to know the initial impact of the initial tsunami model, there are several squared areas that need to be obtained. I decided to focus on the whole Sulawesi and Java islands including islands around them, and parts of Kalimantan and Papua. Once all



the national bathymetry data from the desired areas were obtained, the data is later combined in QGIS as one \*.tiff file and it can be loaded in MIRONE. (Figure 11)

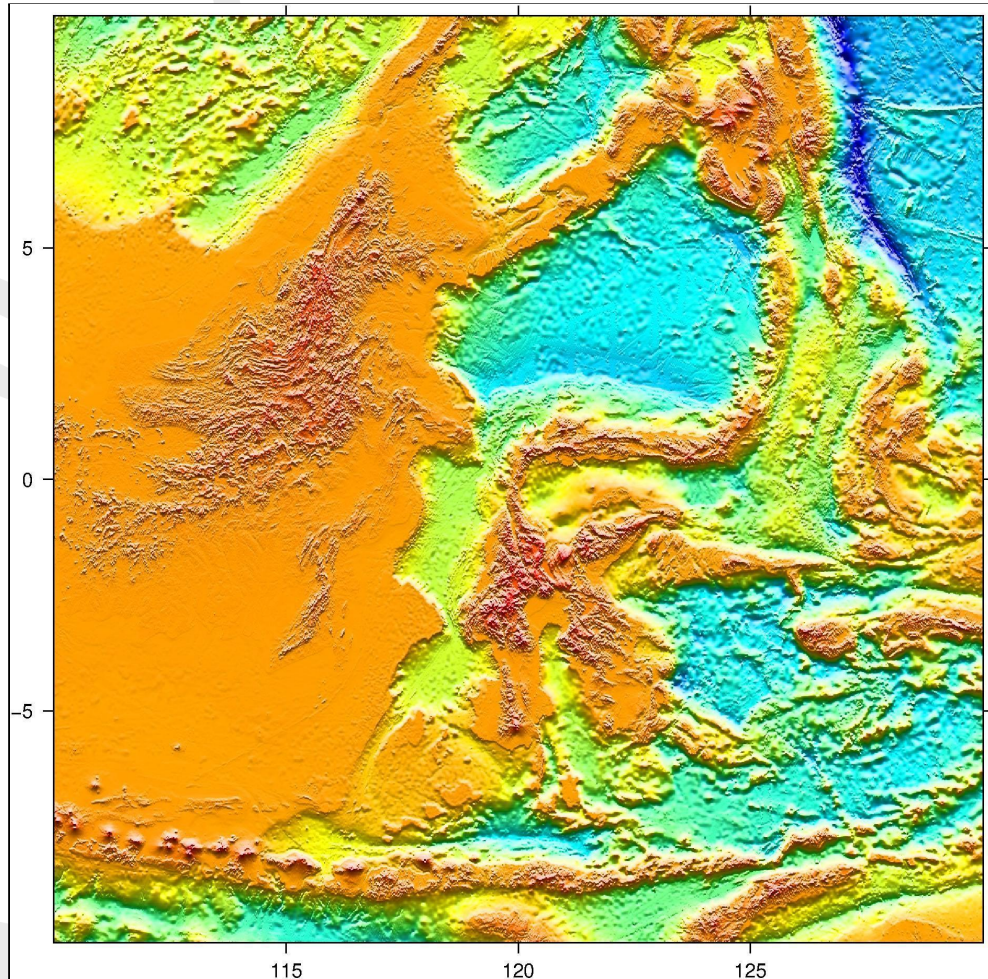


Figure 12 Loaded National Bathymetry in MIRONE

#### 4.1.2. Seismic Elastic Deformation

The second data used is earthquake data that occurred along the Palu-Koro fault. The data is taken from USGS website (<https://earthquake.usgs.gov/earthquakes/eventpage/us1000h3p4/executive>) which stated that this tsunami was triggered by an earthquake with a magnitude of at least 7.5. USGS provided multipatch data regarding the fault after the earthquake. Multipatch data is used to represent the surface, in this case the fault, in a three dimensional area (ESRI, 2008). For MIRONE, the finite fault multipatch in the format of \*.fsp is very suitable. The fsp stands for finite-source parameter, which defines several modeling and the finite-source rupture parameters. It starts with a header block, followed with multiple source parameters on the fault plane, as seen in Appendix A.

Earthquakes ~~in general~~ do not only involve one point, but more like fault area where slip happened where it is significantly related to the magnitude of the event. Then, the magnitude can be modeled via a “finite fault inversion”, which utilizes the traces of the earthquake that create a possibility reconstruct its slip. This would result in “finite fault models” which can either be kinematic or static.

MIRONE can easily visualize this by using the ‘Seismology’ option, then choose ‘Elastic deformation’ and follows it with ‘Import model slip’, because the data is already provided. The result can be seen in Figure 13 and it is clear that the rupture model is given in a column-format that presents a different quantity for each column. Each column has a specialized color that characterizes one point (subfault) on the rupture plane, which would begin from the top left corner of the fault and end with the bottom-right of the faults. The number of columns (source parameters) for this rupture models is 10, and it indicates (in order, see Appendix A): Lat, Lon, X, Y, Z, SLIP, RAKE, TRUP (rupture onset time), RISE time, and SF\_MOMENT

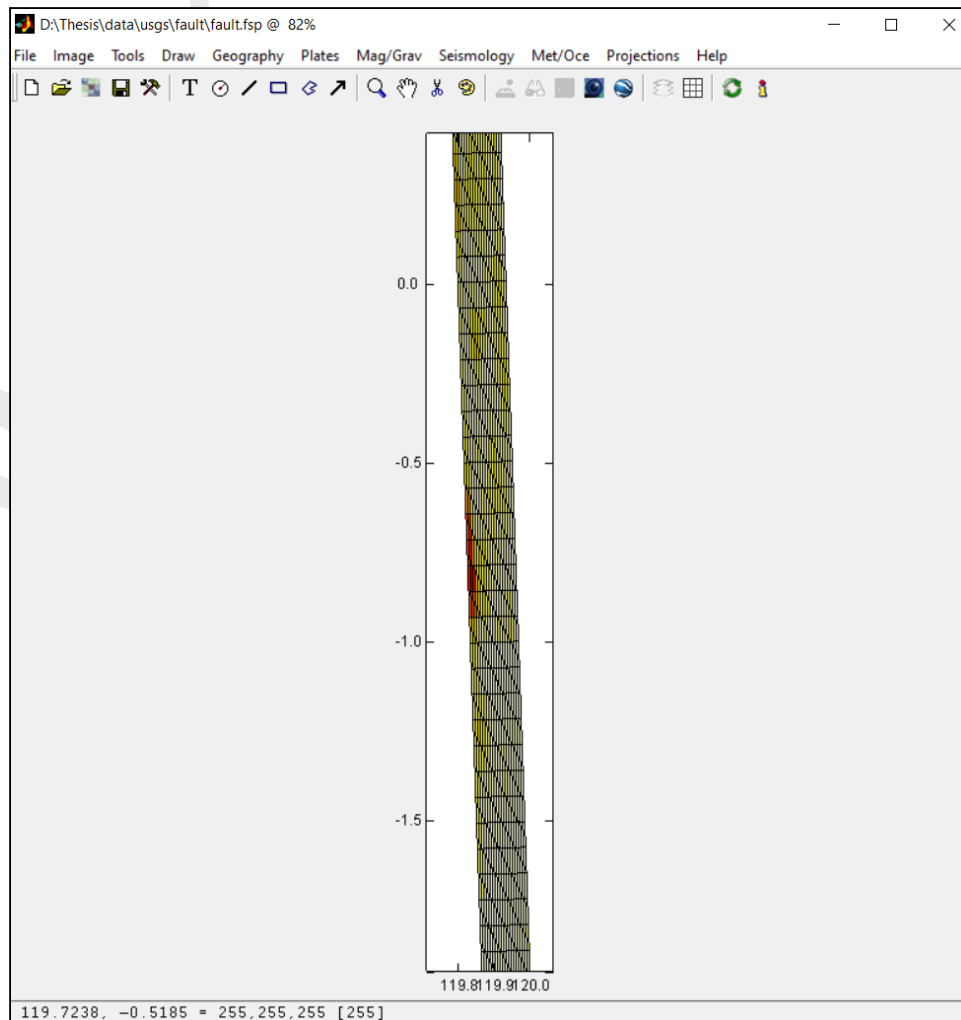


Figure 13 Loaded Finite Source Rupture Model in MIRONE

#### 4.1.3 Tsunami Palu 2018 Initial model

As stated earlier in subchapter 2.4, MIRONE is a MATLAB-based software that can be used to simulate the propagation of a tsunami wave. In order to create the tsunami wave propagation, it only needs a bathymetry grid and the initial condition of water displacement which can be obtained by calculating the seismic parameters data from a certain seismic event, in this case the tsunami Palu 2018. Input initial condition data on MIRONE via its fault parameters formed from the magnitude of the earthquake strength.

According to the data that has been obtained, the steps are:

##### 1. Bathymetry

The process starts by inserting the seabed topography (bathymetry). In MIRONE, it's quite simple and once it's loaded, it can be seen previously in Figure 8 and Figure 11. Since

you don't calculate seismic parameters you use them to calculate the initial condition.

there are 2 bathymetries available, the best one is selected for this model. For tsunami modeling, it is important to have the correct location of the shore. Therefore, one way to see whether the bathymetry is accurate or not is by cross-checking it with Google Earth. To begin, I selected a coastal area in Google earth as seen in Figure 14.



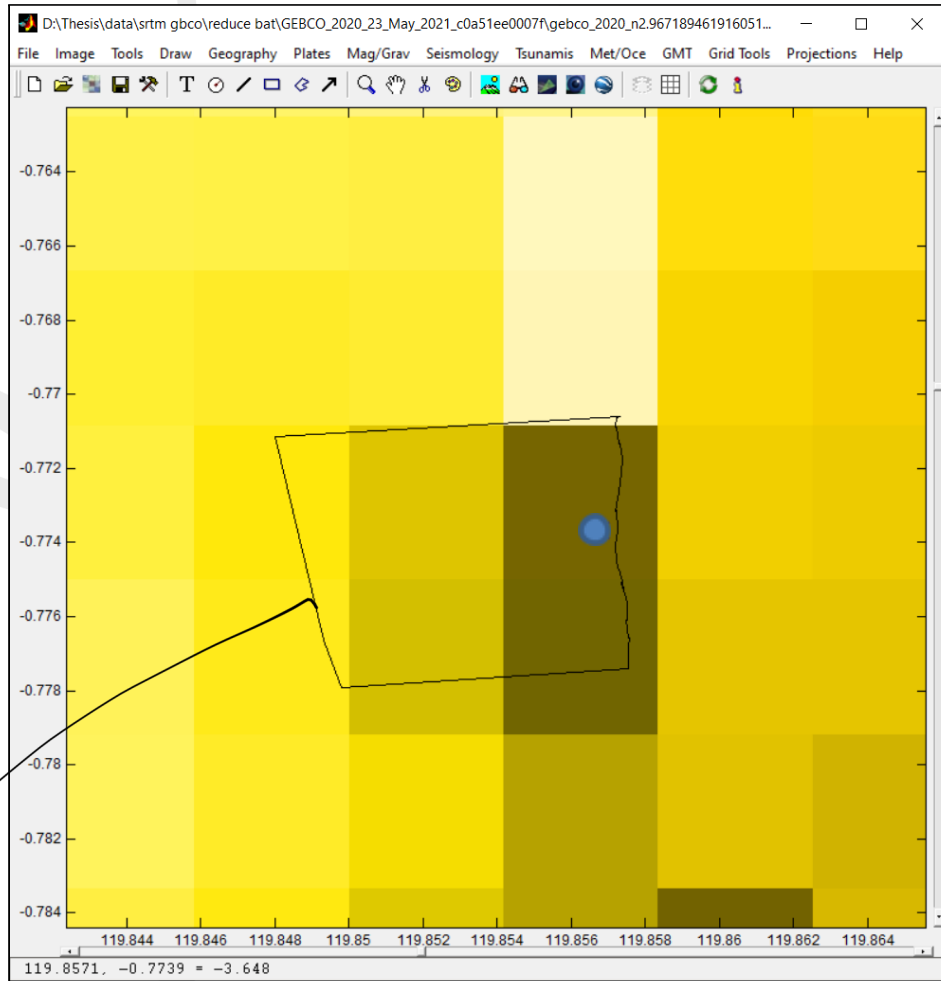
**Figure 14 Coastal Area in Google Earth**

Then, the selected area is imported and compared with both bathymetry data to see whether it the coastline is accurate or not. The results are as following:

- GEBCO 2020 grid

As seen from Figure 15, GEBCO 2020 grid shows quite an accurate value in the coastline, which is -3.6 m and indicates that it is water.





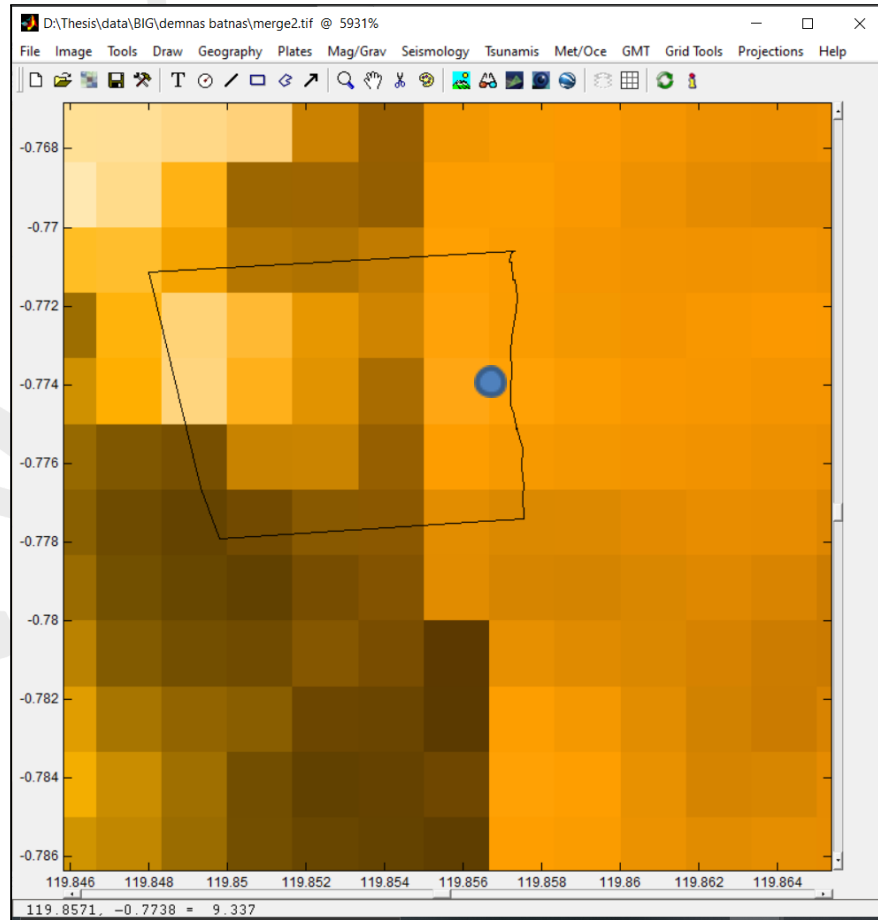
● : Sampling point

Figure 15 GEBCO Coastal Area in MIRONE

- National bathymetry (Batimetri Nasional – BATNAS)

As seen from Figure 16, National bathymetry (Batimetri Nasional – BATNAS) grid shows an inaccurate value in the coastline, which is 9.3 m and indicates that it is land and not water.

→ What is the polygon?



● : Sampling point

Figure 16 BATNAS Coastal Area in MIRONE

Based on the quick assessment above, I chose to proceed with GEBCO 2020 grid, because even though the resolution of national bathymetry is better, the coastal area in national bathymetry is far from accurate.

*See! Not resolution. GRID STEP,*

## 2. Seismic Deformation Computation

Seismic deformation can be loaded once the bathymetry is loaded. It will be placed accordingly (See Figure 17). Therefore, both the bathymetry and deformation grids must have the exact same grid steps and cover the exact same area.



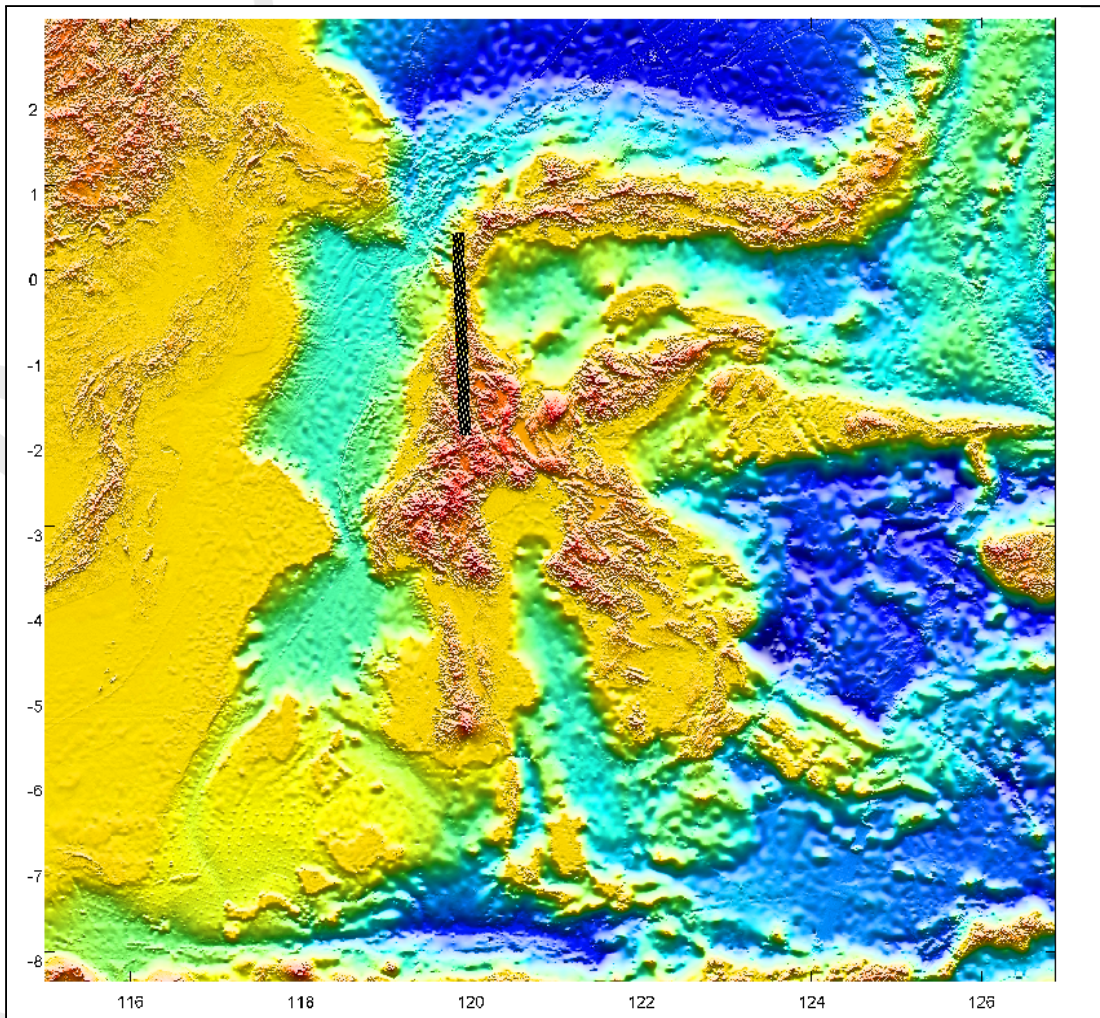


**Figure 17 Loaded Finite Source Rupture Model and Bathymetry in MIRONE**

Once the \*fsp data is placed in the bathymetry, there are two options that can be chosen to compute the deformation: Okada and Masinha.

- Okada:

The main idea of Okada deformation computation is to allow the computation of the vertical seabed deformation (Rashidi et al., 2018) and can later be compared with GPS measurements, which would be perfect for an initial uncalibrated tsunami.

However, Okada deformation could create a significant bias due to its theory that neglects the initial wave current (Jinsong Xie, 2007). More differences between Okada deformation and real tsunami are elaborated in Table 4.

off course it "neglects" It computes the solid Earth deformation, which has nothing to do with water.

Table 4 Differences between Okada Deformation Model and Real Tsunami

No	Okada Deformation Model	Real Tsunami
1	Linear vertical deformation of the Earth	Nonlinear deformation of the Earth
2	No horizontal deformation	Can be up to 3 times more important than the vertical component.
3	The earthquake occurs simultaneously	Slow main shock and lots of aftershocks
4	The water is incompressible	The water is compressible
5	The output is sinusoidal wave	Real tsunami waves are combination of short waves and long waves
6	No initial wave current	Initial wave current
7	One wave	A series of waves
8	Finite fault plane parameters	Unclear

Source: Jinsong Xie (2007)

- Masinha:

The algorithm of Masinha deformation is similar to Okada, the difference is Masinha ignores the hydrodynamic effect because the horizontal part of the wave is adequately greater than the depth of the water at the source (Dao & Tkalich, 2007). Therefore, the initial surface wave is assumed to be identical to the vertical static coseismic displacement of the sea floor which is given for inclined strike-slip and dip-slip faults (Masinha and Smylie (1971) in Dao & Tkalich (2007)).

For the initial simulation, I chose to use Masinha to compute the deformation due to its simplicity yet similar result to Okada. With Okada, the hydrodynamic effect has to be manually neglected which since the required data is only the vertical component. In addition to the two different computation options, MIRONE also gives the option to modify the parameters if later the user wish to manipulate the value of a certain or multiple parameters (See Figure 18). Then, the characteristics of the fault are given in Table 5.

I am sorry but many of these

non-sun

I don't know what you are talking about here

*This is the magnitude of the first patch only. Not the total mag.*

Table 5 Characteristics of USGS Fault

No	Characteristics	Value
1	Magnitude	6.9 Mw
2	Coordinates	119.84E and 0.18S
3	Depth	33.5 km
4	Fault Length	264 km
5	Fault Width	36.75 km
6	Strike ( $\theta$ )	358
7	Dip ( $\bar{D}$ )	66
8	Slip ( $\lambda$ )	0.0838

The screenshot shows a software window titled "Vertical elastic deformation" with several input fields and buttons. The "Fault Geometry" section includes Length (7.9663), Width (1.75), Strike (358), Dip (66), Depth (2.4065), and Depth to Top (0.8078). The "Dislocation Geometry" section includes Strike (358), Rake (343), Slip (0.0838), and a checkbox for "Hide fault planes". The "Gridding Line Geometry" section includes Min, Max, Spacing, and # of lines for both X and Y directions. A "CONFIRM" button is visible, and the "Compute" button is at the bottom right. The "Mu (x10^10)" field is set to 3.0.

Figure 18 Characteristics of the Fault in MIRONE

The result of the computation can be seen in Figure 19. Once this is done, save the result as a new file with a grid format.

color scale.

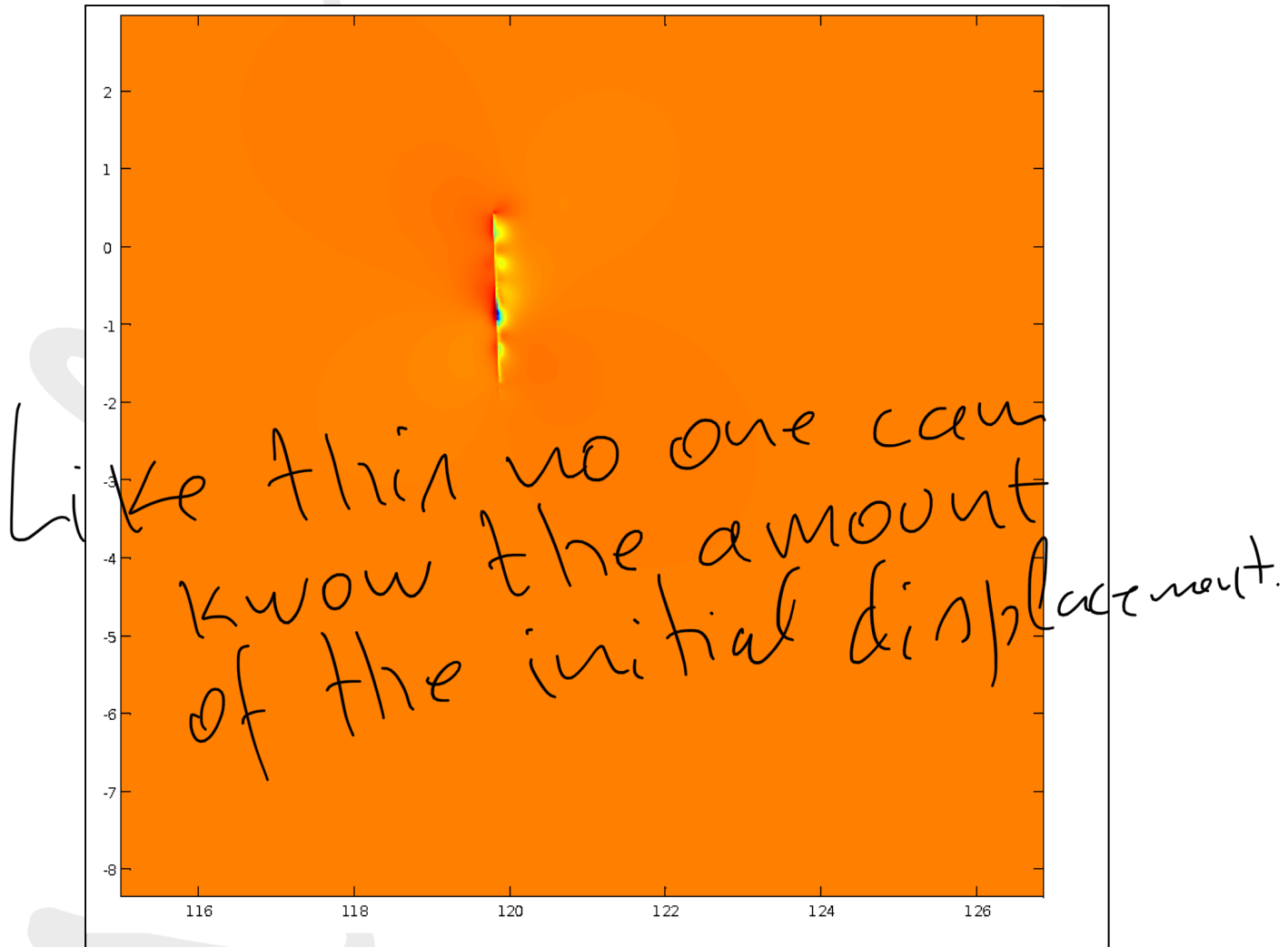


Figure 19 Masinha Fault Computation

With known all these information, the initial tsunami can be created in MIRONE.

### 3. Wave Computation TINTOL (NSWING)

In order to create the wave propagation model, both data need to be combined. Start the combination process by loading the bathymetry data, and then choose the 'TINTOL' option. This would open a new window named the TINTOL (NSWING) that has been mentioned in Subchapter 2.4 and can be seen in Figure 20.



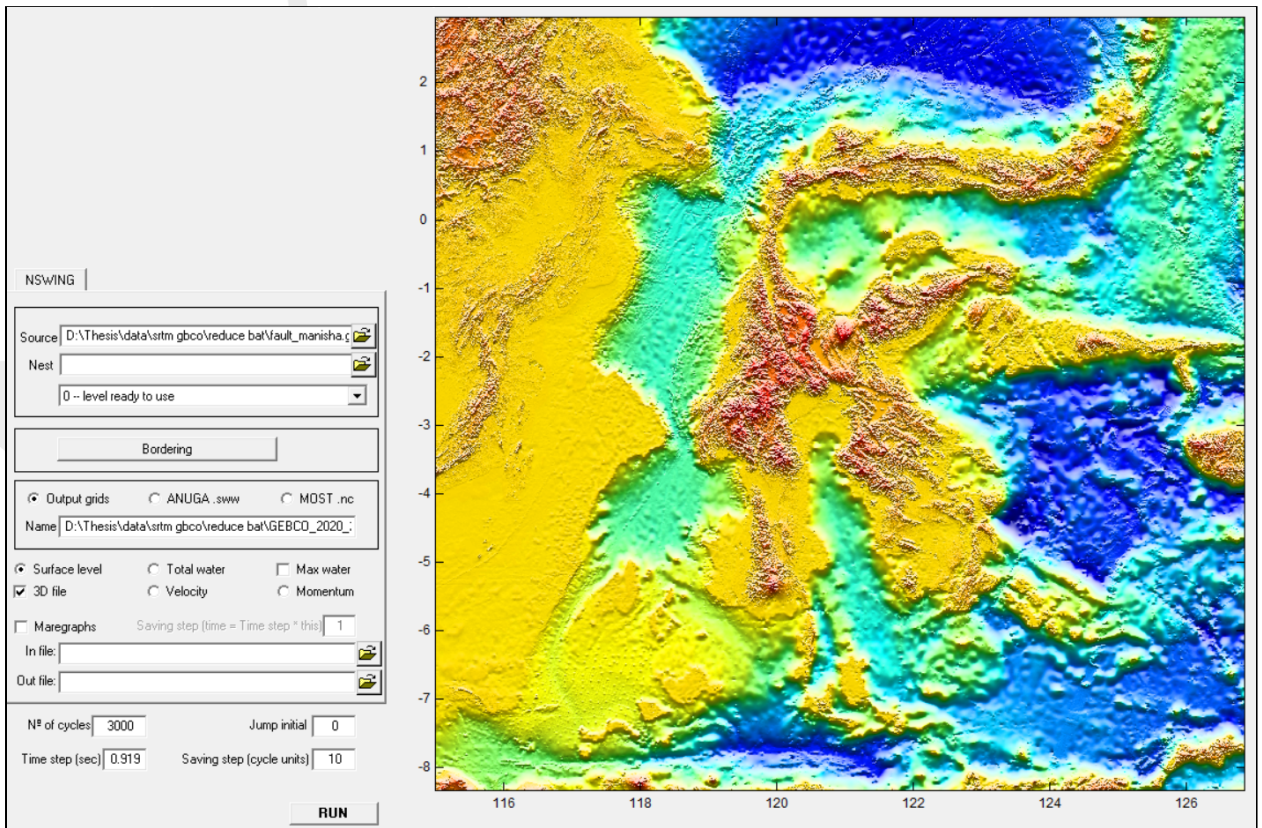


Figure 20 TINTOL Environment

TINTOL allows the user to choose what kind of output is needed (See Figure 20). In this case, the water surface level is selected in a 3D netCDF grid because it is needed for the simulation. Next, decide how many cycles this simulation will run and the time step (in seconds) increment for this simulation.

For the time step, since this model implements a system of coupled nested grids and numerical solution that discretized Shallow Water Equations (SWEs), thus Courant-Friedrichs-Lewy condition (CFL) have to be fulfilled because CFL condition creates stability of unstable numerical methods in a wave model. This discretization would model the problem in a grid with finite cells with a numerical code, NSWING implements an explicit staggered finite leapfrog numerical scheme CFL condition (Wronna, 2015):

$$C = u \times \frac{\Delta t}{\Delta x} \leq C_{max}$$

where:

C: Courant number

$\Delta x$ : length between elements

u: velocity magnitude

$C_{max}$ : maximum Courant number

$\Delta t$ : time step

But you do not have any nested grids here?

you should have rounded it to 0.9

Cmax value for NSWING is 0.5, therefore the time step must satisfy the CFL condition.

MIRONE automatically proposes the time step based on CFL condition and it could be rounded. Both cycle and time step determine to total time of the simulation. For the initial model, we used  $3000 * 0.919$ , resulted in 6000 seconds. Lastly, decide how many saving step that is desired. In this case, the number 10 means saving a step every 15 s of simulation ( $10 * 1.5s = 30s$ ).

#### 4. Visualization

MIRONE is able to view the wave propagation by using Aquamoto tool. To do this, load the \*.nc file from the previous step in the netCDF tab (See Figure 21)

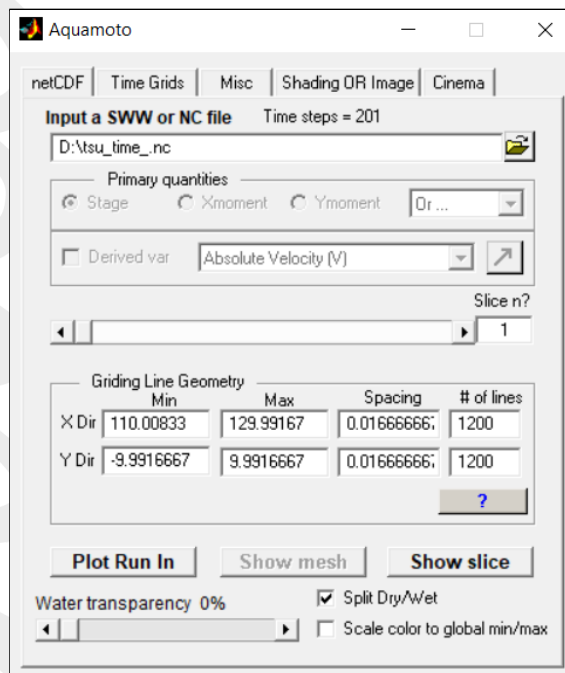


Figure 21 Load \*.nc file

After it's loaded, all the 'Griding Line Geometry' will be filled automatically based on the appropriate number from the file. Next, use the 'Cinema' tab to create a video of the propagation. In Figure 22, decide the movie type (in this case, it's AVI), then also decide the frame/second (in this case, it is 5 fps). Lastly, select the output folder and name the output file.

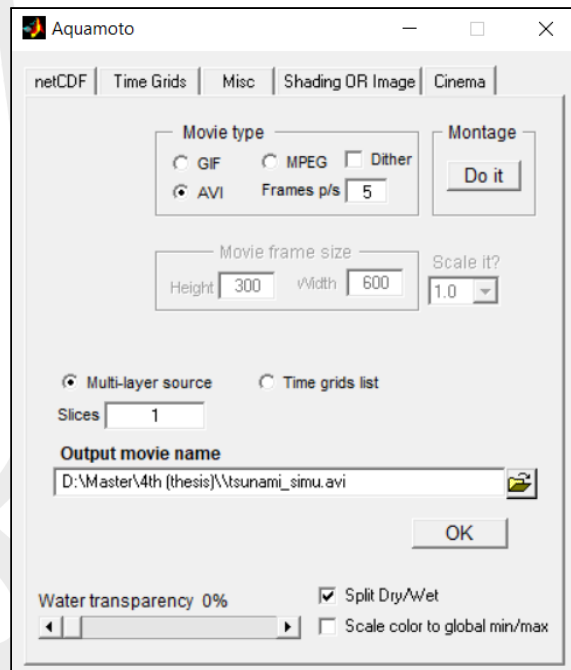
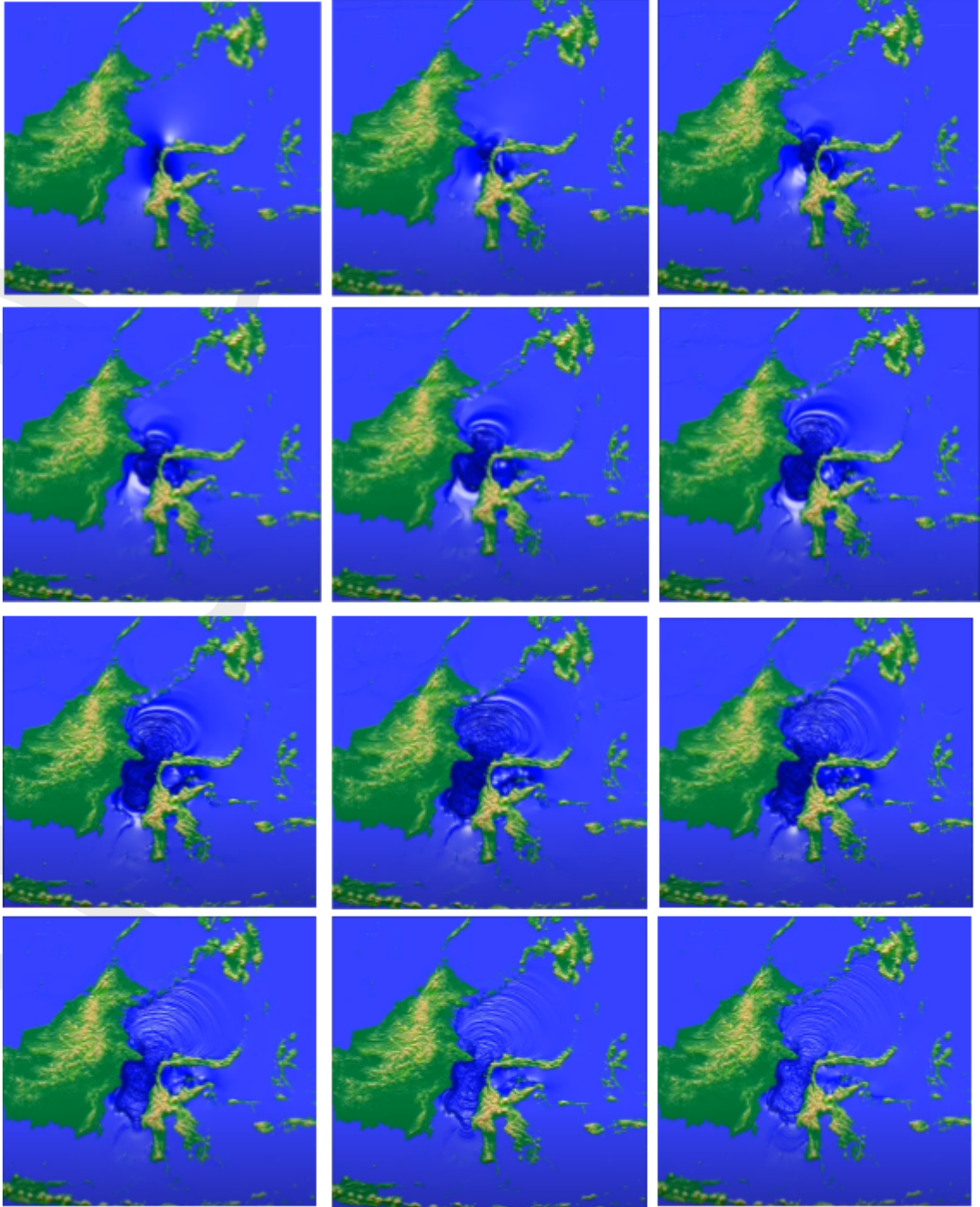


Figure 22 Creating the movie

Once this process is done, the video can be played and this is the result of the initial simulation:





#### 4.2. Result

The most significant result of this model that can be used as a validation method is the maximum wave height produced. MIRONE allows the computation of the wave height through TINTOL environment (See Figure 20) and also through fault computation. Once the result is obtained, the grid file containing the wave height can be loaded in QGIS. To know the exact location of the wave height, load the bathymetry along with the grid file with wave height. The result can be seen in Figure 24.

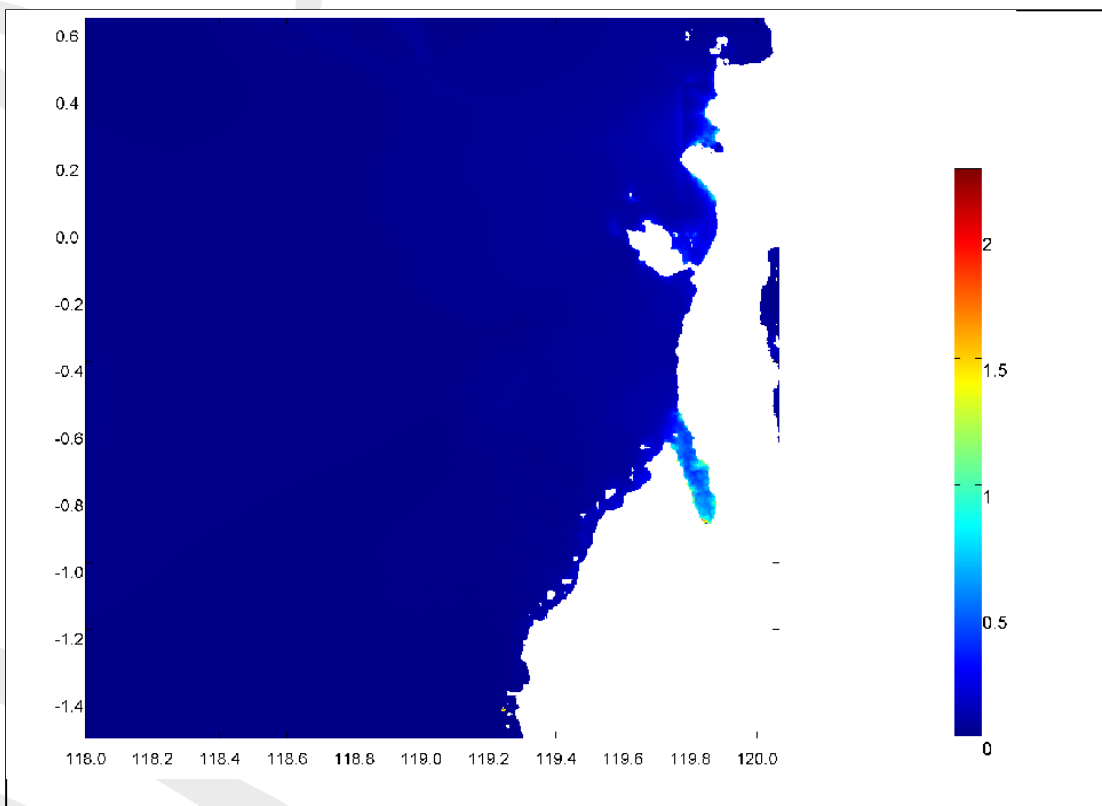


Figure 24 Maximum Wave Height Initial Model

As seen in Figure 24, the highest wave height is found in the Palu bay, which indicated by the white highlight. The value obtained is 2.25 meter, and it is located in the Palu bay.

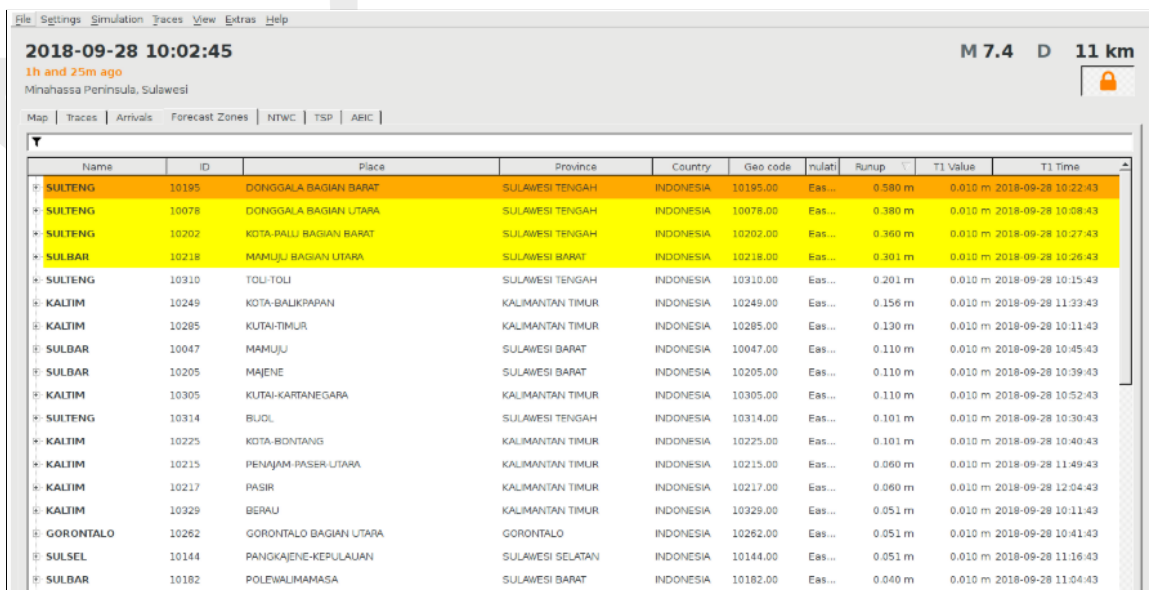
No. There is a pixel or two with  $\approx 2$  m  
There are two maximum wave heights that need to be checked by the initial model:

recorded data and the survey data both by the Meteorology, Climatology, and Geophysical Agency of Indonesia (BMKG).

they are not representative  
I think we discussed this in a room.  
You must show images of the Palu bay  
only. And figures of better  
quality.

#### 4.2.1. Recorded Data

According to Subchapter 2.2.1., the recorded data at Mamuju tide gauge during the event was 6 cm. In addition, on 28 September 2018, BMKG also created a tsunami model based on the earthquake events and obtained a maximum 0.58 m wave height in Palu. The tsunami then resulted in the estimated arrival time at 17:22 WIB, where BMKG issued a tsunami warning. The model result can be seen in Figure 25.



Name	ID	Place	Province	Country	Geo code	Runup	T1 Value	T1 Time
SULTENG	10195	DONGGALA BAGIAN BARAT	SULAWESI TENGAH	INDONESIA	10195.00	0.580 m	0.010 m	2018-09-28 10:22:43
SULTENG	10078	DONGGALA BAGIAN UTARA	SULAWESI TENGAH	INDONESIA	10078.00	0.380 m	0.010 m	2018-09-28 10:08:43
SULTENG	10202	KOTA PALU BAGIAN BARAT	SULAWESI TENGAH	INDONESIA	10202.00	0.360 m	0.010 m	2018-09-28 10:27:43
SULBAR	10218	MAMUJU BAGIAN UTARA	SULAWESI BARAT	INDONESIA	10218.00	0.301 m	0.010 m	2018-09-28 10:26:43
SULTENG	10310	TOLI-TOLI	SULAWESI TENGAH	INDONESIA	10310.00	0.201 m	0.010 m	2018-09-28 10:15:43
KALTIM	10249	KOTA-BALIKPAPAN	KALIMANTAN TIMUR	INDONESIA	10249.00	0.156 m	0.010 m	2018-09-28 11:33:43
KALTIM	10285	KUTAI-TIMUR	KALIMANTAN TIMUR	INDONESIA	10285.00	0.130 m	0.010 m	2018-09-28 10:11:43
SULBAR	10047	MAMUJU	SULAWESI BARAT	INDONESIA	10047.00	0.110 m	0.010 m	2018-09-28 10:45:43
SULBAR	10205	MAJENE	SULAWESI BARAT	INDONESIA	10205.00	0.110 m	0.010 m	2018-09-28 10:39:43
KALTIM	10305	KUTAI-KARTANEGARA	KALIMANTAN TIMUR	INDONESIA	10305.00	0.110 m	0.010 m	2018-09-28 10:52:43
SULTENG	10314	BUDI	SULAWESI TENGAH	INDONESIA	10314.00	0.101 m	0.010 m	2018-09-28 10:30:43
KALTIM	10225	KOTA-BONTANG	KALIMANTAN TIMUR	INDONESIA	10225.00	0.101 m	0.010 m	2018-09-28 10:40:43
KALTIM	10215	PENAJAM-PASER UTARA	KALIMANTAN TIMUR	INDONESIA	10215.00	0.060 m	0.010 m	2018-09-28 11:49:43
KALTIM	10217	PASIR	KALIMANTAN TIMUR	INDONESIA	10217.00	0.060 m	0.010 m	2018-09-28 12:04:43
KALTIM	10329	BERAU	KALIMANTAN TIMUR	INDONESIA	10329.00	0.051 m	0.010 m	2018-09-28 10:11:43
GORONTALO	10262	GORONTALO BAGIAN UTARA	GORONTALO	INDONESIA	10262.00	0.051 m	0.010 m	2018-09-28 10:41:43
SULSEL	10144	PANGKAJENE-KEPULAUAN	SULAWESI SELATAN	INDONESIA	10144.00	0.051 m	0.010 m	2018-09-28 11:16:43
SULBAR	10182	POLEWALIMAMASA	SULAWESI BARAT	INDONESIA	10182.00	0.040 m	0.010 m	2018-09-28 11:04:43

Figure 25 BMKG Model Result

Based on that information, the value of the wave height in the initial model is checked for Mamuju tide gauge to know whether the wave height in that area is indeed 6 cm or not. The value can be seen below (Figure 26) where the tide gauge is marked by yellow triangle, which gives a result of around 0.018 m (marked by red box). It means that the value given by the recorded data is aligned with the initial model given by MIRONE where the wave height is very low.

you can't do this.

First: NO SCREEN CAPTURE FIGS That's awful.

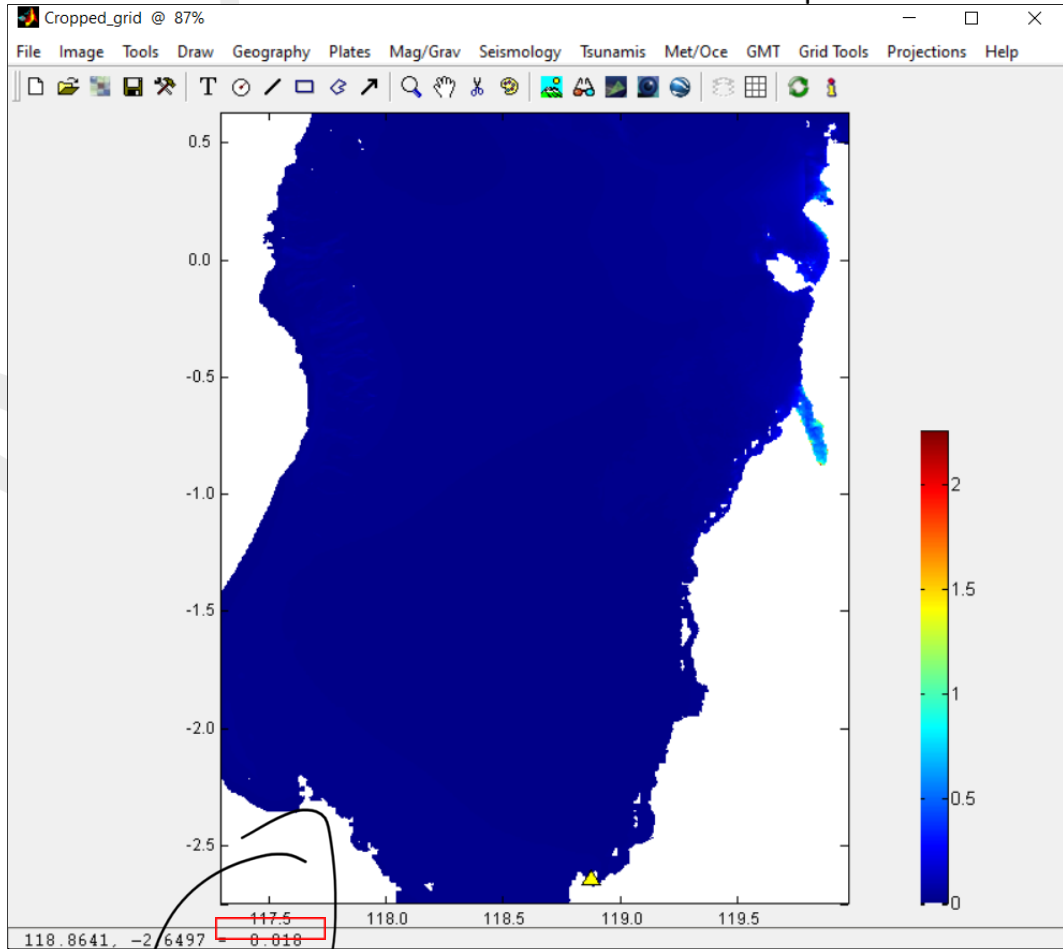


Figure 26 Mamuju Tide Gauge Wave Height

To show something like this you do a zoom and integrate on job.

#### 4.2.2. Survey Data

According to Subchapter 2.2.2., the survey data during the event was 10 meter. In addition, there are additional surveyed data gathered by the Meteorology, Climatology, and Geophysical Agency are displayed below (Table 6).

Table 6 Surveyed Data from Meteorology, Climatology, and Geophysical Agency

No	Location	Latitude	Longitude	Wave Height (m)	Wave Height Tide Correction (m)	Inundation
1	Panggang	-0.71896	119.7746	5.1	5.1	106.7
2	Lolilondo	-0.74715	119.7805	4.0	4.0	97.7
3	Lolipesua	-0.7697	119.7885	7.3	7.3	75.6

<b>No</b>	<b>Location</b>	<b>Latitude</b>	<b>Longitude</b>	<b>Wave Height (m)</b>	<b>Wave Height Tide Correction (m)</b>	<b>Inundation</b>
4	Lolisaluran	-0.84363	119.8189	9.6	9.6	101
5	Primkopal	-0.81755	119.8108	7.1	7.1	74
6	Tipo	-0.86072	119.8286	6.7	6.7	105
7	Silae	-0.87498	119.8349	3.8	3.4	101.8
8	Ruko Lere	-0.88111	119.8401	5.6	5.7	320
9	Grandmall Palu	-0.88223	119.8429	5.6	6.1	320
10	Mercure Palu	-0.88361	119.8495	9.2	10.0	468.8
11	TVRI Palu	-0.88583	119.8629	10.9	7.6	428.9
12	Kp Nelayan	-0.8639	119.8781	7.1	7.6	75
13	Citraland	-0.8318	119.8798	7.0	6.7	197
14	Tondo	-0.83658	119.881	11.3	10.7	165
15	Pergudangan	-0.82354	119.8824	8.3	9.1	378.9
16	Kp Mambaro	-0.8016	119.8766	6.7	7.0	247,1
17	Poltekes	-0.79002	119.8645	6.6	6.2	42
18	Resort Taipa	-0.78183	119.8589	5.8	5.1	145.3
19	PLTU Tawaeli	-0.73204	119.8551	8.7	9.3	168.8
20	Pantoloan	-0.70846	119.8518	11.1	10.2	216
21	Ngada Wani	-0.69501	119.8403	7.1	7.2	158.4
22	Labuan	-0.66251	119.8166	4.4	3.9	29.3
23	TPI Lero	-0.62912	119.8115	6.8	6.0	132.7
24	Pasir Marana	-0.59529	119.7893	3.9	3.0	41.2
25	Tondo Lendi	-0.24924	119.7962	2.3	2.3	133.8

What means "Recorded Data"  
Recorded how?

N o	Location	Latitude	Longitude	Wave Height (m)	Wave Height Tide Correction (m)	Inundation
26	Mapaga Sirenja	-0.23105	119.8022	2.2	2.2	136.7

Based on that information, the value of the wave height in the surveyed model is checked for all the sampling points to know whether the wave heights in those areas are correct or not. Some of the sampling values are located on land, which cause MIRONE to not be able to read the wave height. The value comparison can also be seen in Table 7, which is very different. It means that the value given by the surveyed data is not aligned with the initial model given by MIRONE where the wave height is very low.

**Table 7 Wave Height Comparison from Simulation Data and Surveyed Data**

N o	Location	Latitude	Longitude	Wave Height Recorded Data (m)	Wave Height Surveyed Data (m)	Wave Height Difference (m)
1	Panggung	-0.71896	119.7746	0.7	5.1	4.4
2	Lolilondo	-0.74715	119.7805	0.7	4.0	3.3
3	Lolipesua	-0.7697	119.7885	0.7	7.3	6.6
4	Lolisaluran	-0.84363	119.8189	1	9.6	8.6
5	Primkopal	-0.81755	119.8108	0.9	7.1	6.2
6	Tipo	-0.86072	119.8286	0.7	6.7	6
7	Silae	-0.87498	119.8349	Land	3.4	-
8	Ruko Lere	-0.88111	119.8401	1.5	5.7	4.2
9	Grandmall Palu	-0.88223	119.8429	1.6	6.1	4.5
10	Mercure Palu	-0.88361	119.8495	2.2	10.0	7.8
11	TVRI Palu	-0.88583	119.8629	0.9	7.6	6.7
12	Kp Nelayan	-0.8639	119.8781	1	7.6	6.6
13	Citraland	-0.8318	119.8798	1.1	6.7	5.6
14	Tondo	-0.83658	119.881	1.2	10.7	9.5

<b>N o</b>	<b>Location</b>	<b>Latitude</b>	<b>Longitud e</b>	<b>Wave Height Recorded Data (m)</b>	<b>Wave Height Surveyed Data (m)</b>	<b>Wave Height Difference (m)</b>
15	Pergudangan	-0.8235 4	119.8824	1.5	9.1	7.6
16	Kp Mambaro	-0.8016	119.8766	0.7	7.0	6.3
17	Poltekes	-0.7900 2	119.8645	0.7	6.2	5.5
18	Resort Taipa	-0.7818 3	119.8589	0.7	5.1	4.4
19	PLTU Tawaeli	-0.7320 4	119.8551	0.5	9.3	8.8
20	Pantoloan	-0.7084 6	119.8518	1	10.2	9.2
21	Ngada Wani	-0.6950 1	119.8403	0.6	7.2	6.6
22	Labuan	-0.6625 1	119.8166	Land	3.9	-
23	TPI Lero	-0.6291 2	119.8115	0.5	6.0	5.5
24	Pasir Marana	-0.5952 9	119.7893	0.5	3.0	2.5
25	Tondo Lendi	-0.2492 4	119.7962	0.2	2.3	2.1
26	Mapaga Sirenja	-0.2310 5	119.8022	0.2	2.2	2

## 5. Sensitivity analysis

In this chapter, I will discuss the sensitivity analysis of the obtained initial model of tsunami Palu 2018. This serves a purpose to see whether the recorded data during the event and the data gathered after the event could be achieved through the initial model by modifying some parameters through hypothetical scenarios.

During earthquake events, uncertainties usually come from the fault parameters and not the epicenter location and magnitude. The generation of tsunami because of an earthquake, the commonly applied theory is the dislocation theory developed by Mansinha and Smylie in 1971. This theory is based on the linear elastic theory and predicts the seafloor displacement based on the fault plane characteristics described by several parameters (Gica et al., 2007).

Tsunami generation is a very complex phenomenon, therefore further sensitivity studies on more than one tsunami event originated from different value for fault plane parameters can be challenging to determine and may remain unknown (Gica et al., 2007). Once those parameters have been modified, it can be seen which parameter plays a more significant role. The effect of each parameter can be examined by focusing on a specific event and determining how changes in parameter affect the maximum wave height produced (Aagaard et al., 2004)

### 5.1. Process

The sensitivity analysis of tsunami modeling results can be executed by running multiple simulations with varying several parameters and then examining the relation of the changes in results based on each parameter's variation.

The goal of this sensitivity analysis process is to reach the surveyed data through data manipulation. The altered variables are bathymetry map and seismic elastic deformation. In this study, variable seismic elastic deformation characteristics include the depth, size of fault area, slip displacement, strike, dip, and rake angles are taken into account (Gica et al., 2007). This process is done by the selected software, MIRONE.

The bathymetry, GRID not MAP, is not a variable.

### 5.1.1. Bathymetry Map

Bathymetry is an essential part of the model since it provides the topography of the desired area. Previously, as seen in subchapter 4.1.1, the initial model uses the GEBCO bathymetry. Therefore, in this subchapter, I will use other bathymetries to see if it gives a significant wave height difference. The other bathymetries are:

#### 1. National bathymetry (Batimetri Nasional – BATNAS)

National bathymetry or BATNAS, as described in Subchapter 4.1.1, is produced by Geospatial Information Agency. It has a ~~better resolution~~ compared to GEBCO, which is 6 arcsec. Based on the result from the initial model, the bathymetry reached only a certain part of area. Therefore, I reduced the survey area in BATNAS which could greatly help minimize the calculation process. The selected area displayed with MIRONE can be seen in Figure 27.

*smaller grid step.*

*X anid*



What is this rectangular frame?

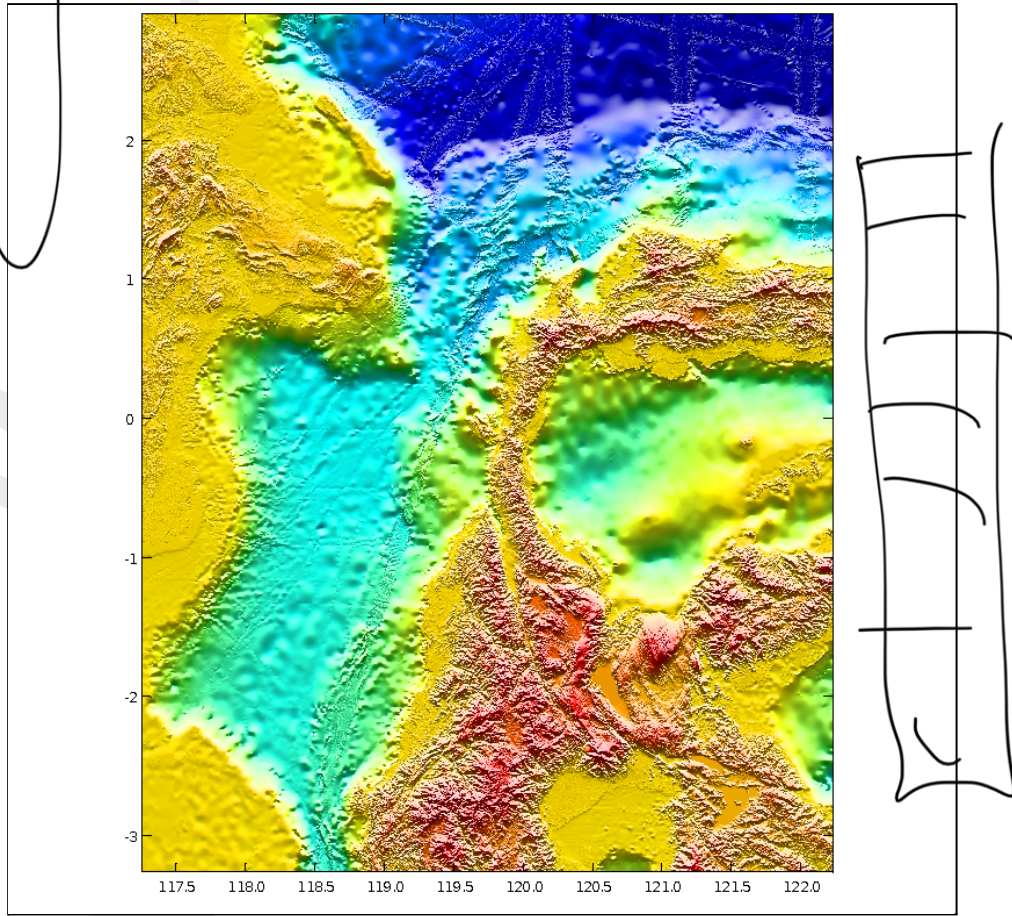


Figure 27 National Bathymetry (Batimetri Nasional – BATNAS) in MIRONE

## 2. GEBCO combined with National bathymetry (Batimetri Nasional – BATNAS)

As seen in Subchapter 4.1.1, the main issue with GEBCO is its resolution, meanwhile the main issue with BATNAS is its inaccurate coastal area. Therefore, in order to have both good resolution and accurate coastal area, it might be useful to combine GEBCO and BATNAS. This can be done by selecting the coastal area in GEBCO and replace it with a higher resolution coastal area from BATNAS. First, the coastal area was selected with Google Earth (Figure). Then the selected area is imported and loaded into MIRONE. MIRONE allows the combination of two bathymetries and will match the two resolutions. The result is a more accurate coastal area with high resolution (6 arcsec) that can be seen in Figure 28.

But you said BATNAS was bad on the coast and now you are going to replace GEBCO with it?

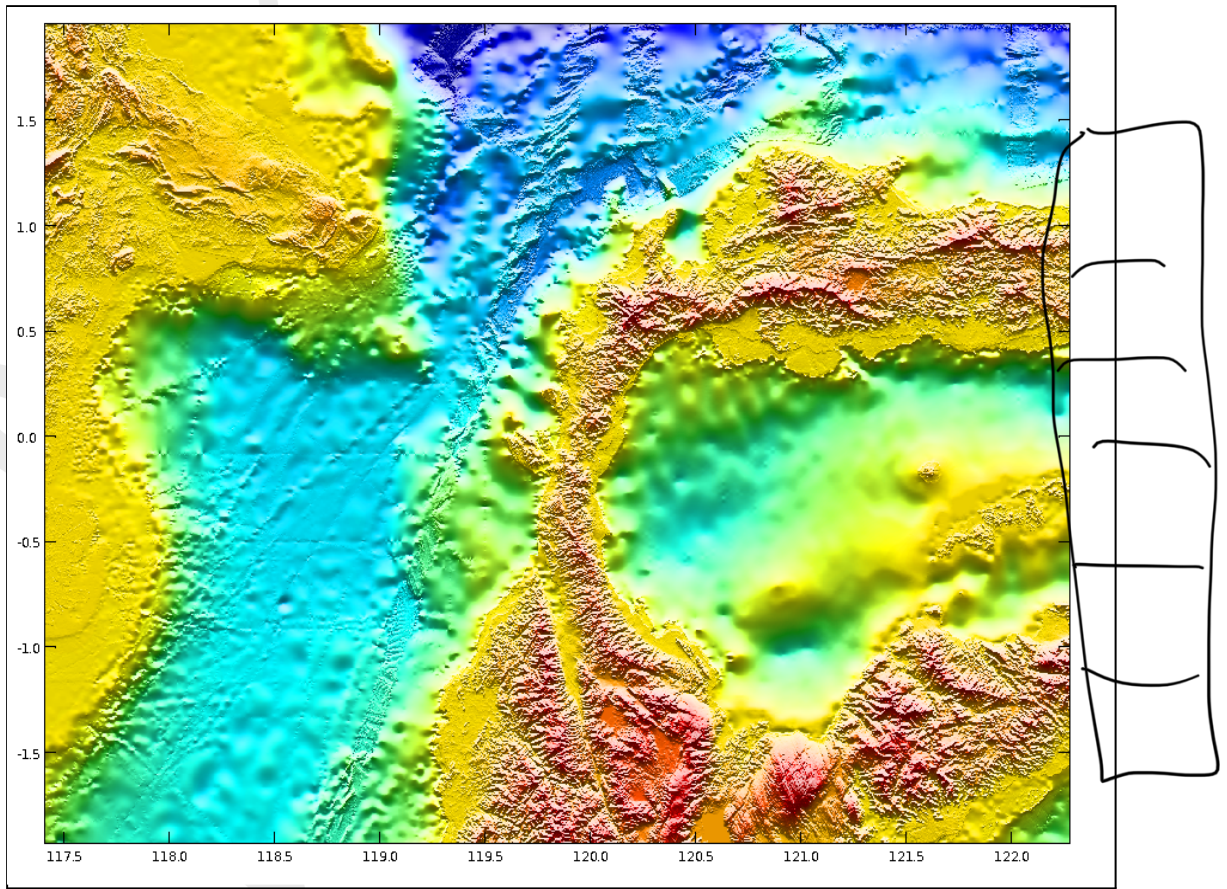


Figure 28 GEBCO Combined with National bathymetry (Batimetri Nasional – BATNAS) in MIRONNE

### 5.1.2. Fault parameters

As mention previously, a significant parameter for this tsunami propagation model is the fault, which triggers the earthquake. Then, seafloor deformation caused by the earthquake will then cause the sea level to be restored by gravity force known as tsunami waves (Sepúlveda et al., 2020). The faulting, in this case a strike-slip event, has a certain geometry that is illustrated by focal mechanism (Kiratzi, 2014).

The faults do not trigger earthq.

The role of focal mechanism is to describe the orientation of the fault based on several angles: strike, dip, and rake angle (Kiratzi, 2014):

- strike ( $\varphi$ ): the angle that defines fault-trace direction ( $0^\circ < \varphi < 360^\circ$ ) relative to North
- dip ( $\delta$ ): the angle of the fault plane relative to the horizontal plane ( $0^\circ < \delta < 90^\circ$ )
- rake ( $\lambda$ ): the angle between the direction of slip and the horizontal measured on the fault plane ( $0^\circ < \lambda < 360^\circ$ )

NO. Focal mechanism describe the earthquake, not the fault.

In addition to those angles, seafloor displacement caused by a submarine earthquake is calculated based on several equations by Mansinha and Smylie 1971 which is also used in MIRONÉ. These equations take account other parameters:

d. Depth: in this case, it is depth to top, which is the depth between fault's top to the surface

e. Slip displacement: on a fault, slip typically is a maximum near the center of the fault and decreases to zero near the end of a fault.

f. Size of fault area: the area depends on both length and width, meanwhile the length is not easily manipulated (can only have length variation by creating new fault), therefore width is chosen as the manipulated parameter.

Therefore, all the modifying parameters that will be discussed are:

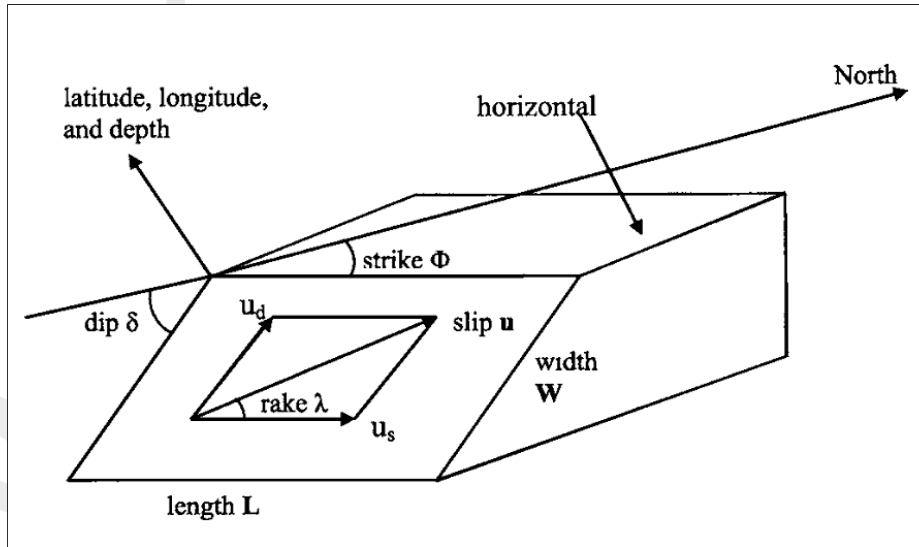
- Depth
- Slip displacement
- Area of fault
- Rake angles
- Strike
- Dip

The parameters involved in such as the fault dislocation, dip, and rake angles are also difficult to determine as they may not be known from the earthquake recordings directly (Gica et al., 2007). The fault deformation itself has several parameters that could be modified one by one according to different available parameters. The goal is to find out whether it is actually possible to reproduce the real wave height (Fang et al., 2018).

yes, but not in the simple model of a single patch.

→ No. Focal mechanisms tell us that.





Source: Gica et al., (2007)

**Figure 28 Definition sketch of fault plane dimension and geometry**

Since the purpose of sensitivity analysis is to know how a certain parameter affects the maximum wave height without any impact from neighboring parameters, the fault used in this section is single dimension and can only accommodate one value of each parameter. These limitations leads to highlighting the specific behavior in the parameters which can be easily interpreted.

The fault that is used in the seismic elastic deformation sensitivity analysis will be created from MIRONE. The initial fault that is being used is provided by USGS in a multipatch format. Since it would be overly complicated to modify, most of the modification will use new fault.

The process of creating the new fault can simply be done by choosing the 'Draw Fault' option in Seismology tab. The new fault created by MIRONE has characteristics that can be seen below in Table 8 and displayed in Figure 29.

**Table 8 Characteristic of New Fault by MIRONE**

No	Characteristics	Value
1	Magnitude	7.6 Mw
2	Coordinates	114.99E and -8.34S
3	Depth	45.6 km
4	Fault Length	214.85 km
5	Fault Width	36.75 km
6	Rake	90°

?? But the Earthquake was strike-slip

No	Characteristics	Value
7	Dip ( $\delta$ )	$25^\circ$
8	Slip ( $\lambda$ )	1
9	Strike ( $\alpha$ )	$176^\circ$

Unil

Why insisting in showing a large area and therefore not being able to show the details in the zone of interest?

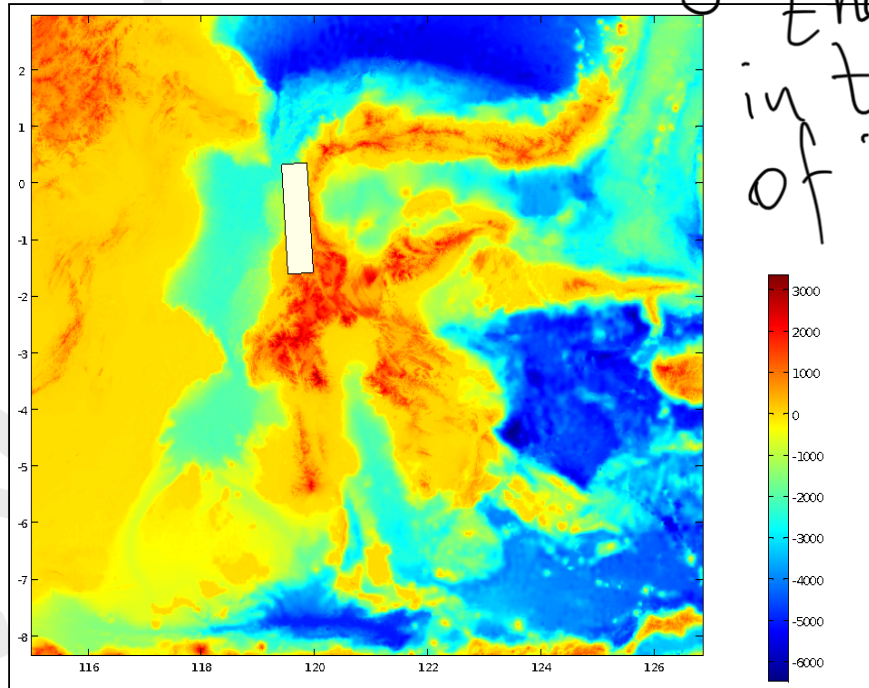


Figure 30 New Fault by MIRONE

Once the new fault is created, I investigated the maximum wave height produced from the new fault. Based on Figure 30, the maximum wave height produced is 0.9 m.

These maximums include interactions with waves reflected and therefore not exactly representative

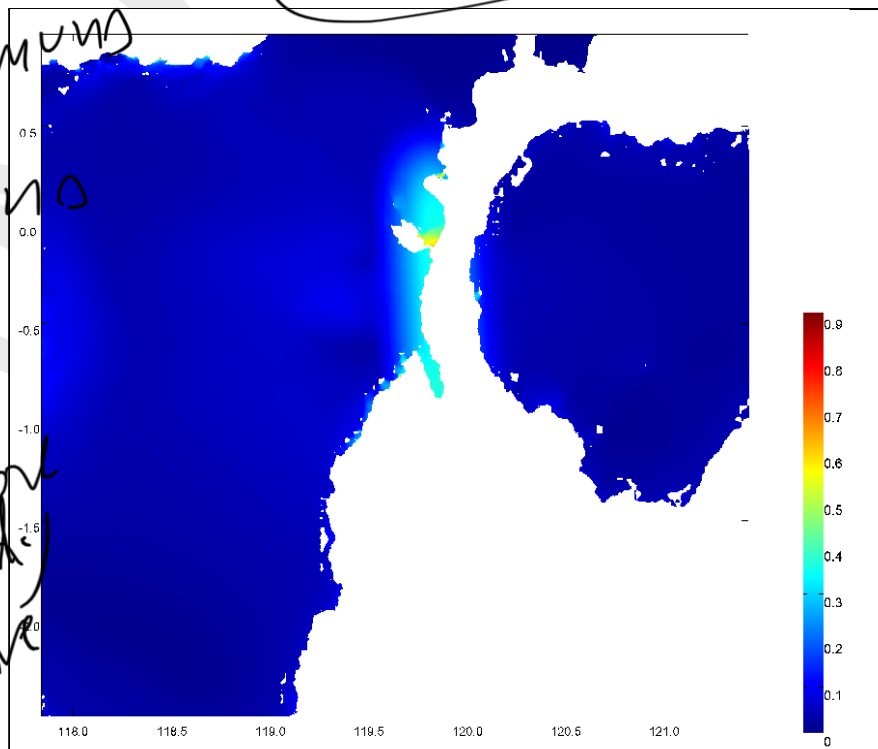


Figure 31 Maximum Wave Height (New Fault)

## 5.2. Result

This subchapter will show the result of sensitivity analysis based on the two main parameters mentioned above. The bathymetry map and seismic elastic deformation.

### 5.2.1. Bathymetry Map

#### 1. National bathymetry (Batimetri Nasional – BATNAS)

As seen in Figure 31, the maximum wave height is found in the Palu bay, which indicated by the white highlight. The value obtained is 3.6 meter.

SO sorry  
I can't  
see  
nothing  
because  
you show  
a TOO BIG  
figure.

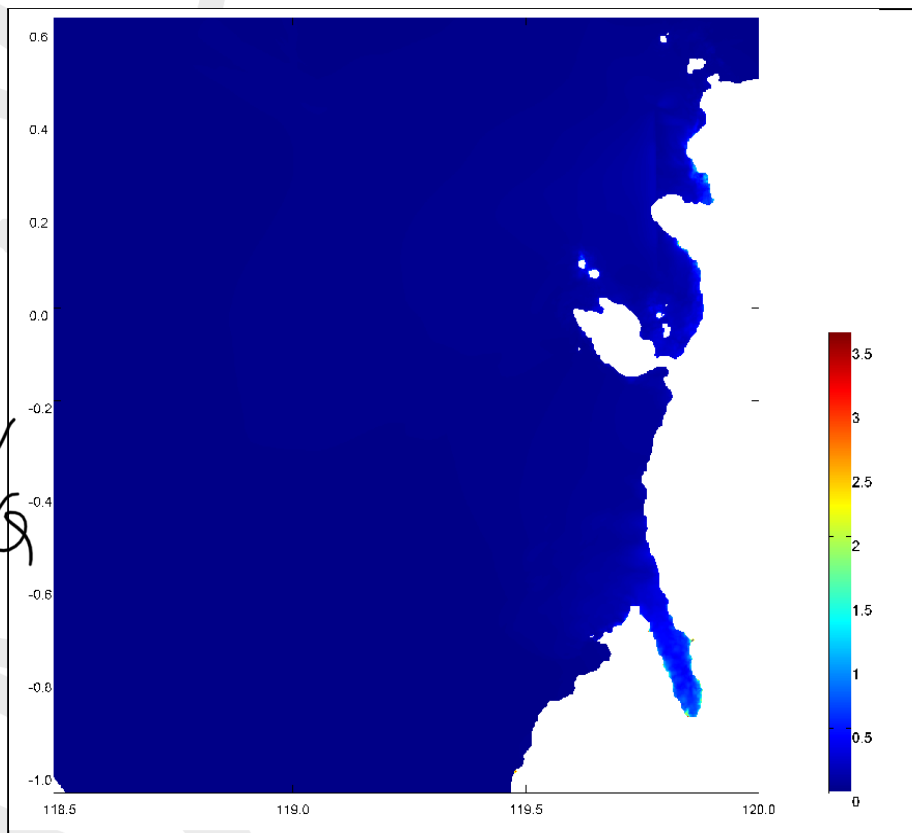


Figure 32 Maximum Wave Height (BATNAS)

#### 2. GEBCO combined with National bathymetry (Batimetri Nasional – BATNAS)

As seen in Figure 32, the highest wave height is found in the Palu bay, which indicated by the white highlight. The value obtained is 2.35 meter.

?

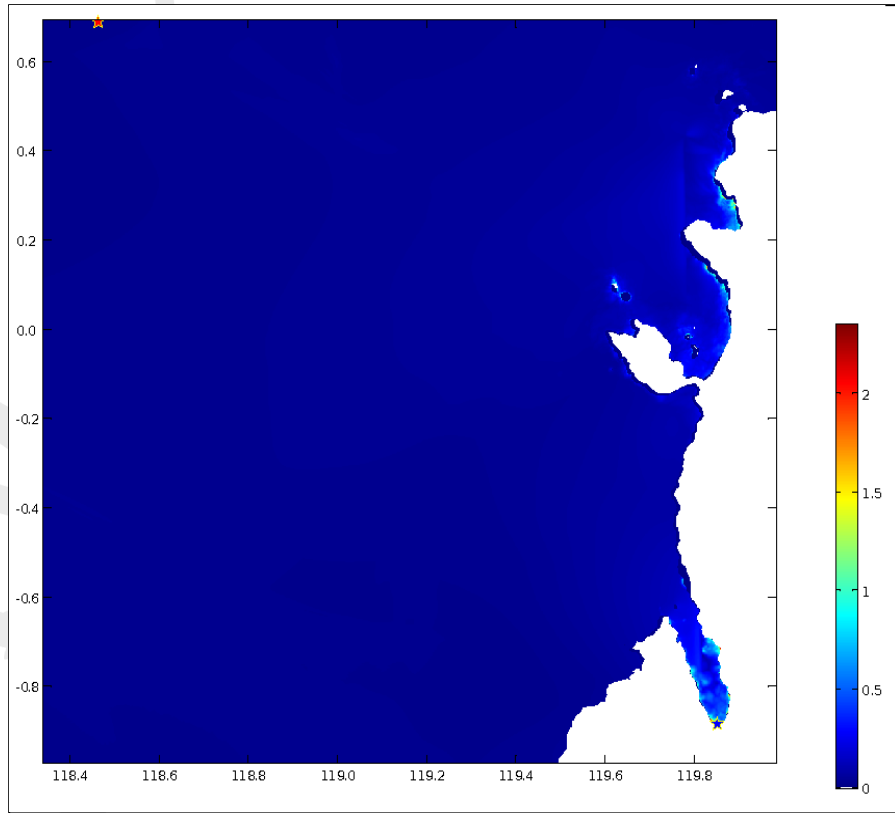


Figure 33 Maximum Wave Height (GEBCO Combined with BATNAS)

Then, the results can be summarized as seen in Table 9.

Table 9 Maximum Wave Heights from Different Bathymetries

Bathymetry	Max. Wave Height (m)
GEBCO (initial model)	2.25
BATNAS	3.6
GEBCO+BATNAS	2.35

*all not reliable because they occur in only one pixel.*

### 5.2.2. Fault parameters

#### 1. Depth

The first modification would be to take the depth to top. The original value of depth is 22.827 km and the modification is done by adding the original depth with 5 and 10, subtracting the original depth with 5 and 10 and finally dividing the depth by 10 and 100.

The result can be seen in Figure 33 and Table 10 below.

*down to meter precision??  
Not possible.*



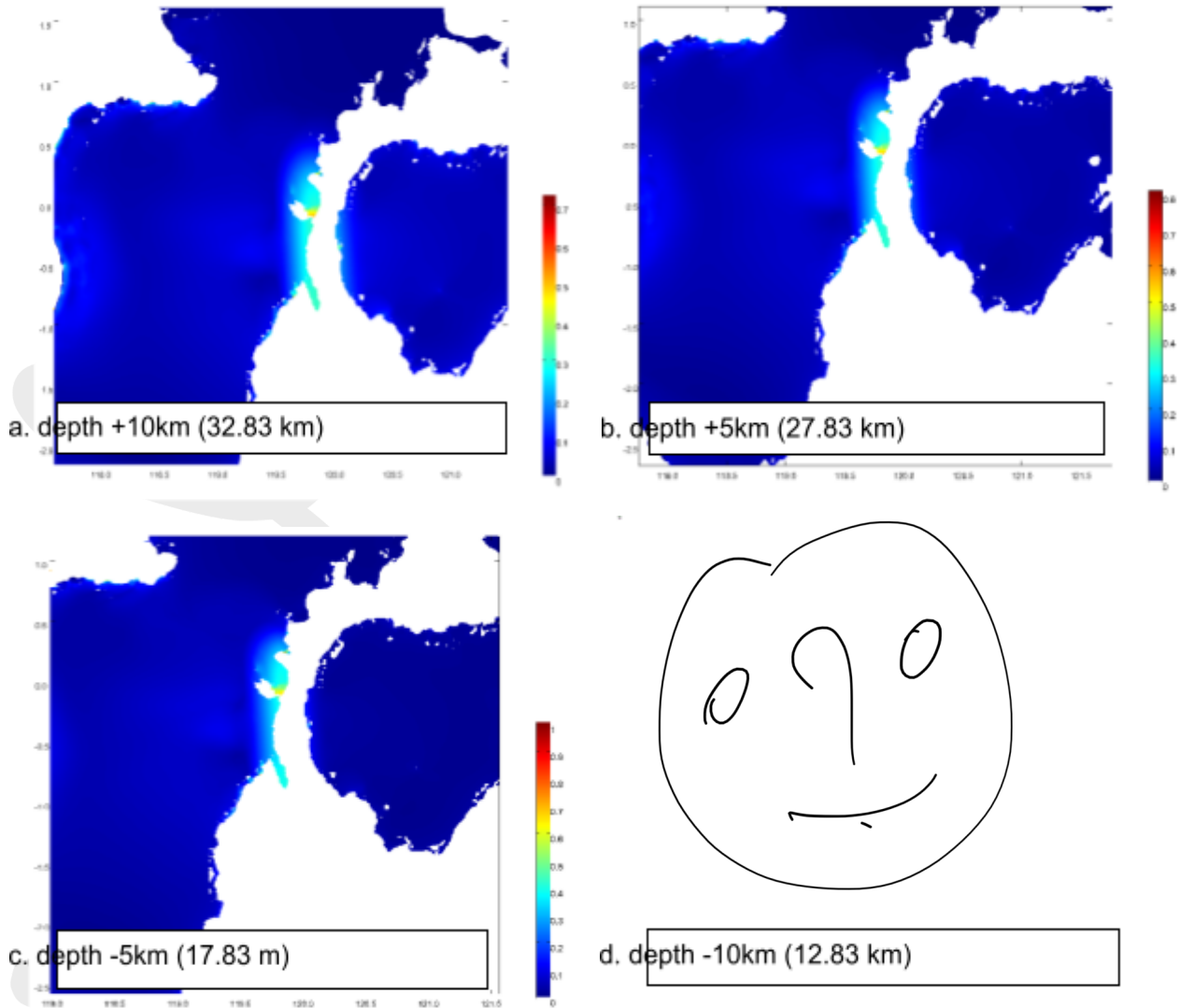


Figure SEQ Figure 1\* ARABIC 34 Maximum Wave Height with Depth Variation

Table 10 Maximum Wave Height with Depth Variation

Depth to top (km)	Max. Wave Height (m)
0.23	0.78
2.28	0.93
12.83	1.13
17.83	1.00
22.83 (initial model)	0.90
27.83	0.80
32.83	0.72

→ what is this?  
where are they coming all those decimals?  
0.23 km??

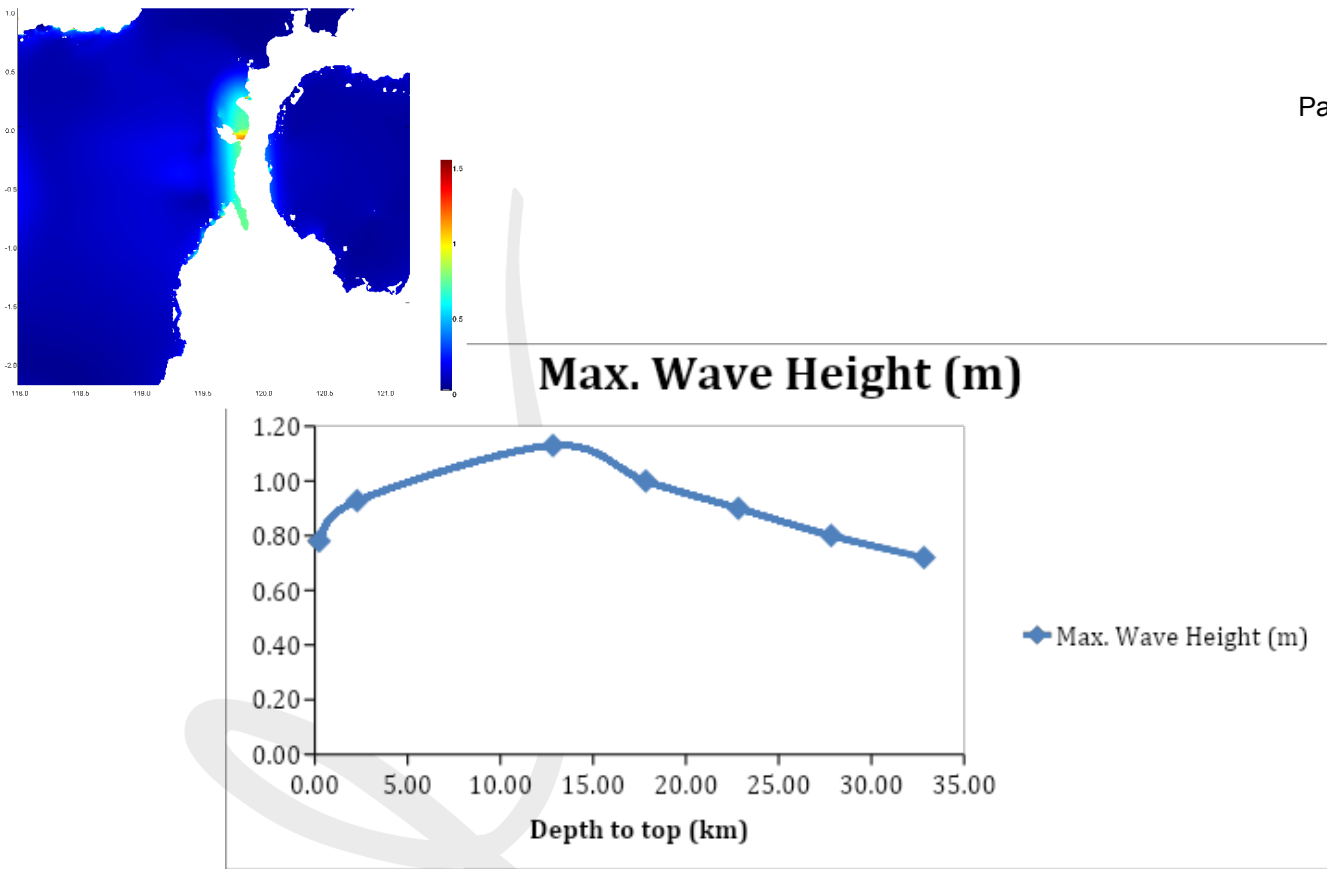


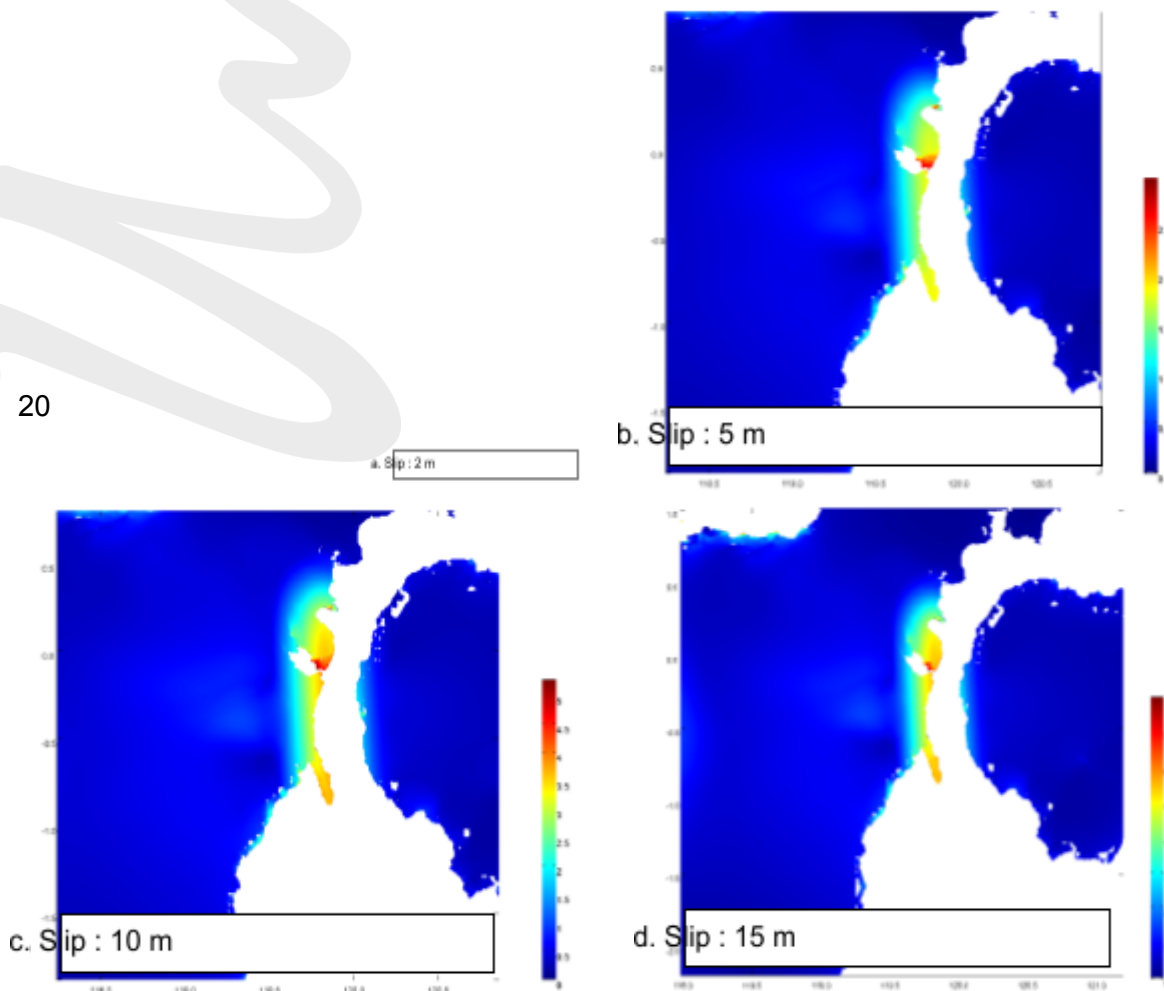
Figure 35 Maximum Wave Height VS Depth to Top

2. Slip

*default*

The second modification is slip, which has the original value of 1 meter. The modification of slip was also done by multiplying the original value by different factors, which are: 2, 5, 10, 15, 20, and 25. The results can be seen in both Figure 35 and Table 11.

20



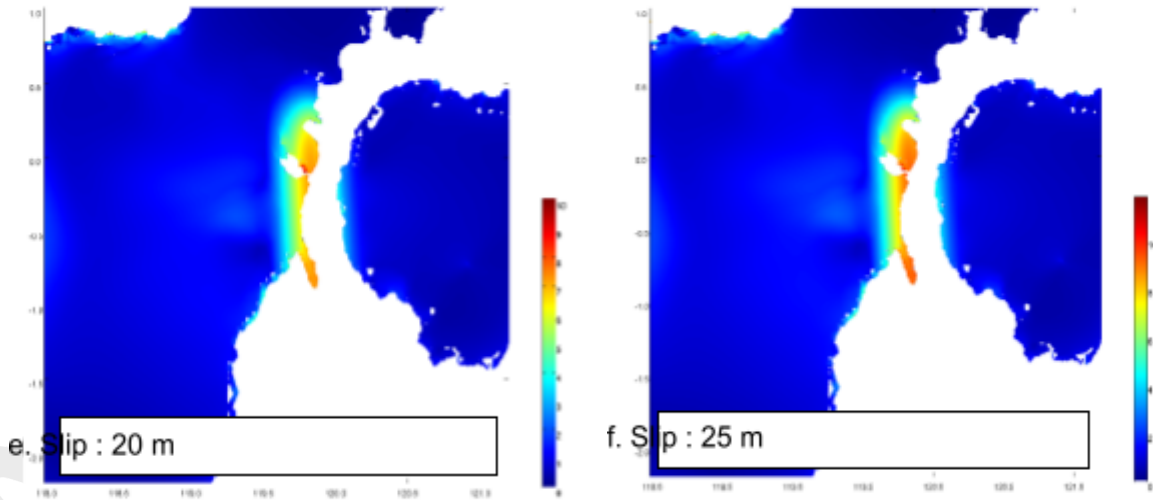


Figure SEQ Figure \\* ARABIC 36 Maximum Wave Height with Slip Variation

Table 11 Maximum Wave Height with Slip Variation

Slip (m)	Max. Wave Height (m)
1 (initial model)	0.9
2	1.52
5	3
10	5.3
15	8
20	10
25	11.7

obvious  
The magnitude  
is increasing  
to unreasonable  
numbers.

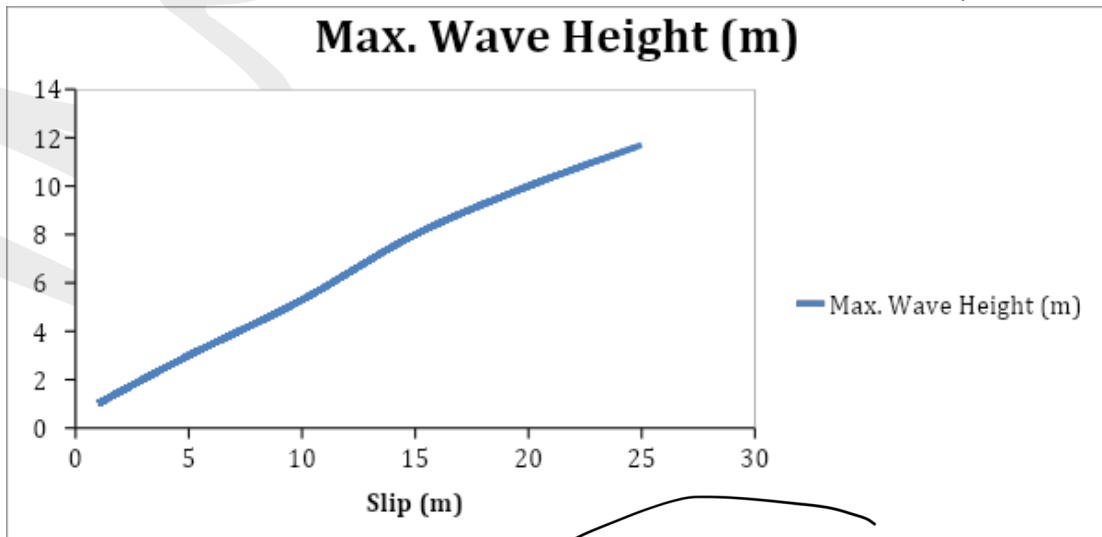


Figure 37 Maximum Wave Height VS Depth to Top

wrong legend.

*This is not a nice word.*

**3. Area (width)**

Area is the third manipulated parameter. The original value of the depth is of the fault is 54.01 km. The modification of width was done by dividing and multiplying the original value by a factor of 10.

The results can be seen in Figure 37 and Table 12.

*→ why .01? Don't get it.*

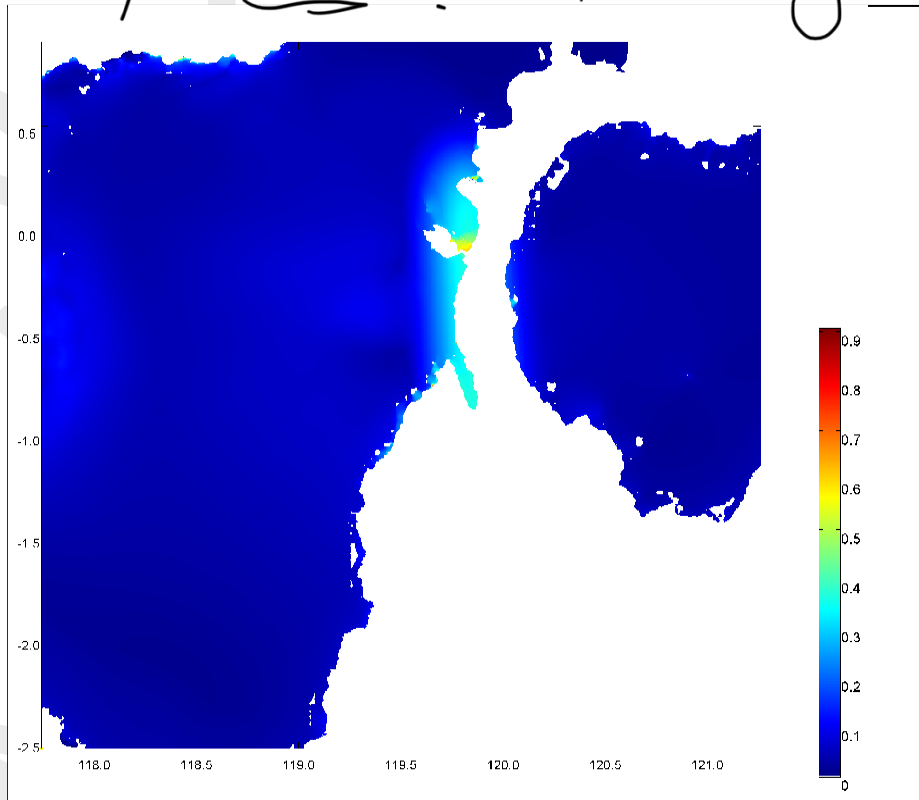


**Figure 38 Maximum Wave Height with Width Variation**

**Table 12 Maximum Wave Height with Width Variation**

Width (km)	Max. Wave Height (m)
0.5401	0.9
5.401	0.9
54.01 (initial model)	0.9
540.1	0.9
5401	0.9

*→ Now you go to the decimeter.*

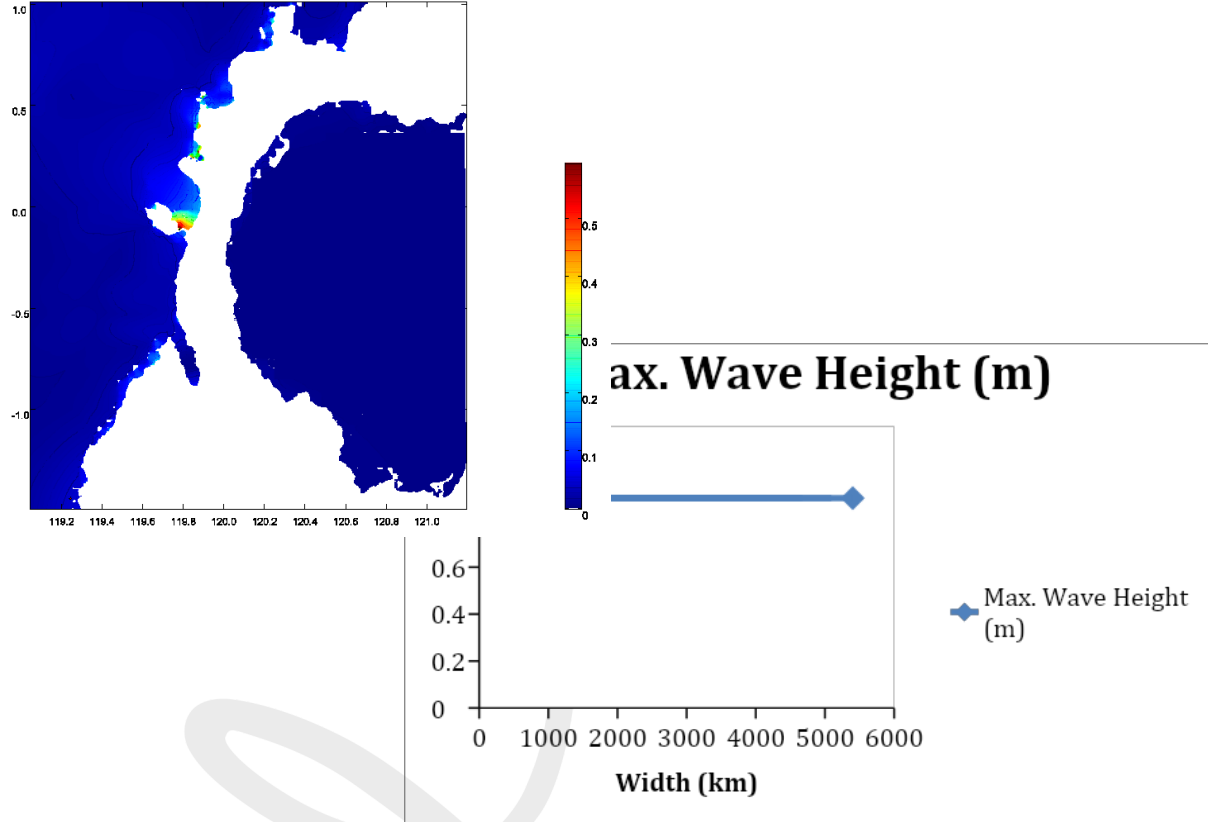
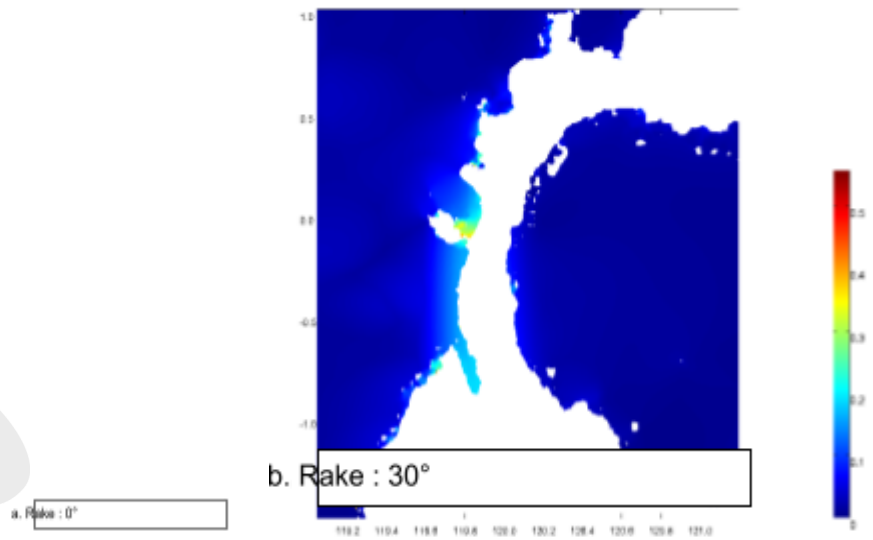


Figure 39 Maximum Wave Height VS Width

**4. Rake (slip angle)**

The initial value of rake is  $90^\circ$ . Because rake is angle of slip, the angle is increased or decreased by  $30^\circ$ .

The result can be seen in Figure 39 and Table 13.



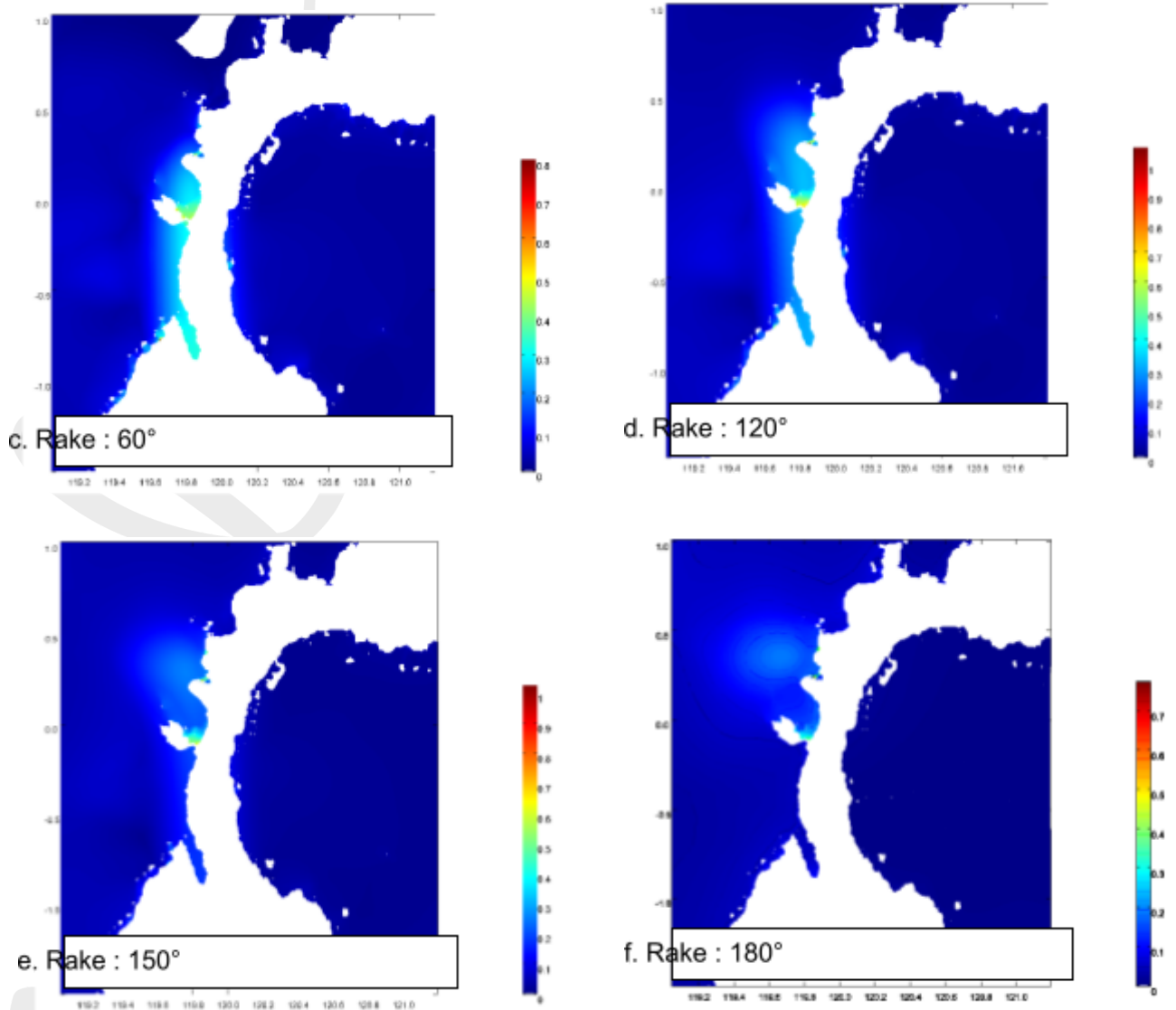


Figure SEQ Figure \\* ARABIC 40 Maximum Wave Height with Rake Angle Variation

Table 13 Maximum Wave Height with Rake Angle Variation

Rake (°)	Max. Wave Height (m)
0	0.5
30	0.55
90 (initial)	0.9
120	1
150	1
180	0.77

Theoretically these should be equal.



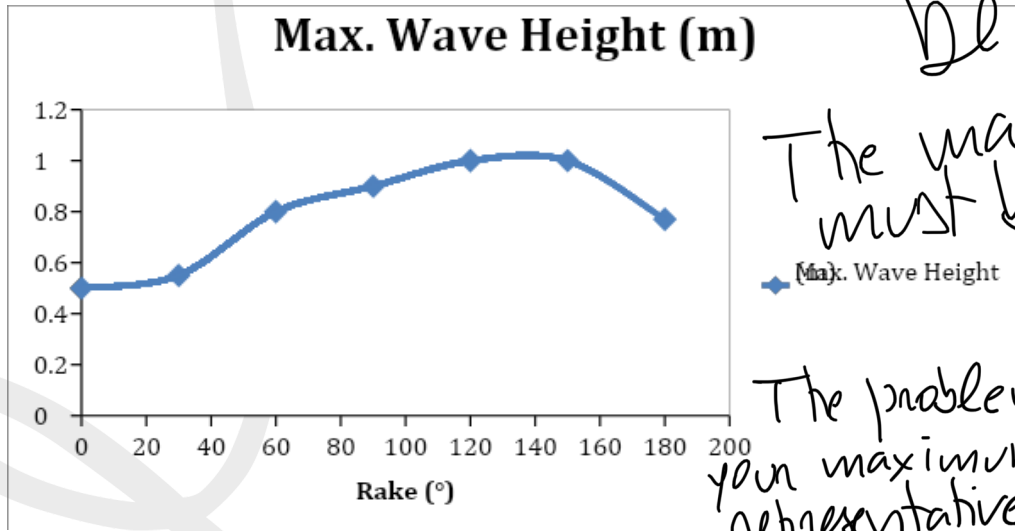


Figure 41 Maximum Wave Height VS Rake Angle

5. Dip

The initial value of dip angle is 25°. Because according to a research by Geist, (1998), the usual value of dip angles are between 10° to 35°, in this study, the angle is increased or decreased by 5°.

The result can be seen below.

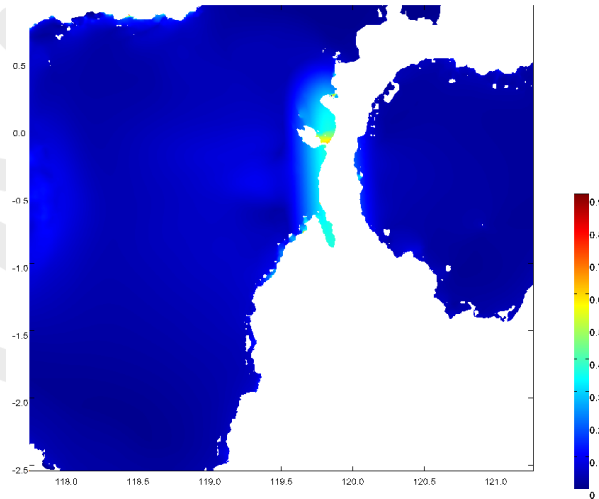


Figure 42 Maximum Wave Height with Dip Angle Variation

This can't be correct

The maximum must be at 90°

The problem is that your maximums are not representative because they occur on individual coastal pixels, very affected by errors

I told you to pay attention to that.

**Table 14 Maximum Wave Height with Dip Angle Variation**

Dip (°)	Max. Wave Height (m)
10	0.9
15	0.9
20	0.9
25	0.9
30	0.9
35	0.9
40	0.9

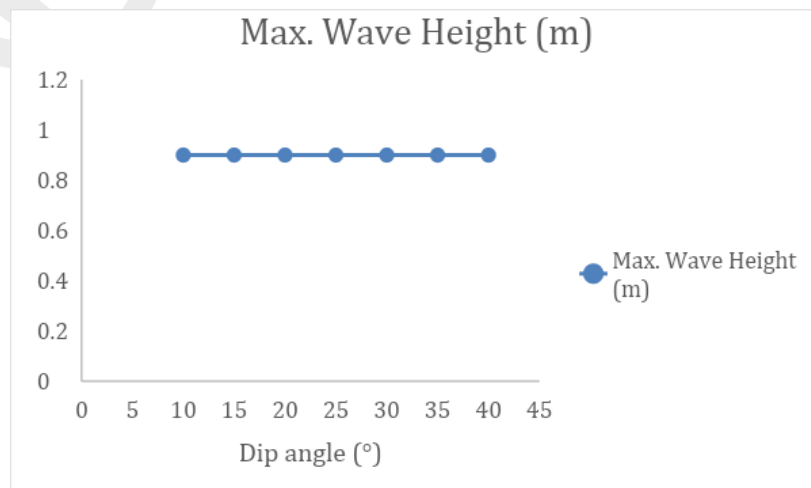


**Figure 43 Maximum Wave Height VS Dip Angle**

### 6. Strike

The initial value of strike angle is 176°. According to a research by Necmioğlu & Özel, (2014) where they stated that wide range of strike angle value could cause different conclusions, therefore the modification of strike angles for this study is by increasing or decreasing the initial strike value by 10°. The result can be seen below.

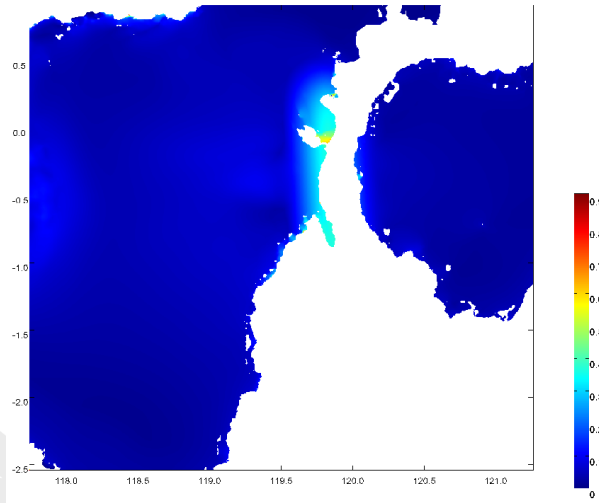
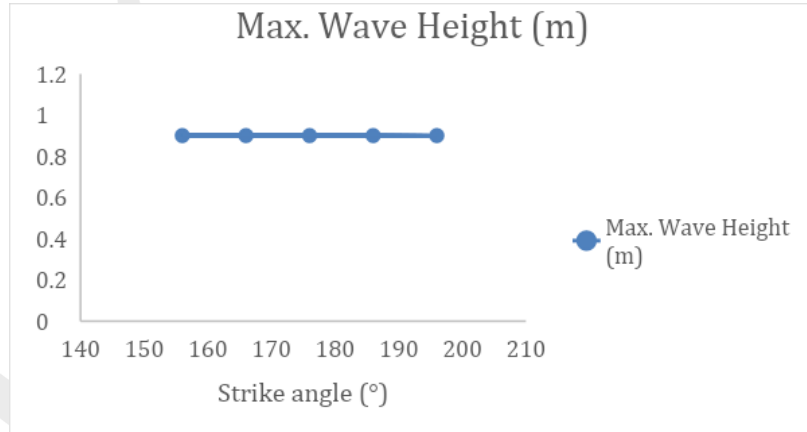


Figure 43 Maximum Wave Height with Strike Angle Variation

Table 14 Maximum Wave Height with Strike Angle Variation

Dip (°)	Max. Wave Height (m)
156	0.9
166	0.9
176	0.9
186	0.9
196	0.9



## 6. Discussion

The strike-slip fault where the Palu earthquake happened has raised a discussion due to its abnormal cause of event. This further leads to an assumption that it is not just a regular event and perhaps the Palu tsunami was triggered primarily by the deformation beneath Palu Bay or landslides triggered by the earthquake (Cilia et al., 2021).

The models created here in this report are exclusively the simulating the earthquake on a strike-slip fault.

### 6.1. Initial model

Based on the result achieved in subchapter 4.2, we can see that there are two important results:

1. The result of recorded data at Mamuju tide gauge is 6 cm **matches** with the result of initial model created in MIRONE, which is 1.8 cm (See Figure 26).
2. The data collected after the tsunami event **don't match** any of measurement. The biggest wave height difference is 9.5 m, and the smallest wave difference is 2 meter, which leads to average wave height difference of 5.8 m (See Table 7).

Therefore, results of the initial simulation agrees with the result from recorded data and not from the survey data, which means that the earthquake and could lead to two main causes:

what limitations? Give example.

#### 6.1.1. Computational limitations

As mentioned previously, tsunami relies on many different parameter which are not only complex, but also difficult to be accurately determined. One possibility of the wave height difference is the simulation might be affected by significant uncertainties caused by computational limitations since a research done by Ulrich, (2019) emphasized the possibility that the source of tsunami due to earthquake displacement in the strike-slip.

Phragm  
with  
no-  
mean  
ing

On one hand, based on a study done by the Pacific Tsunami Warning Center personal communications in 2005, the scientists in this field are usually capable of determining some fault plane parameters quite fast (around 30 mins after the earthquake event), which are:

- epicenter location accuracy to  $\pm 50$  km

magnitude accuracy to  $\pm 0.2$

hypocenter focal depth accuracy to  $\pm 15$  km

They explained that these are estimated numbers, and the uncertainty in these parameters for any particular event may be much larger. On the other hand, according to Costas et al., (1997), uncertainties for the fault parameters after the earthquake that is obtained ranges from 25 to 50%. However, for parameter strike, slip, length and width, the errors can ranges from 75 to 90%.

Therefore, this leads to the sensitivity analysis that is also done in this report.

#### 6.1.2. Landslide induced tsunami

Even though the external trigger of submarine landslides are not always clear, seismicity is often considered as the main trigger setting off submarine landslides. (Harbitz, 2014). In this Palu tsunami case, it is very likely that landslide tsunami happened due to several reason based on two observable occasions during the tsunami event:

1. Survivors of Palu tsunami mentioned that the first tsunami wave arrived immediately after the earthquake. This could imply that the changes in water surface which lead to tsunami was very fast (Takagi et al., 2019).
2. Even though it is proven that both historical and recent tsunamis can be caused by strike-slip earthquakes, their amplitudes were much smaller than Palu tsunami event (Carvajal et al., 2019).

This leads to a suspicion that the tsunami is not primarily caused by earthquake, but submarine landslide. Submarine landslides tend generate quite shorter period tsunamis compared to those caused by earthquakes, but also tend to cause higher wave height (Yavari-Ramshe & Ataie-Ashtiani, 2016). Moreover, in this tsunami case, there are local tsunamis which can be caused by earthquake that triggers submarine landslides at several locations around Palu Bay (Muhari et al., 2018).

Those findings lead to many research which stated that Palu tsunami event cannot be only caused by the earthquake displacement in the strike-slip alone:

1. Carvajal et al., (2019) did an analysis of satellite imagery from Google Earth and also from several amateur videos collected from people in nearby locations.

Why submarine?  
There videos of coastal landslides.



Then, it is clear that the video footage shows tsunami inundation happened only within 1–2 min after the main shock. This is shorter than those recorded by the local tide gauge, which cannot be explained by the earthquake fault slip alone. Surveys done after tsunami in the coastline surveys combined with modelled tsunami travel times supports the dominance of submarine landslides in tsunami generation.

2. Nakata et al., (2020) simulated the 2018 tsunami with submarine landslide sources and was able to produce the similar result as observed in video footage. The research stated that the earthquake is positively the main cause of the tsunami, however in their studies, all the earthquake tsunami models could not produce and explain the observed/surveyed data.

In addition to that, this research also discussed how the earthquake source models in previous studies done by Ulrich et al. 2019 seemed to have overestimate subsidence or uplift around the Pantoloan tide gauge station where considerable average tidal level change was not observed.

3. UNESCO-IOC along with Indonesian Meteorology, Climatology, and Geophysical Agency (BMKG) International Symposium. (2019)., and Widiyanto et al., (2019b) further reinforced the possibility of landslide induced tsunami based on their findings through 3D LIDAR, drones, and video footage.

Video footage shows evidence of submarine landslides and it is observed along the east and west coast. The research also emphasized that the landslide acted as secondary contributions to the tsunami generation.

How?

A generation of tsunami by submarine landslide is a complex process, and various numerical models have been developed to analyze the propagation of the resultant tsunamis. This creates more uncertainties and affect the generation of numerical models. Landslide induced tsunami would need more parameter sources and complex tsunami propagation models compared to earthquake induced tsunami. Furthermore, the fact that landslide-induced tsunamis happen less frequent than earthquake induced tsunamis creates more gap about the knowledge regarding this models. Therefore, it would take more time to simulate or build a model for this event.

In addition to their complexity, landslide induced tsunamis also shows a great variety. Since most of the landslide induced tsunamis are displaying in more local effects compared to

earthquake-induced tsunamis, due to different source characteristics. Examples of landslide induced tsunamis are (Harbitz, 2014):

- 1899 Ceram event caused a 12 m tsunami wave height
- the 1929 Grand Banks event caused a 13 m tsunami wave height
- the 1979 Nice event caused a 3 m tsunami wave height
- the 1992 Flores event caused a 26 m tsunami wave height or 19.6 m based on the average value of wave height from four nearby measurements
- the 1998 Papua New Guinea event caused a 15 m tsunami wave height

Those examples emphasize the fact submarine landslides may cause larger tsunami inundation compared to earthquake-induced.

## 6.2. Sensitivity analysis

The sensitivity analysis is done to quantify and further examine how the different fault parameters affected the tsunami event, including the maximum wave height. My interest is to understand how sensitive the predicted tsunami wave height is to the variations or uncertainties in the fault plane parameters that include epicenter location, rake, dip and strike angles, fault length and width, slip displacement, and the focal depth. (Gica et al., 2007)

### 6.2.1. Bathymetry Map

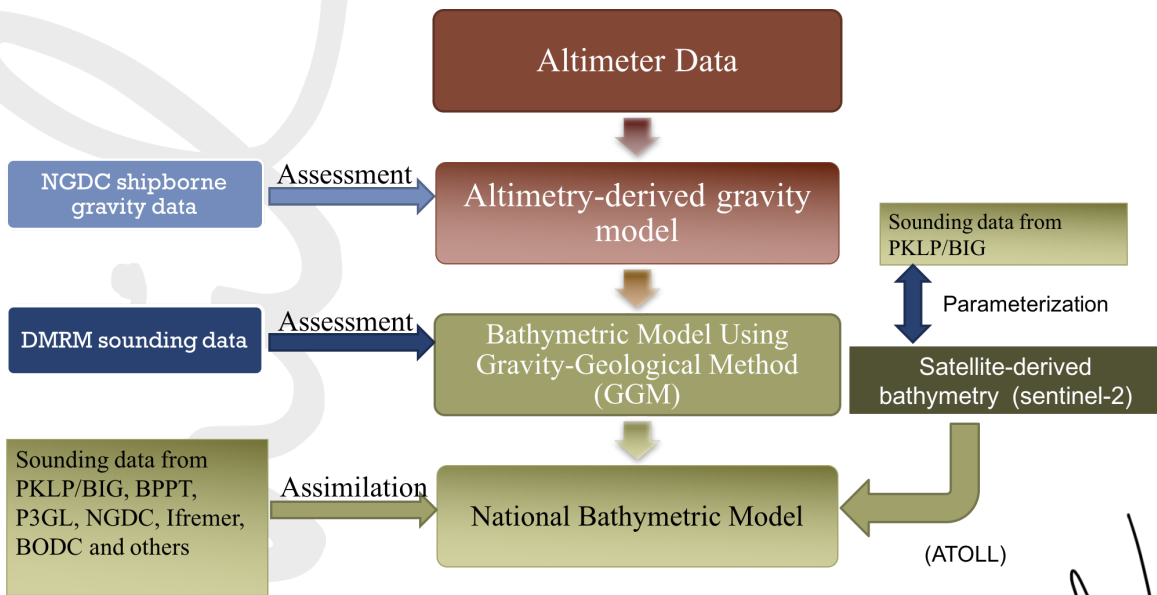
Maximum wave heights in surveys after tsunami is difficult to measure because the value normally depends on debris lines transported during the inundation process and are obtained several days after the tsunami. The distribution of wave heights is also very dependent on the features of the bathymetry, which makes it important to have an accurate one.

Based on the result achieved in Subchapter 5.2.1., bathymetry does play a role in changing the maximum wave height, although not reaching the surveyed maximum wave height. The highest maximum wave height achieved by National Bathymetry (BATNAS) which is 3.6 meter, followed by another variation of bathymetry, which is a combination of GEBCO and BATNAS, which produced a maximum wave height of 2.35 meter. It is interesting how the different bathymetry could produce 1 meter difference of wave height.

The bathymetric do not achieve wave heights.  
None of those numbers

mean anything because you didn't do a real tsunami propagation model. You limited to look at the grid of wave heights that had noise at coastal locations.

BATNAS, the bathymetry that produces the biggest maximum wave height value, has advantages in coastal areas and shallow waters using surveys from the Center for Marine and Coastal Environment (PKLP). The development of the BATNAS gridded model data starts from the calculation of the free air gravity anomaly data, which then leads to the bathymetry data using the Gravity-Geological Method (GGM). Details of using the GGM model can be found in Hsiao et al., (2016), and methods of assimilating generalization data into bathymetric data is available in Becker et al., (2009).



Source: <http://tides.big.go.id/DEMNAS/>

Figure 43 Bathymetric data processing flow chart (modified from Hsiao et al., 2016)

↳ what is the interest of this for your work?

The assessment of the accuracy of the free air gravity anomaly data (altimeter data) is carried out by comparing the model results against shipborne data. The results of the accuracy test show that the marine gravity model developed by Geospatial Information Agency has adequate accuracy, as the basis for estimating the bathymetry model at a resolution of 1m (1 minute) prior to the iteration of the general data assimilation, from 1m to 6-arcsecond resolution.

The results of the hydrographic survey on the Digital Marine Resource Mapping (DMRM) activity were used as data validators for the National Bathymetry gridded model, from 1m, 30-seconds, 15-seconds resolution. Assimilation of general data in shallow waters and

coastal areas would mean that BATNAS will have the best accuracy in the coastal areas of the Indonesian archipelago, compared to other bathymetric model data.

Therefore, although the BATNAS data at several points don't match with the real condition from Google Map, BATNAS still provides the best option as a bathymetry for tsunami simulation.

### 6.2.2. Fault parameters

Strike-slip faults are vertical faults that have mostly moved horizontally. In this case, inaccuracies for the fault parameters after the earthquake that is obtained straightaway ranges from 25 to 50%. However, for parameter strike, slip, length and width, the errors can range from 75 to 90% (Costas et al., 1997).

In this approach the earthquake source is parameterized through its size (depth and width of the fault), its orientation (strike and dip angles), and two kinematic rupture parameters (the slip and its direction in the fault plane, the rake angle).

Based on the result achieved in Subchapter 5.2.2., the variables will be discussed below:

#### 1. Depth

The highest maximum wave height was achieved by 2.2827 km depth to top, which is 0.1 times the original depth of the new fault. However, once the depth is decreased further, it can be seen that the highest maximum wave height doesn't increase, but rather, decreased.

The wave height would first increase ~~due to the fact~~ that the fault is closer to the water, making it more impactful due to the short distance. This agrees with the equation stated below:

Then, interestingly, once the fault distance got decreased once more by a factor of 10, the maximum wave height decreased, and it is even lower than the original maximum wave height. This is because once the depth is too shallow; it cannot produce bigger energy even though it is near the water.

In addition to that, depth can have counter intuitive effect. While deeper depth may cause smaller wave height due to its distance from the water surface, it can also produce longer

why? Faith! The faults don't move.

How can you say this?

fault param. determined by seismic inversion or just focal mechanisms

are very accurate.

wrong, you saw it ~20 km depth produce the highest amplitudes.

wavelength deformation, which cause longer surface waves that can carry higher wave heights to further distance. Therefore, the modification would be both to test shallow and deep fault depths. With MIRONE, fault can be easily adjusted even though it is multi patch. By opening it with Notepad, the value of depth can easily be modified

## 2. Slip

The results show that an increase in the slip displacement cause a significant increase in the maximum tsunami wave heights even when other parameters are is kept the same. Slip is also the only parameter that could reproduce the maximum wave height from the survey data since as seen in Table 11, slip 25 m could produce 11.7 m wave height. From another research that took a case in Chile, a 100% increase in slip displacement in an earthquake produced double the wave height in Hawaii's offshore (Gica et al., 2007). Therefore, it can also be seen that from the graph that slip creates a constant change in seismic moment, which can be explained by a following equation:

$$M_0 = \mu DLW \text{ (Eq. 4)}$$

Where:

$M_0$  = seismic moment

$\mu$  = shear modulus/rigidity of earth

$D$  = average slip displacement (m)

$W$  = fault width (m)

As shown in Eq. 4, slip displacement affect seismic moment.

Seismic moment is a measure of the size of an earthquake based on the area of fault rupture, the average amount of slip, and the force that was required to overcome the friction sticking the rocks together that were offset by faulting. Seismic moment can also be calculated from the amplitude spectra of seismic waves.

Then, the seismic moment is linked to the moment magnitude since the log of seismic moment is a fonction of moment magnitude. It can be seen from the following equation:

$$M_w = \frac{2}{3} \log \log M_0 - 10.7 \text{ (Eq. 5)}$$

Where:

$M_w$  = moment magnitude

$M_0$  = seismic moment

This implies that slip has a direct relation with the magnitude of earthquake, which links to amplitude of tsunami. The result is consistent with this equation and confirms that slip has a strong relation to  $M_w$  which leads to a greater amount of maximum wave height.

However, slip value is usually not more than 10 m because slip is linked to moment magnitude that has the maximum value recorded of 9.5. Therefore, this simulation is based on a hypothetical situation and could not represent any real event.

### 3. Area (width)

Following the previous point about slip, area of fault also plays a role in determining the value of seismic moment. The size of the fault can be changed by increasing or decreasing the width and length. In this case, the parameter modified is the width of fault, because the length of fault would require making new fault and could risk affecting other parameters (and could not isolate the area alone as a parameter).

According to Gica et al., (2007), the fault dimensions include length and width (resulting in area) are one of the most uncertain fault plane parameters. In addition to that, another research by Synolakis et al. (1997) in Gica et al., (2007) mentioned that “the deformation area estimated from aftershocks is often twice that estimated from geodetic data” and that the errors for length and width can be as high as 75%.

Based on this, I examine how a large variation in fault width affect the wave height. As shown in Eq. 4, the seismic moment magnitude is a function of both fault dimension and average slip displacement. However, based on the results obtained, it seems like the width does not affect the maximum wave height. This implies that fault width have an effect mostly in the wavelength and waves with larger wavelength are able to propagate further with less energy decay. So, even though width is a significant factor, it is not directly impacting on the initial wave height.

This is aligned with a research done by Gica et al., (2007) where they did a study on a variation in the length/width ration of a fault. They found that an increase in length combined with decrease in width produces more wave height change compared to the increase in width combined with decrease in length. In addition to that, another research by Geist, (1998) identified that for huge earthquakes, the fault area will most likely have an elongated shape, and the width usually does not exceed 300 km.



#### 4. Rake (slip angle)

Rake is the angle of slip that gives a direction of where the hanging wall moves over foot wall (See Figure 28). This also means that the rake angle could indicate the type of faulting style:

- $0^\circ$  or  $180^\circ$  is a strike-slip fault, where there is no vertical slip.  $0^\circ$  is left lateral strike slip and  $180^\circ$  is right lateral strike slip.
- $+90^\circ$  is a reverse thrusting fault, where the hanging wall moves upwards
- $270^\circ$  or  $-90^\circ$  is a normal fault, where the hanging wall moves downwards
- All other values indicate some form of oblique faulting.

Faulting style is important because it controls the ratio between vertical and horizontal coseismic sea floor displacement.

In addition to that, rake also has crucial parts in determining the magnitude and other characteristics of near-source ground motions. (Aagaard et al., 2004). It is because the rake angle controls two things that are important to represent tsunamigenic strength which are (Gibbons et al., 2022): The displaced water volume and its distribution, and the depth of tsunami generation that influences the relative contribution of shoaling. Even though the rake angle is difficult to determine accurately immediately after an earthquake occurs, the uncertainty is usually less than  $45^\circ$ .

The results that I obtained in Table 13 show the changes in the wave height, where the highest maximum wave height is achieved by both  $120^\circ$  and  $150^\circ$  which is 1 meter, the lowest maximum wave height is achieved by  $0^\circ$  rake angle, which is 0.5 meter, half the value of the highest maximum wave height. This result does not agree with a research done by Gica et al., (2007) where they stated that when the rake angle equals  $90^\circ$ , the highest waves would be generated (note: other parameters are kept the same). This happens because of the physics of  $90^\circ$  rake angle that would cause biggest vertical displacement of the fault plane, and leads to creating higher wave. This small mismatch might be caused by an error in the data that could be further investigated.

For the lowest maximum wave height value obtained by  $0^\circ$ , which corresponds to left strike slip fault (similar to the Palu 2018 tsunami case), it is expected the strike slip faulting cause a small wave heights. Then, as for the other angles result in very similar waveforms

to the normal and reverse faulting ( $90^\circ$  and  $270^\circ$ ) but at lower amplitudes (Gibbons et al., 2022).

### 5. Dip Angle

Geist, (1998) describes the dip angle that could be obtained based on aftershock information quite accurately. Dip angle is a permanent attribute and from the present earthquake data the values of dip angle are usually between  $10^\circ$  and  $35^\circ$ . In this study, the dip angle is varied from  $10^\circ$  to  $40^\circ$  with the increase of  $5^\circ$ . The results of these simulations are shown in Figure 42 and Table 14. Based on the result, it can be seen that with the usual variation of dip angle values does not cause any variation in wave height.

A research by done by Gica et al., (2007) shares a similar result with Titov et al. (1999). Both agree with the result of this study that realistic variations and uncertainties in dip angle will not introduce significant changes in the maximum wave height.

### 6. Strike Angle

Strike angle could be described as the orientation of the fault plane (See Figure 29) since the strike line is the intersection between an inclined surface and a horizontal plane and the strike angle is the direction where the strike line points in. This angle can be assessed based on the impacted area (Gica et al., 2007).

In this study, the strike angle is varied by  $10^\circ$  which is common for most earthquake induced tsunami cases. The original value of the slip and its maximum wave height is then compared to the result of each simulation's maximum wave height. The results obtained by the simulations show no changes with the strike angle variation. This is aligned with a research done by Gica et al., (2007) where they did a simulation of various strike angle for far field tsunami waves at the mouth of Hilo where the earthquake is located in Japan. Based on their research, variation in strike angle will not introduce a significant change to the resulting wave heights. Interestingly, in the same research, it is stated that for an earthquake in Chile, a change in the strike angle is seen to cause a large relative change in wave heights in Hilo Bay. It shows that the sensitivity of the far field wave heights to a strike angle does not always significant.

However, for the near field tsunami, strike plays an important role according to (Necmioğlu & Özel, 2014) where the strike of a fault in an earthquake induced tsunami event is possibly the best known parameter of those selected in their study. They even stated that a change in strike strongly affects the tsunami amplitude in the impact zone, suggesting that it is important to consider an earthquake fault's strike in any tsunami hazard assessment. A research by Gibbons et al., (2022) also mentioned that strike generate a maximum inundation area near  $0^\circ$  and  $180^\circ$  meanwhile the minimum inundation area would be near  $90^\circ$  and  $270^\circ$ .

Therefore, the results obtained from MIRONE might not represent the real effect of strike in a tsunami event due to the poor quality of the fault, or the MIRONE generates the difference in inundation area and not the wave height.

This is  $\pm$  repeated from  
the sensitive analysis  
section and it's not  
really a discussion.

## 7. Conclusion

This study have executed multiple numerical earthquake-generated tsunami simulations in Palu, related to the Palu tsunami in 2018 where it was considered as an ambiguous tsunami event. Meteorology, Climatology, and Geophysical Agency of Indonesia stated that the tide gauge near this tsunami event recorded only 6 cm in wave height meanwhile the real event showed around 11 m wave height after a post tsunami survey was done. This leads to a question on why this fatal error happened. Therefore, a numerical code which is a Non-linear Shallow Water Model with Nested Grids (NSWING) is used to model the tsunami which is embedded in a matlab-based software, MIRONE. This model was used with a system of nested grids and also combined with TSUNAMI N2 to model shoaling, flooding and coastal amplification of the tsunami waves.

The first part of this study examines the initial model, where the earthquake data is obtained through USGS, containing all the information in the fault related to the earthquake that caused or triggered the tsunami event. Then, the source of bathymetry used in the initial model is obtained from General Bathymetric Chart of the Oceans (GEBCO) 2020 grid. The results are:

1. A maximum wave height of 2.25 m, which is far from the tsunami wave height (11 m)
2. The wave height acquired in the simulation at the tide gauge is only 1.8 cm, which is aligned with the result from the tide gauge recording during the tsunami event (6 cm)
3. Huge gaps on the value of wave heights from the simulation data compared to survey data in all the survey points. The average difference of wave height value is 5.8 m.

This leads to a conclusion that there are some uncertainties that needs to be checked by completing a sensitivity analysis, or the tsunami was not caused by only earthquake, but rather, induced by submarine landslide.

The second part of this study focuses on tackling the uncertainties caused by computational limitations that might be the reason for the big gap in wave height values. This is done by performing sensitivity analysis on several parameters related to the

*you didn't do any of these*

*Again TSUNAMI N2? (NOT TSUNAMI N2)  
where did you do that? (you didn't)*

earthquake event, namely: bathymetry and fault parameters. Fault parameters consist of: depth, slip, area, rake angle, dip angle and strike angle. It is important to know that the fault for sensitivity analysis is not the one used for initial simulation, but instead it was made with MIRONE to simplify the process. The source of bathymetry used for sensitivity analysis is still from General Bathymetric Chart of the Oceans (GEBCO) 2020 grid. The results are:

1. The new fault generated a 0.9 m maximum wave height
2. Bathymetry variation models achieved higher wave heights than initial model where the highest maximum wave height is obtained by National Bathymetry (Batimetri Nasional – BATNAS) which is 3.6 m.
3. Fault parameters:
  - a. Depth: The highest maximum wave height was achieved by 12.827 km depth to top (-10 km the original depth of the new fault), which is 1.13 m, meanwhile the lowest maximum wave height was achieved by 32.827 km depth to top (+10 km the original depth of the new fault), which is 0.72 km.
  - b. Slip: The only parameter that could recreate the tsunami wave height. The highest maximum wave height was achieved by 25 m slip (25 times the original slip of the new fault), which is 11.7 m, meanwhile the lowest maximum wave height was achieved by 1 m slip (the original slip of the new fault), which is 0.9 m.
  - c. Area (width): Width is chosen to represent the area since it is much simpler to manipulate. This parameter does not change the wave height at all.
  - d. Rake angle: The highest maximum wave height was achieved by 120° and 150° m rake angles (+30° and +60° the original rake angle of the new fault), which is 1 m, meanwhile the lowest maximum wave height was achieved by 0° rake angle (-90° the original rake angle of the new fault), which is 0.5 m.
  - e. Dip angle: Dip angle does not change the wave height at all.
  - f. Strike angle: Strike angle does not change the wave height at all.

Knowing that offshore tsunami height is a complex function of earthquake parameters, based on the significant differences caused by different parameters, it is confirmed that the sensitivity of wave height to these parameters is very dependent for some and not as much for others. Based on the simulation done by MIRONE, slip is the only parameter

that could reach the survey tsunami wave height, which is 11.7. Then, bathymetry, depth, and rake are able to generate differences in maximum wave height. However, width, dip angle and strike angle don't cause any differences. But this does not mean that these parameters have no impact at all. In several other research, strike is proven to be one of the most important parameters for earthquake induced tsunami. Therefore, this could be caused by the poor quality of fault data or MIRONÉ generated a difference in inundation area, and not wave height.

All these results leads to a strong indication of submarine landslide, because the parameters in sensitivity analysis is not able to recreate the real event based on survey data, except for slip. However, the value of slip that could recreate the value is not realistic and only serves a purpose in showing the significance of slip as a parameter. Therefore, it can be concluded that Palu tsunami 2018 was a landslide induced tsunami that was triggered by earthquakes. This emphasizes the importance of fully understanding the bathymetry and geological condition of tsunami prone area to prevent similar event in the future.

The problem is that your sensitivity analysis experimented cases that have nothing, but really nothing to do with the Palu earthquake so any comparison doesn't really make much sense.



## References

- Aagaard, B. T., Hall, J. F., & Heaton, T. H. (2004). Effects of fault dip and slip rake angles on near-source ground motions: Why rupture directivity was minimal in the 1999 Chi-Chi, Taiwan, earthquake. *Bulletin of the Seismological Society of America*, *94*(1), 155–170. <https://doi.org/10.1785/0120030053>
- André, D., & Conde, S. (2012). *A Tsunami in Lisbon Where to run ? Engenharia Civil*.
- Bao, H., Ampuero, J. P., Meng, L., Fielding, E. J., Liang, C., Milliner, C. W. D., Feng, T., & Huang, H. (2019). Early and persistent supershear rupture of the 2018 magnitude 7.5 Palu earthquake. *Nature Geoscience*, *12*(3), 200–205. <https://doi.org/10.1038/s41561-018-0297-z>
- Becker, J. J., Sandwell, D. T., Smith, W. H. F., Braud, J., Binder, B., Depner, J., Fabre, D., Factor, J., Ingalls, S., Kim, S. H., Ladner, R., Marks, K., Nelson, S., Pharaoh, A., Trimmer, R., von Rosenberg, J., Wallace, G., & Weatherall, P. (2009). Global Bathymetry and Elevation Data at 30 Arc Seconds Resolution: SRTM30\_PLUS. *Marine Geodesy*, *32*(4), 355–371. <https://doi.org/10.1080/01490410903297766>
- Bellier, O., Siame, L., Beaudouin, T., Villeneuve, M., & Braucher, R. (2001). High slip rate for a low seismicity along the Palu-Koro active fault in Central Sulawesi (Indonesia). *Terra Nova*, *13*(6), 463–470. <https://doi.org/10.1046/j.1365-3121.2001.00382.x>
- Bock, Y. (2003). Crustal motion in Indonesia from Global Positioning System measurements. *Journal of Geophysical Research*, *108*(B8). <https://doi.org/10.1029/2001jb000324>
- Bryant, E. (2008). *Tsunami The Underrated Hazard (Second Edition)*. In *Geophysical Sciences*.
- Carvajal, M., Araya-Cornejo, C., Sepúlveda, I., Melnick, D., & Haase, J. S. (2019). Nearly Instantaneous Tsunamis Following the Mw 7.5 2018 Palu Earthquake. *Geophysical Research Letters*, *46*(10), 5117–5126. <https://doi.org/10.1029/2019GL082578>
- Chenan, C. M., Jayaraf, N., & Vaidyanathan S., G. (2010). Artificially intelligent tsunami early warning system. *UKSim2010 - UKSim 12th International Conference on Computer Modelling and Simulation*, 39–44. <https://doi.org/10.1109/UKSIM.2010.16>
- Cilia, M. G., Mooney, W. D., & Nugroho, C. (2021). Field Insights and Analysis of the 2018 Mw 7.5 Palu, Indonesia Earthquake, Tsunami and Landslides. *Pure and Applied Geophysics*, *4340*. <https://doi.org/10.1007/s00024-021-02852-6>
- Costas, S., Philip, L., Abelson, P. H., George, C., & Harry, Y. (1997). Tsunamigenic Sea-Floor Deformations. *Science*, *278*(5338), 598–600. <https://doi.org/10.1126/science.278.5338.598>

- Dao, M. H., & Tkalich, P. (2007). Tsunami propagation modelling - A sensitivity study. *Natural Hazards and Earth System Science*, 7(6), 741–754. <https://doi.org/10.5194/nhess-7-741-2007>
- ESRI. (2008). The Multipatch Geometry Type. *White Paper, December*, 156.
- Fang, J., Xu, C., Wen, Y., Wang, S., Xu, G., & Zhao, Y. (2018). *The 2018 Mw 7.5 Palu Earthquake: A Supershear Rupture Event Constrained by InSAR and Broadband Regional Seismograms. Figure 1*, 1–15.
- GEBCO Bathymetric Compilation Group 2020. (2020). *The GEBCO\_2020 Grid - a continuous terrain model of the global oceans and land*. British Oceanographic Data Centre, National Oceanography Centre, NERC. <https://doi.org/doi:10.5285/a29c5465-b138-234d-e053-6c86abc040b9>
- Geist, E. L. (1998). Local Tsunamis and Earthquake Source Parameters. *Advances in Geophysics*, 39(C), 117–209. [https://doi.org/10.1016/S0065-2687\(08\)60276-9](https://doi.org/10.1016/S0065-2687(08)60276-9)
- Gibbons, S. J., Lorito, S., de la Asunción, M., Volpe, M., Selva, J., Macías, J., Sánchez-Linares, C., Brizuela, B., Vöge, M., Tonini, R., Lanucara, P., Glimsdal, S., Romano, F., Meyer, J. C., & Løvholt, F. (2022). The Sensitivity of Tsunami Impact to Earthquake Source Parameters and Manning Friction in High-Resolution Inundation Simulations. *Frontiers in Earth Science*, 9(January), 1–23. <https://doi.org/10.3389/feart.2021.757618>
- Gica, E., Teng, M. H., Liu, P. L.-F., Titov, V., & Zhou, H. (2007). Sensitivity Analysis of Source Parameters for Earthquake-Generated Distant Tsunamis. *Journal of Waterway, Port, Coastal, and Ocean Engineering*, 133(6), 429–441. [https://doi.org/10.1061/\(asce\)0733-950x\(2007\)133:6\(429\)](https://doi.org/10.1061/(asce)0733-950x(2007)133:6(429))
- Goda, K., Mori, N., Yasuda, T., Prasetyo, A., Muhammad, A., & Tsujio, D. (2019). Cascading Geological Hazards and Risks of the 2018 Sulawesi Indonesia Earthquake and Sensitivity Analysis of Tsunami Inundation Simulations. *Frontiers in Earth Science*, 7(September). <https://doi.org/10.3389/feart.2019.00261>
- HAMZAH, L., PUSPITO, N. T., & IMAMURA, F. (2000). Tsunami Catalog and Zones in Indonesia. *Journal of Natural Disaster Science*, 22(1), 25–43. <https://doi.org/10.2328/jnds.22.25>
- Harbitz, C. B. (2014). *Submarine landslide tsunamis: How extreme and how likely? and how likely? January 2015*. <https://doi.org/10.1007/s11069-013-0681-3>
- Harnantyari, A. S., Takabatake, T., Researcher, I., Esteban, M., & Valenzuela, V. P. (2019). *Tsunami awareness and evacuation behaviour during the 2018 Sulawesi Earthquake*

- tsunami Tsunami Awareness and Evacuation Behaviour during the 2018 Sulawesi Earthquake Tsunami. November.* <https://doi.org/10.1016/j.ijdr.2019.101389>
- Hsiao, Y. S., Hwang, C., Cheng, Y. S., Chen, L. C., Hsu, H. J., Tsai, J. H., Liu, C. L., Wang, C. C., Liu, Y. C., & Kao, Y. C. (2016). High-resolution depth and coastline over major atolls of South China Sea from satellite altimetry and imagery. *Remote Sensing of Environment*, 176, 69–83. <https://doi.org/10.1016/j.rse.2016.01.016>
- Jinsong Xie. (2007). *u Ottawa Department of Civil Engineering Numerical Modeling of Tsunami Waves.*
- Khare, V., Khare, C., Nema, S., & Baredar, P. (2019). Optimum Sizing and Modeling of Tidal Energy Systems. In *Tidal Energy Systems*. <https://doi.org/10.1016/b978-0-12-814881-5.00004-1>
- Kiratzis, A. A. (2014). Mechanisms of Earthquakes in Aegean. *Encyclopedia of Earthquake Engineering, November.* <https://doi.org/10.1007/978-3-642-36197-5>
- Kowalik, Z., Knight, W., Logan, T., & Whitmore, P. (2005). Numerical Modeling of The Global Tsunami : Indonesian Tsunami of 26 December 2004. *Science of Tsunami Hazards*, 23(1), 40–56.
- Kurniasih, A., Marin, J., & Setyawan, R. (2020). Belajar dari Simeulue: Memahami Sistem Peringatan Dini Tsunami di Indonesia. *Jurnal Geosains Dan Teknologi*, 3(1), 21. <https://doi.org/10.14710/jgt.3.1.2020.21-30>
- Liu, P. L. F., Woo, S.-B., & Cho, Y.-S. (1998). Computer programs for tsunami propagation and inundation. *Cornell University*, 25.
- Luis, J. F. (2007). Mirone: A multi-purpose tool for exploring grid data. *Computers and Geosciences*, 33(1), 31–41. <https://doi.org/10.1016/j.cageo.2006.05.005>
- Miranda, J. M., Luis, J. F., Reis, C., Omira, R., & Baptista, M. A. (2015). Validation of NSWING , a multi-core finite difference code for tsunami propagation and run-up. *Poster, April*, 1–2.
- Muhari, A., Imamura, F., Arikawa, T., Hakim, A. R., & Afriyanto, B. (2018). Solving the Puzzle of the September 2018 Palu, Indonesia, Tsunami Mystery: Clues from the Tsunami Waveform and the Initial Field Survey Data. *Journal of Disaster Research*, 13(Scientific Communication), sc20181108. <https://doi.org/10.20965/jdr.2018.sc20181108>
- Nahak, P. G., Djunaedi, D., & Wonlele, T. (2017). Studi Perencanaan Mitigasi Bencana Tsunami di Daerah Wisata Pantai Tablolong. *Potensi: Jurnal Sipil Politeknik*, 19(2), 83–89. <https://doi.org/10.35313/potensi.v19i2.898>
- Nakata, K., Katsumata, A., & Muhari, A. (2020). Submarine landslide source models consistent

- with multiple tsunami records of the 2018 Palu tsunami , Sulawesi , Indonesia. *Earth, Planets and Space*. <https://doi.org/10.1186/s40623-020-01169-3>
- Necmioğlu, Ö., & Özel, N. M. (2014). An earthquake source sensitivity analysis for tsunami propagation in the Eastern Mediterranean. *Oceanography*, 27(2), 76–85. <https://doi.org/10.5670/oceanog.2014.42>
- Papadopoulos, G. A., Daskalaki, E., Fokaefs, A., & Novikova, T. (2014). Tsunamigenic potential of local and distant tsunami sources threatening SW Peloponnese. *Bollettino Di Geofisica Teorica Ed Applicata*, 55(2), 469–484. <https://doi.org/10.4430/bgta0097>
- Parker, B. (2010). *The Power of the Sea: Tsunams, Storm Surges, Rogue Waves and our Quest to predict disasters*.
- Paulik, R., Gusman, A., Williams, J. H., Pratama, G. M., Lin, S. lin, Prawirabhakti, A., Sulendra, K., Zachari, M. Y., Fortuna, Z. E. D., Layuk, N. B. P., & Suwarni, N. W. I. (2019). Tsunami Hazard and Built Environment Damage Observations from Palu City after the September 28 2018 Sulawesi Earthquake and Tsunami. *Pure and Applied Geophysics*, 176(8), 3305–3321. <https://doi.org/10.1007/s00024-019-02254-9>
- Pribadi, S., Gunawan, I., Nugraha, J., Haryono, T., Susanto, E., Utara, K., Belum, T., & Donggala, K. (2018). *Merekam Jejak Tsunami Teluk Palu 2018. September*, 1–7.
- PuSGen, T. (2018). Kajian Gempa Palu Provinsi Sulawesi Tengah 28 September 2018 (M7.4). In *Pusat Litbang Perumahan dan Pemukiman, Balitbang PUPR Pusat* (Vol. 1, Issue).
- Rashidi, A., Shomali, Z. H., Dutykh, D., Faraj, N. K., Rashidi, A., Shomali, Z. H., Dutykh, D., Keshavarz, N., Khah, F., Rashidi, A., Shomali, Z. H., & Dutykh, D. (2018). *Evaluation of tsunami wave energy generated by earthquakes in the Makran subduction zone To cite this version: HAL Id: hal-01719939 Evaluation of tsunami wave energy generated by earthquakes in the Makran subduction zone*.
- Roy, A. B. (2014). Facts about Tsunami : Its origin , earthquake link and prediction : An Opinion. *INSA Honorary Scientist*, 18(3), 330–335.
- Sepúlveda, I., Haase, J. S., Carvajal, M., Xu, X., & Liu, P. L. F. (2020). Modeling the Sources of the 2018 Palu, Indonesia, Tsunami Using Videos From Social Media. *Journal of Geophysical Research: Solid Earth*, 125(3), 1–22. <https://doi.org/10.1029/2019JB018675>
- Simandjuntak, T. O., & Barber, A. J. (1996). Contrasting tectonic styles in the neogene orogenic belts of Indonesia. *Geological Society Special Publication*, 106(106), 185–201. <https://doi.org/10.1144/GSL.SP.1996.106.01.12>
- Sotiris Valkaniotis, Ganas, A., Tsironi, V., & Barberopoulou, A. (2018). *A preliminary report on*

*the M7.5 Palu earthquake co-seismic ruptures and landslides using image correlation techniques on optical satellite data. October, 1–15.*  
<https://doi.org/10.5281/zenodo.1467128>

- Suppasri, A., Koshimura, S., Imamura, F., Ruangrassamee, A., & Foytong, P. (2013). A review of tsunami damage assessment methods and building performance in Thailand. *Journal of Earthquake and Tsunami*, 7(5). <https://doi.org/10.1142/S179343111350036X>
- Symposium, B. I. (2019). *Lesson Learnt from the 2018 Tsunamis in Palu and Sunda Strait. September.*
- Takagi, H., Pratama, M. B., Kurobe, S., Esteban, M., Aránguiz, R., & Ke, B. (2019). Analysis of generation and arrival time of landslide tsunami to Palu City due to the 2018 Sulawesi earthquake. *Landslides*, March. <https://doi.org/10.1007/s10346-019-01166-y>
- Triyono, R., Prasetya, T., Daryono, Anugrah, S. D., Sudrajat, A., Setiyono, U., & Gunawan, I. (2018). *Katalog Tsunami Indonesia Tahun 416-2018.*  
<https://cdn.bmkg.go.id/Web/Katalog-Tsunami-Indonesia-pertahun-416-2018.pdf>
- Ulrich, T. (2019). *Coupled , Physics-Based Modeling Reveals Earthquake Displacements are Critical to the 2018 Palu , Sulawesi Tsunami. 176, 4069–4109.*  
<https://doi.org/10.1007/s00024-019-02290-5>
- UNESCO/IOC. (2019). *Limitations and Challenges of Early Warning Systems Case Study: IOC/2019/TS/150, 100.*
- Wessel, P., Luis, J. F., Uieda, L., Scharroo, R., Wobbe, F., Smith, W. H. F., & Tian, D. (2019). The Generic Mapping Tools Version 6. *Geochemistry, Geophysics, Geosystems*, 20(11), 5556–5564. <https://doi.org/10.1029/2019GC008515>
- Widiyanto, W., Santoso, P. B., Hsiao, S. C., & Imananta, R. T. (2019a). Post-event field survey of 28 September 2018 Sulawesi earthquake and tsunami. *Natural Hazards and Earth System Sciences*, 19(12), 2781–2794. <https://doi.org/10.5194/nhess-19-2781-2019>
- Widiyanto, W., Santoso, P. B., Hsiao, S., & Imananta, R. T. (2019b). *Post-event field survey of 28 September 2018 Sulawesi earthquake and tsunami. 1(September 2018), 2781–2794.*
- Wronna, M. (2015). *Deterministic tsunami hazard assessment of Sines - Portugal. 56.*
- Yavari-Ramshe, S., & Ataie-Ashtiani, B. (2016). Numerical modeling of subaerial and submarine landslide-generated tsunami waves—recent advances and future challenges. *Landslides*, 13(6), 1325–1368. <https://doi.org/10.1007/s10346-016-0734-2>

## Appendix A: Finite-Source Rupture Model from USGS

```

% ----- FINITE-SOURCE RUPTURE MODEL -----
%
% Event : MINAHASSA PENINSULA, SULAWESI 2018/09/28 [Hayes (NEIC,2014)]
% EventTAG: 1000h3p4HAYES
%
% Loc : LAT = -0.1781 LON = 119.8401 DEP = 10.4
% Size : LEN = 264 km WID = 36.75 km Mw = 7.52 Mo = 2.5479443e+20 Nm
% Mech : STRK = 358 DIP = 66 RAKE = 343 Htop = 0 km
% Rupt : HypX = 196 km Hypz = 11.375 km avTr = 3.12 s avVr = 3.93 km/s
%
% ----- inversion-related parameters -----
%
% Invs : Nx = 33 Nz = 21 Fmin = 0.002 Hz Fmax = 1 Hz
% Invs : Dx = 8 km Dz = 1.75 km
% Invs : Ntw = 6 Nsg = 1 (# of time-windows,# of fault segments)
% Invs : LEN = 1.8 s SHF = 0.9 s (time-window length and time-shift)
% SVF : Asymmetriccosine (type of slip-velocity function used)
%
% Data : SGM TELE TRIL LEVEL GPS INSAR SURF OTHER
% Data : 0 57 0 0 0 0 57 0
% Data : 0 76.43 0 0 0 0 76.43 0
% Data : 0 32.59 0 0 0 0 32.59 0
%
% -----
%
% VELOCITY-DENSITY STRUCTURE
% No. of layers = 7
%
% DEPTH P-VEL S-VEL DENS QP QS
% [km] [km/s] [km/s] [g/cm^3]
% 0.00 2.30 1.20 2.20 1000 500
% 1.50 3.20 1.60 2.30 1000 500
% 3.50 6.00 3.40 2.70 1000 500
% 13.50 6.60 3.70 2.90 1000 500
% 23.00 7.20 4.00 3.10 1000 500
% 31.00 8.08 4.47 3.38 1200 500
% 227.00 8.59 4.66 3.45 360 140
%
% -----
% 16-Oct-2018 created by GPH (mguy@usgs.gov)
%
% SOURCE MODEL PARAMETERS
% Nsbfs = 693 subfaults
% X,Y,Z coordinates in km; SLIP in m
% if applicable: RAKE in deg, RISE in s, TRUP in s, slip in each TW in m
%
% Coordinates are given for center of each subfault or segment: '|'
% Origin of local coordinate system at epicenter: X (EW) = 0, Y (NS) = 0
% LAT LON X==EW Y==NS Z SLIP RAKE TRUP RISE SF_MOMENT
% -----
-1.9063 119.8620 2.0729 -192.1641 0.8078 0.0838 353.6272 48.0000 3.4000 3.72e+15
-1.8343 119.8595 1.7950 -184.1584 0.8078 0.3005 375.1458 46.6000 3.6000 1.33e+16
-1.7623 119.8570 1.5172 -176.1528 0.8078 0.0777 353.9919 44.6000 4.0000 3.44e+15

```